Evaluation of neuroprotective strategies in inflammatory and degenerative animal models by visual system readouts

Inaugural-Dissertation

zur Erlangung des Doktorgrades
der Mathematisch-Naturwissenschaftlichen Fakultät
der Heinrich-Heine-Universität Düsseldorf

vorgelegt von

Michael Dietrich
aus Villingen-Schwenningen

Düsseldorf, September 2019

Aus der Klinik für Neurologie des
Universitätsklinikums Düsseldorf
und dem Institut für Neurobiologie
der Heinrich-Heine-Universität Düsseldorf

Gedruckt mit der Genehmigung der
Mathematisch-Naturwissenschaftlichen Fakultät der
Heinrich-Heine-Universität Düsseldorf

Berichterstatter:

1.PD Dr. Philipp Albrecht

2. Prof. Dr. Christine R. Rose

Tag der mündlichen Prüfung: 27. April 2020

Summary

In the relapsing remitting and in progressive forms of Multiple Sclerosis (MS), neuronal degeneration is the main cause of long-term disability. While great advances have been made in preventing the inflammatory relapses, strategies to effectively prevent the chronic neurodegenerative processes or promote repair are still lacking. Experimental autoimmune encephalomyelitis (EAE) is a commonly used animal model for MS and recapitulates most pathological hallmarks, allowing a preclinical evaluation of novel therapeutic strategies. The implementation and application of preclinical, longitudinal *in vivo* readouts that can be translated to clinical applications, is of great scientific interest. Optical coherence tomography (OCT) is a fast, non-invasive, interferometric technique allowing high resolution imaging of the eye's retina. In MS patients and EAE mice, the retinal alterations not only represent a morphological correlate of the functional visual deficits, but also mirror the overall disability and the brain atrophy. This makes OCT an ideal tool for visualizing the degenerating processes in inflammatory and degenerative animal models.

In this thesis, the first task was to establish retinal OCT measurements in a preclinical setting. We therefore created a holder with optional inhalant anesthesia, where the beam-to-target angle can be adjusted by a manual rotation of the tube housing the animal. We then provided a video manual and detailed protocol for confocal scanning laser ophthalmoscopy (cSLO)/OCT and optokinetic response (OKR) in rodents. OKR can be used to determine the visual acuity of rodents, providing the functional readout to support the structural data from OCT. As an animal model for MS, EAE is a frequently used model, but comparative studies between the different EAE models using visual system readouts are still lacking. In the third work of this thesis, we first identified the ideal OCT scanning protocol in mice with best reproducibility and reliability. We then compared the longitudinal progression of pathology, inducing EAE in transgenic and wildtype mouse lines with different antigens, measuring OCT and OKR, and performing histological analyses. EAE in C57Bl/6J mice using the myelin oligodendrocyte glycoprotein, fragment 35-55 (MOG_{35-55}) was concluded as the most suitable model. Using this model, we tested the antioxidant alpha-lipoic acid (LA) with the established systems, after evaluating the suitable compound in cell culture. This is a highly relevant approach, as clinical optic neuritis studies (ON) are increasingly being used to evaluate new neuroprotective or remyelinating strategies. We found LA having both neuroprotective and anti-inflammatory properties. However, we also determined, that only a prophylactic LA treatment resulted in significant protective effects detected by OCT. Therefore, the translation to an optic neuritis trial might not be recommendable, as therapy would only be started at the onset of symptoms. However, we conclude that EAE-ON is a very suitable *in vivo* model, recapitulating the pathological hallmarks of acute autoimmune infiltration, demyelination and neuroaxonal

damage, as well as possible remyelination and repair after therapy. The fact that all of these pathologies can easily be assessed in the retina and/or optic nerve makes the anterior visual pathway an ideal model for the preclinical evaluation of novel therapeutic strategies.

Zusammenfassung

Bei der schubförmigen und der progressiven Form der Multiplen Sklerose (MS) ist Neurodegeneration die Hauptursache für eine Langzeitbehinderung. Während bei der Prävention der entzündungsgeprägten Schübe große Fortschritte erzielt werden konnten, fehlen noch Behandlungsmöglichkeiten, um die chronischen, neurodegenerativen Prozesse effektiv zu verhindern oder Regeneration zu fördern. Die experimentelle autoimmune Enzephalomyelitis (EAE) ist das am häufigsten verwendete Tiermodell für MS und umfasst deren pathologischen Eigenschaften, was eine präklinische Bewertung neuer therapeutischer Ansätze ermöglicht. Die Etablierung und Anwendung präklinischer, longitudinaler *in vivo* Messungen, welche ggf. auf eine klinische Studie übertragen werden können, ist von großem wissenschaftlichen Interesse. Die Optische Kohärenztomographie (OCT) ist eine schnelle, nicht-invasive, interferometrische Methode, die eine hochauflösende Bildgebung der Netzhaut des Auges ermöglicht. Bei MS-Patienten und EAE-Mäusen stellen die Netzhautveränderungen nicht nur ein morphologisches Korrelat der funktionellen Sehdefizite dar, sondern spiegeln auch die allgemeine Behinderung und die Hirnatrophie wieder. Damit ist OCT ein ideales Werkzeug zur Visualisierung von Degenerationsprozessen sowohl in entzündlichen wie in degenerativen Tiermodellen.

In dieser Arbeit war das erste Ziel, retinale OCT-Messungen im präklinischen Rahmen zu etablieren. Deshalb entwickelten wir zunächst eine Halterung für Mäuse und Ratten mit optionaler Inhalationsanästhesie. Mit dieser kann das Tiere in allen Ebenen um das Auge als Fixpunkt rotiert werden, sodass besonders leicht ein orthogonaler Winkel des OCT Messstrahls zur Retina eingestellt werden kann. Anschließend produzierten wir einen Video-Artikel mit einem detaillierten Protokoll für die konfokale Scanning-Laser-Ophthalmoskopie (cSLO), OCT Untersuchung und die Messung der optokinetischen Reaktion (OKR) in Nagetieren. Mit der OKR kann die Sehfunktion von Nagetieren beurteilt werden, um die Ergebnisse der retinalen Morphologie aus der OCT Untersuchung zu untermauern. Als Tiermodell für MS ist die EAE ein häufig verwendetes Modell, aber vergleichende Studien zwischen verschiedenen EAE Modellen hinsichtlich des visuellen Systems sind noch nicht vorhanden. Im dritten Teil dieser Arbeit haben wir daher das OCT-Scanprotokoll in Mäusen mit der besten Reproduzierbarkeit und Verlässlichkeit identifiziert. Wir induzierten EAE in transgenen und Wildtyp-Mauslinien durch Immunisierung mit verschiedenen Antigenen und

verglichen den Krankheitsverlauf mittels OCT-, OKR- und histologische Analysen. Wir identifizierten die Myelin-Oligodendrozyten-Glykoprotein, Fragment 35-55 (MOG_{35-55}), induzierte EAE in C57Bl/6J Mäusen als am besten geeignetes Modell zur Analyse retinaler Neurodegeneration bei Optikusneuritis. Mit diesem Modell untersuchten wir daraufhin das Antioxidans alpha-Liponsäure (LA) mit Hilfe der implementierten Untersuchungsmethoden, nachdem wir zunächst in Zellkultur-Untersuchungen die wirksamste Form der LA identifiziert hatten. Dies ist ein sehr relevanter Ansatz, da bei Patienten zunehmend klinischen Studien an der Optikus-Neuritis (ON) zur Untersuchung neuer neuroprotektiver oder remyelinisierender Strategien eingesetzt werden. Wir fanden heraus, dass LA sowohl neuroprotektive, als auch entzündungshemmende Eigenschaften besitzt. Gleichzeitig stellten wir fest, dass nur eine prophylaktische LA-Behandlung zu signifikant protektiven Effekten in der Retina führt, welche durch das OCT identifiziert werden können. Daher erscheint eine ON-Studie zur Untersuchung der protektiven Wirkung von LA nicht erfolgversprechend.

Wir kommen jedoch zu dem Schluss, dass EAE-ON ein gut geeignetes *in vivo*-Modell ist, um die pathologischen Merkmale der akuten Autoimmuninfiltration, der Demyelinisierung und der neuroaxonalen Schäden sowie der möglichen Remyelinisierung und Regeneration bei entzündlichen Erkrankungen des zentralen Nervensystems zu untersuchen und Therapien zu evaluieren. Die Tatsache, dass all dies in der Netzhaut und/oder im Sehnerv beurteilt werden kann, macht das visuelle System zu einem idealen Modell für die präklinische Bewertung neuer therapeutischer Strategien.

Inhaltsverzeichnis

Introduction

Parts of this thesis have been published in the review article “Assessing the anterior visual pathway in optic neuritis: Recent experimental and clinical aspects” by **Dietrich M**, Aktas O, Hartung H-P, Albrecht P (2019), Current opinion in neurology, 32(3):346-357.

Neurodegenerative disease – Unmet need for effective therapies

In various neurological diseases, including Parkinson’s disease (PD), Alzheimer’s disease (AD), and Multiple Sclerosis (MS), neuronal degeneration is the critical mechanism for chronic clinical deterioration of the patients (Lane et al. 2018; Thenganatt and Jankovic 2014; Thompson et al. 2018). While AD and PD, and other inherited disorders such as Huntington’s disease (Bates et al. 2015), are classical neurodegenerative diseases, the primary pathology in MS is mediated by autoimmune inflammation (Thompson et al. 2018). Although great advances have been made in preventing the inflammatory relapses, strategies to effectively prevent the chronic neurodegenerative processes are still lacking, despite decades of research. Reasons are, among others: a) the complexity of the brain and pathophysiology of neurodegenerative processes, b) the delivery of the therapeutics to the target region is limited due to physiological borders, such as the blood–brain barrier and (c) the complex evaluation of the clinical outcomes makes it difficult to identify new targets and effective therapies (Piguet et al. 2017). While clinical relapse activity and magnetic resonance imaging of lesions are highly sensitive outcomes for inflammatory activity already in the short term follow up, tracking neuroaxonal degeneration, which progresses at a slower rate, is still a great challenge (Miller et al. 2002).

Multiple Sclerosis

MS is an inflammatory autoimmune disorder, which involves demyelination, loss of oligodendrocytes and subsequent axonal damage and eventually degeneration of neurons in the central nervous system. This degeneration is the main reason for the persisting clinical disability of MS patients (Compston and Coles 2008). Pathological changes in MS are generally characterized by infiltration of lymphocytes and macrophages into the brain parenchyma, where they trigger the upregulation of adhesion molecules and promote the recruitment of immune cells by inflammatory cytokines. This leads to glial and neuronal injury in an incompletely understood manner (Thompson et al. 2018; Wingerchuk and Carter 2014). There is, however, an improved understanding of the different parameters, such as genetic, lifestyle and environmental factors, that contribute to the development of the disease (Olsson et al. 2017). It has also been postulated that increased oxidative stress plays a major role in causing neuronal damage (Fischer et al. 2012). Both, the innate and adaptive immune

systems, with their effector cells seem to influence the pathogenesis of multiple sclerosis (Cheng et al. 2018). These findings, and also the discovery that B -cells are major contributors to the disease progression (Lisak et al. 2017), deliver potential new targets and starting points for new therapies.

Optic neuritis - paradigm for new neuroprotective therapies

Optic neuritis (ON) is characterized by subacute visual loss in one eye, usually occurring within hours or days, and is associated with pain during eye movement. (Optic Neuritis Study Group 1991). ON is the initial manifestation in about 25% of MS patients and occurs in the disease course in about 70%, predominantly in the early, relapse-remitting phase (Toosy et al. 2014). Additionally, ON occurs in the context of several other inflammatory disorders of the central nervous system (CNS) including neuromyelitis optica spectrum disorders (Wu et al. 2019) and chronic relapsing inflammatory optic neuropathy (Lee et al. 2018). The pathology of ON reflects the processes of acute inflammation, demyelination and consecutive neuronal degeneration, all hallmarks of MS pathology, which also occur in other parts of the CNS (Dietrich et al. 2019a). Hence, ON is frequently used as a model to investigate new neuroprotective and neuroregenerative therapies (Aktas et al. 2016).

Visual system readouts as window to the brain

The retina is part of the CNS and contains, among others, retinal ganglion cells (RGCs), the neurons of the optic nerve. The functional and structural evaluation of the visual pathway is comparatively easy, little time-consuming and non-invasive. Some parameters, such as retinal nerve fiber layer (RNFL) and ganglion cell/inner plexiform layer (GCIPL) thickness, have reasonable to high correlations with brain atrophy occurring in neurodegenerative disease (Siger et al. 2008; Villoslada et al. 2008; Saidha et al. 2015). The retinal degeneration of MS patients also mirrors the overall disability assessed by the Expanded Disability Status Scale (Galetta et al. 2011; Albrecht et al. 2007; Albrecht et al. 2012). Therefore, assessing the visual pathway can provide insight to the mechanisms occurring during neuro-inflammatory and neurodegenerative disease and is a valuable tool to evaluate new therapeutic approaches.

Optical coherence tomography and confocal scanning laser ophthalmoscopy

Optical coherence tomography (OCT) is a fast, non-invasive, interferometric technique that allows imaging of the retinal structures (Huang et al. 1991). Newest generation OCT provides high-resolution anatomic reconstructions of retinal morphology in a rapid and reproducible manner and permits an objective analysis not only of the RNFL but also of the deeper retinal layers (Frohman et al. 2008). It was recently demonstrated, that the reduction of the retinal

thickness occurs in MS patients also in the absence of optic neuritis (Albrecht et al. 2007; Albrecht et al. 2012; Petzold et al. 2010).

This makes OCT an ideal tool for visualizing the processes of neurodegeneration, neuroprotection and neuro-repair in MS. 3rd generation OCT devices can be modified to obtain and quantify high resolution morphological sections of the mouse and rat retina (Gobel et al. 2013; Dietrich et al. 2019b; Dietrich et al. 2017) which are in good accordance with the results of histological sections of the animals' retina (Fischer et al. 2009). The great advantage of OCT in comparison with histological investigations is that longitudinal analyses are possible to detect dynamic changes (Dietrich et al. 2018), avoiding inter-subject variability and thereby largely reducing the variability and the amount of animals needed per study. Furthermore *in vivo* imaging with OCT is not afflicted with any fixation artifacts such as changes in layer thickness depending on the fixation protocol used in histological sections.

Several OCT devices have the option to simultaneously apply confocal scanning laser ophthalmoscopy (cSLO) imaging. With different adjustable wavelengths, it is possible to gather diagnostic information about retinal pathologies i.e. visualization of lipofuscin deposits or alterations of the retinal pigment epithelium (Ward et al. 2017). Moreover, in vivo imaging of fluorescence labelled cells in transgenic animals can be performed to address several scientific questions (Chauhan et al. 2012; Lidster et al. 2013; Munguba et al. 2014; Kokona et al. 2017; Leung et al. 2008; Dietrich et al. 2019b).

Optokinetic response

In mice and rats, the function of the visual system can be investigated by measuring the optokinetic response (OKR). The animals are placed unrestrained on a platform in the center of a square of TFT monitors displaying a grating of black bars circulating in a virtual cylinder around the mice in varying direction. The mice involuntarily track the moving grating with reflexive head and neck movements. As animals only track in one direction with each eye, separate assessments can be performed for each eye by alternating the direction of rotation of the cylinder. The head movements can be measured and the distance between the black gratings in cycles per degree can be reduced until the mice cannot track anymore and the threshold is reached (Prusky et al. 2004). The optokinetic response is reduced or eliminated in case of reduced visual acuity, thus the functional effect of the neurodegeneration measured by OCT can also be monitored *in vivo* (Dietrich et al. 2019b).

Animal models for MS

"To investigate pathomechanisms and explore new therapeutic strategies, three main experimental approaches replicating major features of MS are applied: Toxic demyelinating

models with lack of primary inflammation and axonal damage (Matsushima and Morell 2001), models induced with viral agents to assess their contribution to disease course (DePaula-Silva et al. 2017) and a variety of experimental autoimmune encephalomyelitis (EAE) models (Miller et al. 2010; Lassmann and Bradl 2017). The latter are the most widely used animal models for human MS, summarized in Table 1" (Dietrich et al. 2019a: 347).

Table 1. Preclinical models of MS/optic neuritis (modified from Dietrich et al. 2019a). Models with the antigen, required for EAE induction in the diverse rodent strains. Myelin basic protein (MBP), proteolipid protein (PLP), myelin oligodendrocyte glycoprotein (MOG), T-cell receptor (TCR).

Strain	**Animal**	**Antigen**
Active EAE		
C57BL/6	Mouse	MOG
C57BL/6	Mouse	PLP
SJL/J	Mouse	PLP
SJL/J	Mouse	MBP
BALB/c	Mouse	PLP
Lewis	Rat	MBP
Brown Norway	Rat	MOG
Sprague Dawley	Rat	MOG
Dark Aguti	Rat	Spinal cord homogenate
Passive EAE-ON		
Various strains	Mouse or rat	Adoptive transfer of myelin specific lymphocytes
Genetic/spontaneous EAE-ON		
2D2/	C57BL/6 Mouse	MOG-specific T-cell receptor (TCR)
2D2xTH	C57BL/6 Mouse	MOG-specific TCR (2D2) MOG-specific B cell receptor (TH)
2D2/SJL/J	SJL/J Mouse	MOG-specific TCR
T⁄R+ H-2u	H-2U Mouse	MBP-specific TCR
HLA-DR15 + MBP-TCR	HLA-DR15 Mouse	MBP-specific TCR
PLPmut	C57BL/6 Mouse	Human PLP1 mutation transgenic

"In most active EAE models activation/infiltration of microglia, macrophages and lymphocytes occurs roughly around 1-2 weeks after immunization leading to demyelination but also degeneration of retinal ganglion cells and their axons" (Dietrich et al. 2019a: 349). In the commonly used MOG peptide, fragment 35-55 (MOG_{35-55}) EAE, an increase of the inner retinal layers (IRL) thickness is observed at disease onset (approx. after one week), followed by a degeneration as the disease progresses (Manogaran et al. 2018; Dietrich et al. 2018).

Aims of the thesis

The thesis aimed to identify and evaluate the molecular mechanisms and neuroprotective potential of established and new compounds and substances using the retina and visual function in inflammatory and neurodegenerative models. Cutting edge *in vivo* retinal imaging and evaluation of visual function were implied for animal use, to test the effect on the progression. Histological stainings and in vitro assays served as additional readouts (Figure 1). As the disability of MS patients is mainly caused by degeneration of neurons, neuroprotective substances are urgently required. Positive findings could provide a rationale for testing the substance in clinical trials using OCT and visual acuity as outcome parameters.

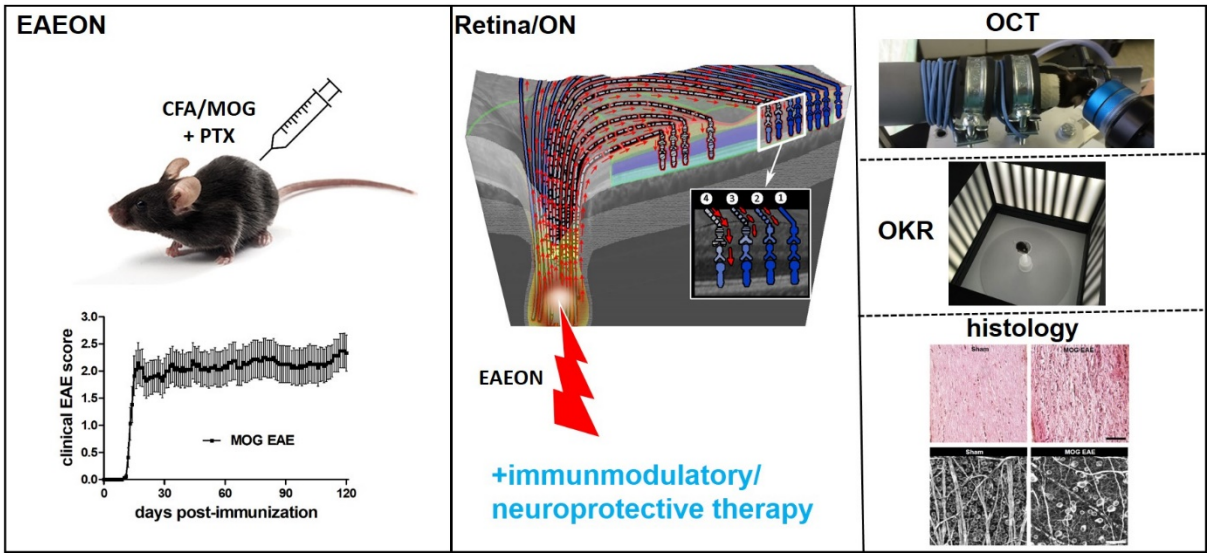

Figure 1. Models and readouts of the visual pathway. After EAE induction, inflammatory-induced axonal damage occurs in the optic nerve and subsequently in the retina. Immunomodulatory and potential neuroprotective therapies are tested and the effects can be evaluated by visual readouts and histology.

Publications as first/shared first author

Whole-body positional manipulators for ocular imaging of anaesthetised mice and rats: a do-it-yourself guide

Michael Dietrich[1], Andrés Cruz-Herranz[2], Hao Yiu[2], Orhan Aktas[1], Alexander U Brandt[3], Hans-Peter Hartung[1], Ari Green[2] and Philipp Albrecht[1]

[1]Department of Neurology, Heinrich-Heine-Universität Düsseldorf, Düsseldorf, Germany
[2]Department of Neurology, University of California San Francisco, San Francisco, California, United States
[3]NeuroCure Clinical Research Center, Charite-Universitätsmedizin Berlin, Berlin, Germany

The presented manuscript was published in “BMJ Open Ophthalmology”, 2016.

Contribution:

-First authorship
-Design of the study, experiments and rodent holder (50%)
-Construction and assembly of the holder (50%)
-Implementing and establishing rodent OCT in the laboratory (50%)
-Execution, analysis and statistics of the OCT experiments (90%)
-Writing and drafting of the manuscript (90%)

BMJ Open Ophthalmology

Whole-body positional manipulators for ocular imaging of anaesthetised mice and rats: a do-it-yourself guide

Michael Dietrich,[1] Andrés Cruz-Herranz,[2] Hao Yiu,[2] Orhan Aktas,[1] Alexander U Brandt,[3] Hans-Peter Hartung,[1] Ari Green,[2] Philipp Albrecht[1]

To cite: Dietrich M, Cruz-Herranz A, Yiu H, *et al*. Whole-body positional manipulators for ocular imaging of anaesthetised mice and rats: a do-it-yourself guide. *BMJ Open Ophth* 2016;**1**:e000008. doi:10.1136/bmjophth-2016-000008

► Prepublication history and additional material is available. To view please visit the journal (http://dx.doi.org/10.1136/bmjophth-2016-000008).

Received 06 June 2016
Revised 27 September 2016

[1]Department of Neurology, Heinrich-Heine-Universität Düsseldorf, Düsseldorf, Germany
[2]Department of Neurology, University of California, San Francisco, San Francisco, California, United States
[3]NeuroCure Clinical Research Center, Charite—Universitätsmedizin Berlin, Berlin, Germany

Correspondence to
Dr. Philipp Albrecht; phil.albrecht@gmail.com

ABSTRACT

Background: In vivo retinal imaging of rodents has gained a growing interest in ophthalmology and neurology. The bedding of the animals with the possibility to perform adjustments in order to obtain an ideal camera-to-eye angle is challenging.

Methods: We provide a guide for a cost-effective, do-it-yourself rodent holder for ocular imaging techniques. The set-up was tested and refined in over 2000 optical coherence tomography measurements of mice and rats.

Results: The recommended material is very affordable, readily available and easily assembled. The holder can be adapted to both mice and rats. A custom-made mouthpiece is provided for the use of inhalant anaesthesia. The holder is highly functional and assures that the rodent's eye is the centre of rotation for adjustments in both the axial and the transverse planes with a major time benefit over unrestrained positioning of the rodents.

Conclusion: We believe this guide is very useful for eye researchers focusing on in vivo retinal imaging in rodents as it significantly reduces examination times for ocular imaging.

Key messages

- While in vivo ocular imaging of small rodents, namely optical coherence tomography (OCT), is gaining increasing importance in ophthalmology and neurology, the available devices often require additional holders to manipulate the animals, especially if different species are to be imaged.
- We provide a do-it-yourself guide for a new whole-body positional manipulator for ocular imaging of mice and rats. It is cost-effective, easily assembled and compatible with any OCT device on the market.
- The holder speeds up OCT and fundus imaging in rodents and enables inhalation anaesthesia, which increases the throughput and reduces the recovery time from anaesthesia.

BACKGROUND

In recent years, in vivo retinal imaging has gained increasing relevance[1–3] not only in ophthalmological[4–8] but also in neurological[9–19] cases. Optical coherence tomography (OCT) and confocal scanning laser ophthalmoscopy (cSLO) have been identified as useful diagnostic tools to evaluate a large variety of retinopathies and retinal manifestations of neurological diseases. OCT allows for fast, non-invasive and high resolution in vivo visualisation of the retinal morphology and has been introduced as an outcome parameter in clinical trials of neuroprotection in multiple sclerosis and optic neuritis.[20–22]

The high resolution of third-generation spectral-domain OCT devices renders in vivo retinal imaging in mice and rats possible, gaining an increasing importance in ophthalmological and neurological preclinical research.[23–33] The obtained results are in good accordance with histological sections of the animals' retinae.[34]

The application of OCT technology in rodent models, however, is still challenging, mainly because of the small size of the rodents' eyes. Even if systems have been developed specifically for the imaging of rodents,[31 35] several commercially available devices require adaptations to image animals of different species. If investigators desire to change the species under investigation, for example, mice to rats, often a different size of holder is required. Animals have to be anaesthetised for measurement, which is largely facilitated by the proposed mouthpiece and holder.[36 37] Positioning the rodent with the option to easily adjust the eye orientation is critical for reproducible and high-quality images. Different holders have been proposed[38–43] to assure an optimal positioning and an adequate camera-to-eye angle. However, not all holders are applicable with all OCT devices. Some holders do not harmonise with the size of the OCT camera on certain devices, some are patented and/or only available together with

OCT devices and most are high priced. We, therefore, aimed to develop a guide and instructional drawing for a do-it-yourself, cost-effective and adjustable holder for bedding of rodents during OCT and cSLO measurements as well as for other ocular imaging techniques. The device is in use at our facilities and delivers excellent results with rodent OCT imaging.

METHODS

Ethics

The set-up was tested and approved in over 2000 measurements with mice and rats. All animal procedures were performed in compliance with the experimental guidelines approved by the regional authorities (State Agency for Nature, Environment and Consumer Protection; AZ 84-02.4.2014.A059) and conform to the Association for Research in Vision and Ophthalmology Statement for the Use of Animals in Ophthalmic and Vision Research.

Material

For the construction of the holder, we recommend the following items (figure 1A):

- Polyvinylchloride (PVC) pipe, inner diameter: ~3.4 cm for mice, ~6–8 cm for rats (eg, standard drainage pipes), approximately US$3;
- Aluminium sheet (20 × 5 × 0.2 cm), approximately US$11;
- Screw (M8, 4 cm), wing screw and plastic washers for the pivot, approximately US$1;
- Two clamps (size matching the PVC pipe, eg, drainage pipe holders), screws and lock nuts, approximately US$5.

Tools

The following tools are needed for the construction of the holder:

- jigsaw (saw blade for metal and plastic)
- drill (bits for metal)

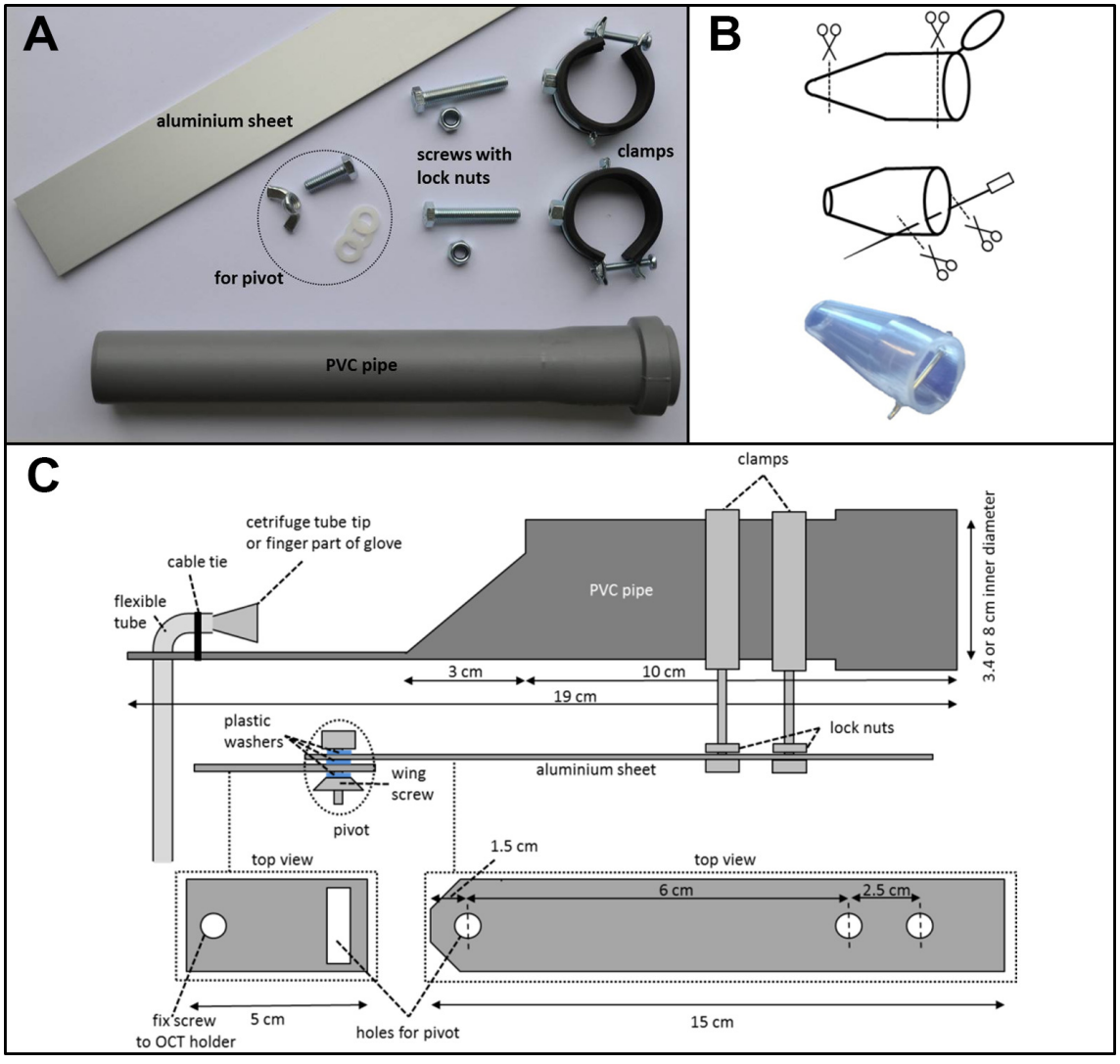

Figure 1 Construction and properties of the holder. (A) Recommended items for the holder, (B) construction of the mouthpiece and (C) diagram for modification of the items and assembly of the holder. OCT, ocular coherence tomography.

- file
- screw wrenches.

Assembly of the holder for mice

The following is a guide for the assembly of a holder for mice. Adaptations necessary for a rat holder are described below. Shorten the PVC pipe to a final length of 19 cm. At 10 cm from one end, cut out the top of the tube in a sloping shape, leaving a 6 cm long and 3 cm wide strip as illustrated in figure 1C. Drill a hole of 0.8 cm diameter into the strip at the front end of the PVC pipe (~2 cm from the front end) to hold the tube for the inhalant anaesthesia supply. Cut the aluminium sheet into two pieces of 15 and 5 cm length. Drill a rectangular excision of 1 × 4 cm at 1 cm from the end of the smaller sheet for a slidable pivot and an additional circular hole for an M8 screw at 0.5 cm from the other end. Slope the tip of one end of the 15 cm aluminium sheet at a 45°° angle using the jigsaw (optional) and drill three M8 holes at 1.5, 7.5 and 10 cm from the sloped end. Assemble the items by inserting the plastic washers between the screw, the two aluminium sheets and the wing screw for smooth movement of the pivot. The tube for inhalant anaesthesia supply (if needed) can be inserted and fixed with a cable tie. To form a mouth piece with an integrated bite bar, cut a centrifuge tube tip at 0.8 and 2.4 cm from the narrow end. Pierce a 20-gauge syringe needle through the bottom third of the tube tip at 0.3 cm from the broad end (figure 1B). This mouthpiece design allows a snug fit for the mouth of adult animals of most commercially available mouse lines (eg, A/J, BALB/cJ, C57BL/6J, DBA/2J, NMRI, SJL) and provides an improved immobilisation of the animal by carefully hooking the upper front teeth over the bite bar. Anaesthesia can be maintained by inhalation of isoflurane vaporised with pure oxygen at concentrations of 2% during measurement.

To maintain the body temperature and ensure immobility, we suggest wrapping the animal in a paper towel during measurement. Additionally, an external heat source, for example, a heat string used for terrariums, can be wrapped around the holder for longer measurements.

Adaptations for a holder suitable for rats

For rat holders (eg, Sprague Dawley, Wistar, Lewis, Long Evans, Brown Norway), the PVC pipe should have an inner diameter of ~6–-8 cm with size-matching clamps. The inhalant anaesthesia supply tube can be modified using the finger part of a laboratory glove, cut open on both sides and fixed on the tube with tape.

OCT device and fixation of the holder

Our experiments were performed using a Heidelberg Engineering Spectralis HRA+OCT device (Heidelberg Engineering GmbH, Heidelberg, Germany). The holder was attached to the platform that holds the chin rest for human subjects and that can be adjusted in the z-axis. However, the device is compatible with any other OCT device on the market and can be attached to a simple xyz table.

Statistics

A paired Student's t-test was performed to compare the time needed to adjust the mouse's eye position for an OCT measurement with and without the use of the rodent holder. Average values are presented as mean with SD. Differences were considered significant at $p<0.05$.

RESULTS

Evaluation of benefits for retinal imaging

Analysing the time needed to achieve correct positioning of the eye-to-camera angle and scanning area in OCT measurements of 11 independent mouse eyes, we observed a highly significant ($p<0.001$) time benefit when using the rodent holder (figure 2). The time expended was almost three times higher (2.8×) when the animal was manually positioned and the angles of imaging were adjusted by moving the OCT camera.

Furthermore, in our experience, the use of the holder seems to reduce the movement artefacts from breathing; however, this was not formally assessed.

DISCUSSION

For in vivo ocular imaging, especially retinal OCT and fundus imaging, a beam path through the middle of the pupil with an orthogonal angle to the target structure (eg, the retina) in all planes is an essential prerequisite for optimal image quality and reproducibility in longitudinal assessments. During live imaging, this can be obtained by modifying the angle of the camera, of the animal or both. Cameras for retinal imaging are often heavy, and the design of camera holders allowing

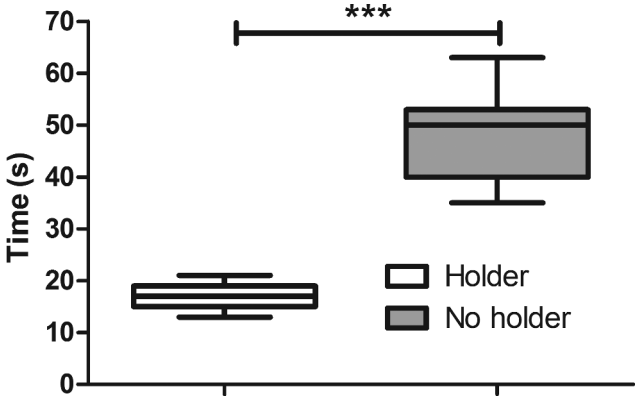

Figure 2 Time to adjust the mouse's optic disc in a centric position for optical coherence tomography imaging with and without the rodent holder. Boxes and whiskers represent the mean, SD and minimum to maximum of results obtained while imaging 11 independent eyes (***p >0.001, Student's t-test).

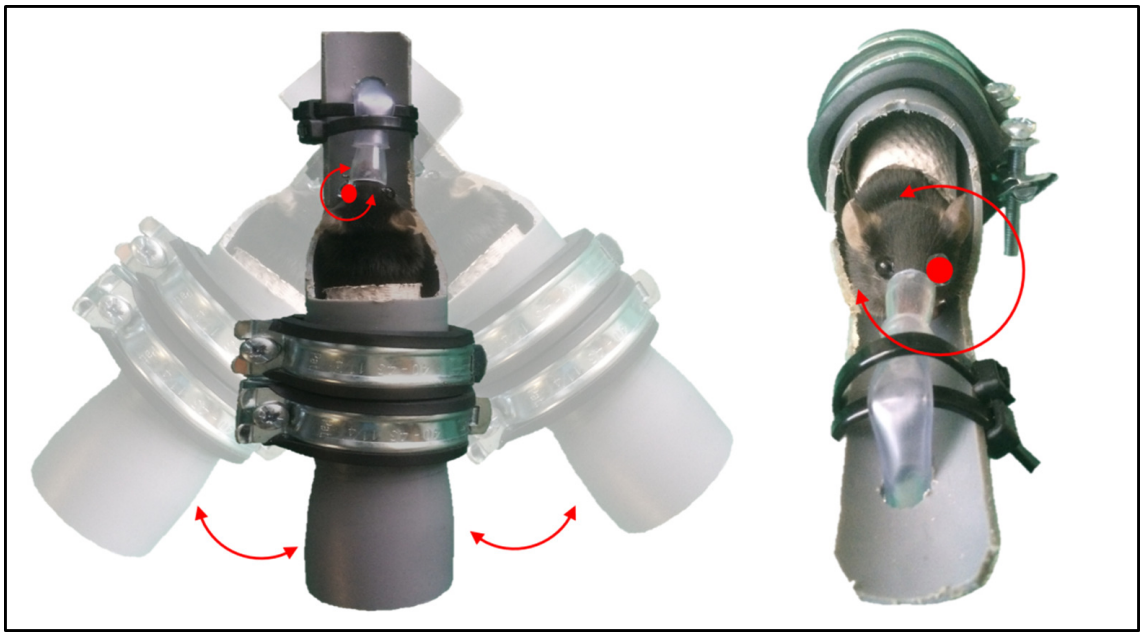

Figure 3 Rotational axis around the rodent eye. Rotation in transverse plane (left) and in axial plane (right).

movements in all planes and angles is challenging. Some OCT devices only allow movements in the vertical axis, so the adjustment of the angle as well as the horizontal and vertical axes has to be performed by moving the animal. An advantage of adjusting the beam-to-target angle by moving the animal is that the camera can be manoeuvred in the z-axis without changing the angle of imaging. This is not possible when the camera is moved from an angled position.

A remarkable strength of the proposed holder is that the rodent's eye is the centre of rotation for rotations in both the axial and transverse planes (figure 3). By adjusting the position of the mouth piece that tightly holds the rodent's head by the upper front teeth, which can be hooked over the bite bar, the eye can be positioned in the centre of the rotational pivot of the aluminium sheets and in the middle of the tube. Therefore, the beam-to-target angle can be adjusted by a manual rotation of the holder tube housing the animal. In most OCT systems, the camera can be moved along the visual axis of the camera to zoom into the eye and provide adjustments of the z-axis. Movements in the x-plane and y-plane can be performed using the pivot of the aluminium sheets of the holder, which is also slidable due to the rectangular excision at the end of the smaller aluminium sheet. If additional movements are needed (ie, if the camera cannot be moved in the z-axis), the holder can be fixed on a simple xyz table. Our experiments demonstrate that this reduces the time needed to find the correct angle in all planes compared with angling of the camera. Considering an average imaging time of 2 min for high-resolution volume scans per eye, the time benefit of 30 s corresponds to a reduction of time needed for imaging by 25%. However, we have to acknowledge that, with the experience and training, imaging can also be performed without the use of a holder by just placing the animals on a stable platform if the camera can be moved and rotated in all angles and planes and operators may become quicker in adjusting the animal with practice. Overall, in our experience, the use of the holder has largely facilitated rodent imaging, reducing acquisition times and served to avoid having to readjust the animals or repeat the measurements due to movement or dislocation of the animal.

Another advantage of the device is that it includes an option for volatile anaesthesia. The combination of fixation of the mouth using the bite bar and volatile anaesthesia serves to reduce breathing artefacts during image acquisition. Furthermore in our experience, volatile anaesthesia (eg, inhalant isoflurane) is safer and easier to control than injectable anaesthesia (eg, ketamine-–xylazine),[44 45] and serves to prevent premature awakening of rodents in case of longer acquisition times. This allows imaging for over 45 min, for example, for funduscopic imaging of fluorescence-labelled cells or complex OCT protocols. However, the combination of ketamine-–xylazine is also an effective anaesthesia method for small laboratory animals[23 34] and in our experience, we have never encountered cataracts or corneal alterations during the first anaesthesia when performing OCT imaging. The method is safe, especially when using low dosages of xylazine (5 mg/kg).

We acknowledge that our holder does show resemblance to other commercially available options. This is owing to the fact that there are only a few ways to design a holder, which allows pivotal rotation of the rodent in two planes with the eye as centre of rotation. Our aim was not to develop an entirely new concept but rather to provide a do-it-yourself guide for researchers to construct a very cost-efficient yet fully functional holder. This will be of greatest help not only

for research groups beginning mouse retinal imaging but also for groups planning to extend their species of interest from mice to rats. Of note, the proposed guide has been developed over a period of 12 months while performing more than 2000 retinal imaging sessions on rodents. During this period, several adaptations have been evaluated iteratively. Options such as stereotactic holders fixing the mice at the mouth or ears have proven to have no advantage in our hands over the proposed breathing mask with the bite bar and were therefore discarded. In our experience, the holder outperforms commercial options, which are available for more than 10 times the price.

A limitation of the proposed holder is that the rotations are performed manually instead of controlled dials, which may reduce the precision of very fine adjustments. In our experience, however, the movements needed for setting the angle for OCT and fundus imaging are not too delicate and can be performed manually at a sufficiently high precision. Furthermore, the proposed guide is not intended as a rigid instruction manual but rather as a prototype for researchers to introduce further refinements, including using higher quality materials, according to their specific needs and interests.

CONCLUSION

In conclusion, we present a do-it-yourself guide for a highly functional and effective rodent holder using materials that are both easily available and very affordable. Using the device speeds up OCT and fundus imaging in rodents and enables inhalation anaesthesia. Together, this increases the throughput and reduces the recovery time from anaesthesia. We believe this guide could be very useful for eye researchers aiming to establish retinal imaging in rodents at their laboratories.

Contributors MD made substantial contributions to the conception and design of the holder, acquisition of data as well as analysis and interpretation of data; he has been involved in drafting and writing the manuscript. AC-H and HY made substantial contributions to the conception and design of the holder and have been involved in drafting the manuscript. AB and HPH have been involved in revising the manuscript critically for important intellectual content and made substantial contributions to the interpretation of data. OA has been involved in revising the manuscript critically for important intellectual content. AG made substantial contributions to the conception and design of the holder and has been involved in revising the manuscript critically for important intellectual content and made substantial contributions to the interpretation of data. PA made substantial contributions to conception and design of the holder, acquisition of data as well as analysis and interpretation of data; he has been involved in drafting and writing the manuscript, and has given final approval of the version to be published and agreed to be accountable for all aspects of the work in ensuring that questions related to the accuracy or integrity of any part of the work are appropriately investigated and resolved.

Funding The rodent holder was developed and refined in the context of research projects that were funded by grants from Dr. Robert Pfleger Stiftung, Forschungskommission der Heinrich Heine University Düsseldorf, Novartis and Biogen to PA.

Competing interests None declared.

REFERENCES

1. Chalam KV, Sambhav K. Optical coherence tomography angiography in retinal diseases. *J Ophthalmic Vis Res* 2016;**11**:84–92.
2. Murthy RK, Haji S, Sambhav K, *et al*. Clinical applications of spectral domain optical coherence tomography in retinal diseases. *Biomed J* 2016;**39**:107–20.
3. Wojtkowski M, Kaluzny B, Zawadzki RJ. New directions in ophthalmic optical coherence tomography. *Optom Vis Sci* 2012;**89**:524–42.
4. Folgar FA, Jaffe GJ, Ying GS, *et al*; Comparison of Age-Related Macular Degeneration Treatments Trials Research Group. Comparison of optical coherence tomography assessments in the comparison of age-related macular degeneration treatments trials. *Ophthalmology* 2014;**121**:1956–65.
5. Mowatt G, Hernández R, Castillo M, *et al*. Optical coherence tomography for the diagnosis, monitoring and guiding of treatment for neovascular age-related macular degeneration: a systematic review and economic evaluation. *Health Technol Assess* 2014;**18**:1–254.
6. Schlanitz FG, Sacu S, Baumann B, *et al*. Identification of drusen characteristics in age-related macular degeneration by polarization-sensitive optical coherence tomography. *Am J Ophthalmol* 2015;**160**:335–44. e1.
7. Makiyama Y, Oishi A, Otani A, *et al*. Prevalence and spatial distribution of cystoid spaces in retinitis pigmentosa: investigation with spectral domain optical coherence tomography. *Retina* 2014;**34**:981–8.
8. Al Rashaed S, Khan AO, Nowilaty SR, *et al*. Spectral-domain optical coherence tomography reveals prelaminar membranes in optic nerve head pallor in eyes with retinitis pigmentosa. *Graefes Arch Clin Exp Ophthalmol* 2016;**254**:77–81.
9. Albrecht P, Blasberg C, Lukas S, *et al*. Retinal pathology in idiopathic moyamoya angiopathy detected by optical coherence tomography. *Neurology* 2015;**85**:521–7.
10. Albrecht P, Fröhlich R, Hartung HP, *et al*. Optical coherence tomography measures axonal loss in multiple sclerosis independently of optic neuritis. *J Neurol* 2007;**254**:1595–6.
11. Albrecht P, Müller AK, Südmeyer M, *et al*. Optical coherence tomography in parkinsonian syndromes. *PLoS One* 2012;**7**:e34891.
12. Albrecht P, Müller AK, Ringelstein M, *et al*. Retinal neurodegeneration in Wilson's disease revealed by spectral domain optical coherence tomography. *PLoS One* 2012;**7**:e49825.
13. Albrecht P, Ringelstein M, Müller AK, *et al*. Degeneration of retinal layers in multiple sclerosis subtypes quantified by optical coherence tomography. *Mult Scler* 2012;**18**:1422–9.
14. Ringelstein M, Albrecht P, Südmeyer M, *et al*. Subtle retinal pathology in amyotrophic lateral sclerosis. *Ann Clin Transl Neurol* 2014;**1**:290–7.
15. Ringelstein M, Albrecht P, Kleffner I, *et al*. Retinal pathology in Susac syndrome detected by spectral-domain optical coherence tomography. *Neurology* 2015;**85**:610–8.
16. Bhaduri B, Nolan RM, Shelton RL, *et al*. Detection of retinal blood vessel changes in multiple sclerosis with optical coherence tomography. *Biomed Opt Express* 2016;**7**:2321–30.
17. Satue M, Rodrigo MJ, Otin S, *et al*. Relationship between visual dysfunction and retinal changes in patients with multiple sclerosis. *PLoS One* 2016;**11**:e0157293.
18. Thomson KL, Yeo JM, Waddell B, *et al*. A systematic review and meta-analysis of retinal nerve fiber layer change in dementia, using optical coherence tomography. *Alzheimers Dement* 2015;**1**:136–43.
19. Knier B, Berthele A, Buck D, *et al*. Optical coherence tomography indicates disease activity prior to clinical onset of central nervous system demyelination. *Mult Scler* 2016;**22**:893–900.
20. Raftopoulos RE, Kapoor R. Neuroprotection for acute optic neuritis-Can it work? *Mult Scler Relat Disord* 2013;**2**:307–11.
21. Sühs KW, Hein K, Sättler MB, *et al*. A randomized, double-blind, phase 2 study of erythropoietin in optic neuritis. *Ann Neurol* 2012;**72**:199–210.

22. Salari M, Janghorbani M, Etemadifar M, *et al*. Effects of vitamin D on retinal nerve fiber layer in vitamin D deficient patients with optic neuritis: preliminary findings of a randomized, placebo-controlled trial. *J Res Med Sci* 2015;**20**:372–8.
23. Groh J, Stadler D, Buttmann M, *et al*. Non-invasive assessment of retinal alterations in mouse models of infantile and juvenile neuronal ceroid lipofuscinosis by spectral domain optical coherence tomography. *Acta Neuropathol Commun* 2014;**2**:54.
24. Knier B, Rothhammer V, Heink S, *et al*. Neutralizing IL-17 protects the optic nerve from autoimmune pathology and prevents retinal nerve fiber layer atrophy during experimental autoimmune encephalomyelitis. *J Autoimmun* 2015;**56**:34–44.
25. Berger A, Cavallero S, Dominguez E, *et al*. Spectral-domain optical coherence tomography of the rodent eye: highlighting layers of the outer retina using signal averaging and comparison with histology. *PLoS One* 2014;**9**:e96494.
26. Hein K, Gadjanski I, Kretzschmar B, *et al*. An optical coherence tomography study on degeneration of retinal nerve fiber layer in rats with autoimmune optic neuritis. *Invest Ophthalmol Vis Sci* 2012;**53**:157–63.
27. Hariri S, Moayed AA, Choh V, *et al*. In vivo assessment of thickness and reflectivity in a rat outer retinal degeneration model with ultrahigh resolution optical coherence tomography. *Invest Ophthalmol Vis Sci* 2012;**53**:1982–9.
28. Shariati MA, Park JH, Liao YJ. Optical coherence tomography study of retinal changes in normal aging and after ischemia. *Invest Ophthalmol Vis Sci* 2015;**56**:2790–7.
29. Baran U, Zhu W, Choi WJ, *et al*. Automated segmentation and enhancement of optical coherence tomography-acquired images of rodent brain. *J Neurosci Methods* 2016;**270**:132–7.
30. Baumann B, Rauscher S, Glösmann M, *et al*. Peripapillary rat sclera investigated in vivo with polarization-sensitive optical coherence tomography. *Invest Ophthalmol Vis Sci* 2014;**55**:7686–96.
31. Jian Y, Zawadzki RJ, Sarunic MV. Adaptive optics optical coherence tomography for in vivo mouse retinal imaging. *J Biomed Opt* 2013;**18**:56007.
32. Zawadzki RJ, Zhang P, Zam A, *et al*. Adaptive-optics SLO imaging combined with widefield OCT and SLO enables precise 3D localization of fluorescent cells in the mouse retina. *Biomed Opt Express* 2015;**6**:2191–210.
33. Zhang P, Zam A, Jian Y, *et al*. In vivo wide-field multispectral scanning laser ophthalmoscopy-optical coherence tomography mouse retinal imager: longitudinal imaging of ganglion cells, microglia, and Müller glia, and mapping of the mouse retinal and choroidal vasculature. *J Biomed Opt* 2015;**20**:126005.
34. Fischer MD, Huber G, Beck SC, *et al*. Noninvasive, in vivo assessment of mouse retinal structure using optical coherence tomography. *PLoS One* 2009;**4**:e7507.
35. Hammer DX, Ferguson RD, Mujat M, *et al*. Multimodal adaptive optics retinal imager: design and performance. *J Opt Soc Am A Opt Image Sci Vis* 2012;**29**:2598–607.
36. Kim KH, Puoris'haag M, Maguluri GN, *et al*. Monitoring mouse retinal degeneration with high-resolution spectral-domain optical coherence tomography. *J Vis* 2008;**817**:1–11.
37. Seeliger MW, Beck SC, Pereyra-Muþoz N, *et al*. In vivo confocal imaging of the retina in animal models using scanning laser ophthalmoscopy. *Vision Res* 2005;**45**:3512–9.
38. Gabriele ML, Ishikawa H, Schuman JS, *et al*. Reproducibility of spectral-domain optical coherence tomography total retinal thickness measurements in mice. *Invest Ophthalmol Vis Sci* 2010;**51**:6519–23.
39. Kocaoglu OP, Uhlhorn SR, Hernandez E, *et al*. Simultaneous fundus imaging and optical coherence tomography of the mouse retina. *Invest Ophthalmol Vis Sci* 2007;**48**:1283–9.
40. Pennesi ME, Michaels KV, Magee SS, *et al*. Long-term characterization of retinal degeneration in rd1 and rd10 mice using spectral domain optical coherence tomography. *Invest Ophthalmol Vis Sci* 2012;**53**:4644–56.
41. Song W, Wei Q, Jiao S, *et al*. Integrated photoacoustic ophthalmoscopy and spectral-domain optical coherence tomography. *J Vis Exp* 2013;**15**:e4390.
42. Galichanin K, Wang J, Löfgren S, *et al*. A new universal rat restrainer for ophthalmic research. *Acta Ophthalmol* 2011;**89**:e67–71.
43. Maurice DM, Singh T. An improved method for restraining rabbits for examination of the eye. *Invest Ophthalmol Vis Sci* 1984;**25**:1220–1.
44. Calderone L, Grimes P, Shalev M. Acute reversible cataract induced by xylazine and by ketamine-xylazine anesthesia in rats and mice. *Exp Eye Res* 1986;**42**:331–7.
45. Szczesny G, Veihelmann A, Massberg S, *et al*. Long-term anaesthesia using inhalatory isoflurane in different strains of mice–the haemodynamic effects. *Lab Anim* 2004;**38**:64–9.

Using optical coherence tomography and optokinetic response as structural and functional visual system readouts in mice and rats

Michael Dietrich[1], Christina Hecker[1], Alexander Hilla[2], Andrés Cruz-Herranz[3], Hans-Peter Hartung[1], Dietmar Fischer[2], Ari Green[3], Philipp Albrecht[1]

[1]Department of Neurology, Heinrich-Heine-University Düsseldorf, Germany
[2]Department of Cell Physiology, Faculty of Biology and Biotechnology, Ruhr-University Bochum, Germany
[3]Division of Neuroinflammation and Glial Biology, Department of Neurology, University of California San Francisco, United States

The presented manuscript was published in the “Journal of Visualized Experiments”, 2018.

Contribution:
-First authorship
-Design of the study, experiments, protocols and video script (80%)
-Implementing and establishing EAE- and OKR-methodology in the laboratory (70%)
-Video shooting (80%)
-Execution, analysis and statistics of the EAE experiments (including retinal histology), OCT and OKR measurements (90%)
-Writing and drafting of the manuscript (80%)

Video Article

Using Optical Coherence Tomography and Optokinetic Response As Structural and Functional Visual System Readouts in Mice and Rats

Michael Dietrich[1], Christina Hecker[1], Alexander Hilla[2], Andrés Cruz-Herranz[3], Hans-Peter Hartung[1], Dietmar Fischer[2], Ari Green[3], Philipp Albrecht[1]

[1]Department of Neurology, Heinrich-Heine-University Düsseldorf

[2]Department of Cell Physiology, Faculty of Biology and Biotechnology, Ruhr-University Bochum

[3]Division of Neuroinflammation and Glial Biology, Department of Neurology, University of California San Francisco

Correspondence to: Philipp Albrecht at phil.albrecht@gmail.com

URL: https://www.jove.com/video/58571
DOI: doi:10.3791/58571

Keywords: Neuroscience, Issue 143, Optical coherence tomography, optokinetic response, ocular imaging, visual pathway, holder, rodent models

Date Published: 1/10/2019

Citation: Dietrich, M., Hecker, C., Hilla, A., Cruz-Herranz, A., Hartung, H.P., Fischer, D., Green, A., Albrecht, P. Using Optical Coherence Tomography and Optokinetic Response As Structural and Functional Visual System Readouts in Mice and Rats. *J. Vis. Exp.* (143), e58571, doi:10.3791/58571 (2019).

Abstract

Optical coherence tomography (OCT) is a fast, non-invasive, interferometric technique allowing high-resolution retinal imaging. It is an ideal tool for the investigation of processes of neurodegeneration, neuroprotection and neuro-repair involving the visual system, as these often correlate well with retinal changes. As a functional readout, visually evoked compensatory eye and head movements are commonly used in experimental models involving the visual function. Combining both techniques allows a quantitative in vivo investigation of structure and function, which can be used to investigate the pathological conditions or to evaluate the potential of novel therapeutics. A great benefit of the presented techniques is the possibility to perform longitudinal analyses allowing the investigation of dynamic processes, reducing variability and cuts down the number of animals needed for the experiments. The protocol described aims to provide a manual for acquisition and analysis of high quality retinal scans of mice and rats using a low cost customized holder with an option to deliver inhalational anesthesia. Additionally, the proposed guide is intended as an instructional manual for researchers using optokinetic response (OKR) analysis in rodents, which can be adapted to their specific needs and interests.

Video Link

The video component of this article can be found at https://www.jove.com/video/58571/

Introduction

The examination of the visual pathway, as a part of the central nervous system, has been proven to be an effective starting point in addressing not only ophthalmologic[1,2,3,4,5], but also neurologic[6,7,8,9,10,11,12,13,14,15,16] questions. In recent years, OCT and OKR have been identified as useful analytic, non-invasive tools to evaluate a large variety of retinopathies and retinal manifestations in various rodent models[17,18,19,20,21,22,23,24,25]. OCT allows for fast and high resolution *in vivo* visualization of the retinal morphology and structure in mice and rats, with results in good accordance with histological sections of the animals retinae[26]. OKR constitutes a fast and robust method to quantitatively assess visual function.

Many OCT devices allow simultaneous confocal scanning laser ophthalmoscopy (cSLO) imaging with different wavelengths, which provides diagnostic information about retinal pathologies, i.e., visualization of lipofuscin deposits or alterations of the retinal pigment epithelium[27]. Furthermore, *in vivo* imaging of fluorescence labelled cells in transgenic animals is possible[28,29,30,31,32]. However, the application of OCT technology in rodent models is still challenging, mainly because of the small eye size. Several commercially available devices require adaptations and often a different size of holder is required to image the animals of different species. Additionally, animals require anesthesia for measurement.

OKR devices can be used to assess the visual function in rodents. The animals are placed on a platform in the center of an actual or virtual cylinder displaying a moving grating, which the animals track with reflexive head and neck movements. This optokinetic response is reduced or eliminated in the case of the reduction or loss of visual function.

The aim of this protocol is to present a manual for the measurement of retinal thickness using a commercially available OCT device with a custom holder providing inhalant anesthesia. The protocol illustrates how to analyze volume scans using the software provided by the manufacturer. For visual testing, the aim is to provide instructions on how to use a commercially available system to assess the OKR.

Protocol

All animal procedures were performed in compliance with the experimental guidelines approved by the regional authorities (State Agency for Nature, Environment and Consumer Protection; reference number 84-02.04.2014.A059) and conform to the Association for Research in Vision

and Ophthalmology (ARVO) Statement for the Use of Animals in Ophthalmic and Vision Research and the European directive 2010/63/EU on the protection of animals used for scientific purposes.

1. Confocal Scanning Laser Ophthalmoscopy-optical Coherence Tomography

NOTE: The protocol for cSLO-OCT measurement is adaptable for all strains of laboratory mice and rats.

1. Set-up and pre-imaging preparations
   NOTE: The system configuration of the OCT device used in this protocol has already been described elsewhere[31].
2. **Rodent preparation for inhalant anesthesia**
   1. Place the rodent in an induction chamber and set the vaporizer to an isoflurane concentration of 2% at 2 L/min O_2.
   2. Check if the rodent is anesthetized by pinching the tail, remove it from the chamber and wrap it in paper towel to keep it warm.
   3. Place the rodent in the custom holder[33] and hook the maxillary incisors on the integrated bite bar of the mouth piece, connected to the vaporizer (2.5% isoflurane at 2 L/min O_2).
   4. Apply one drop of Phenylephrine 2.5%-Tropicamide 0.5% on each eye for pupillary dilation.
   5. Wipe off any excess liquid of eye drops after 1 min and lubricate the eyes with methyl-cellulose based ophthalmic gel (e.g., hypromellose 0.3% eye drops) to avoid drying out and turbidity of the cornea.
   6. Place custom contact lens (+4 diopters) on the mouse eye by hand or using forceps. Cover the rat eye with a glass plate (e.g., round 12 mm diameter glass coverslip) without optical properties to assure a plane surface.
      NOTE: Monitor respiratory rate during anesthesia. Increase or decrease Isoflurane concentration if required.

3. **Measurement and analysis**
   NOTE: Make sure to perform and report the OCT measurements in line with the APOSTEL recommendations[34] and perform quality control according to the OSCAR-IB consensus criteria[35]. As these recommendations have been developed for human OCT images, some criteria are not or only partially applicable.
   1. To image the left eye, position the holder as presented in **Figure 1A** to ensure that the left eye bulb of the rodent faces the camera.
   2. Press the **Start** button in the right corner of the control panel display to start the acquisition mode.
   3. Set the filter lever to **R** and select **BR+OCT** for **Blue reflectance** fundus imaging and B-scan acquisition on the control panel.
   4. Set the focus distance to approx. 38 diopters using the focus knob on the back of the camera and zoom in on the retina until the OCT scan is visible on the screen.
      NOTE: At the first measurement, the reference arm has to be adapted for rodent measurement. Press the combination Ctrl+Alt+Shift +O and adjust the value of the reference arm in the open window until the OCT-scan appears on the screen.
   5. To ensure a beam path through the middle of the pupil with an orthogonal angle to the retina in all planes, position the optic disc in the middle of the illuminated field (BR) and adjust the horizontal and vertical line B-scans to a horizontal level by rotating/turning the holder (**Figure 1B**) or moving the camera.
   6. Select the volume scan mode and set it to 25 B-scans in high-resolution mode at 50 automatic real-time tracking (ART, rasterized from 50 averaged A-Scans) on the software screen.
   7. Center the middle of the volume scan grid on the optic disc and start acquisition by pressing the black sensitivity knob and then **AQUIRE** on the control panel.
   8. Set the filter lever to **A**, select **Blue Auto Florescence** (BAF) on the control panel and adjust image brightness with the sensitivity knob. Press the sensitivity knob and then **AQUIRE** to image fluorescent cells (e.g., EGFP) or auto fluorescent deposits.
   9. Apply ophthalmic gel on the eye of the rodent to prevent dehydration and put the animal in a separate cage with a heat source.
   10. Supervise the rodent until it is fully recovered from anesthesia, in a separate cage and individually housed. When the animal is ambulatory, return it to the home cage.
   11. For analysis of the volume scans, use the automated segmentation of the OCT device's software by right-clicking on the scan and select **Segmentation** then **All Layers**. Make sure that the quality of the OCT images is sufficient and define quality cutoffs for each set of experiments, *e.g.*, >20 decibels.
   12. Perform manual correction of the layers by double clicking on the desired scan, select **Thickness Profile** and click on **Edit Layer Segmentations**. Select one layer, e.g., press ILM for **Inner limiting membrane**, and, if necessary, correct the green line by moving the red dots by drag and drop to the correct position.
       NOTE: Make sure the investigator performing the manual correction is blinded for the experimental groups.
   13. Select the tab **Thickness Map** and choose the **1, 2, 3 mm** early treatment of diabetic retinopathy study (ETDRS) grid. Center the inner circle on the optic disc (**Figure 2**, left).
   14. Calculate the thickness of retinal layers from the thickness values provided by the software for the different retinal sectors of interest. To compute the mean thickness values from volume scans, use the whole 1, 2, 3 mm ETDRS grid, which covers an angle of approximately 25°, excluding the inner 1 mm circle, which contains the optic disc (**Figure 2**, right).
   15. Perform the statistical analysis using adequate software. If both eyes of an animal are included, consider a statistical model accounting for within subject inter-eye correlations (e.g., generalized estimating equations or mixed linear models), as the eyes of one subject are statistically dependent[36].

2. Optokinetic Response

NOTE: In the following, a detailed manual for OKR measurements of mice and rats is provided, which can be adapted to individual specific needs.

1. **Set-up and pre-measurement preparations**
   1. Turn on the computer. After the system has booted, turn on the screens of the testing chamber as described in more detail elsewhere[37].

2. Select a suitable platform for the measurement of mice or rats.
   NOTE: The platform size is selected based on the body size of the rodent. The animal should be able to sit properly on the platform without the ability to walk around.
3. Open the pre-settings window by double-clicking on the software, select **New group** and choose the group name, the number of subjects, the species and strains. Select a variable stimulus: spatial/temporal frequency, contrast sensitivity, speed or orientation in the drop-down menu, then press **Create New Group**.
4. Focus on the platform by manipulating the focus ring of the camera on top of the chamber and calibrate the system by aligning (drag and drop) the red circle around the black circle on the platform.

2. **Measurement and analysis**
   1. Place the animal on the platform, let it adapt to the environment for ~5 min. Lift the animal back on platform if it drops (**Figure 3A**).
   2. Select **Subject** number and **Condition** on the top right corner of the software screen (**Figure 3B**). One stimulus is variable, the other stimuli are kept constant. This is confirmed by the **Open lock** or **Closed lock** symbol next to the stimulus.
   3. Start measurement by selecting ◄ for **Yes** or ■ for **No**, if the animal tracks or does not track, respectively.
      NOTE: Clockwise tracking corresponds to the left and counterclockwise tracking to the right eye. The software randomly changes the direction of the moving grid.
   4. Select the step size of the stimulus manually by clicking on the **Up** and **Down** arrows next to the variable stimulus or let it adapt automatically by the software if stimulus threshold converges.
   5. For optimal results, animate the animal, e.g., by high whistling sounds and blanking, by clicking the black or white box symbol on the software screen. Perform these actions repeatedly in the case of prolonged measurements.
   6. For data analysis, select the **Summary** tab and click on **File** | **Export Table/Graph** to export the desired data set.
   7. Perform the statistical analysis using the desired software (see also Step 1.3.15).

Representative Results

Using 3rd generation OCT imaging in myelin oligodendrocyte glycoprotein (MOG) peptide induced experimental autoimmune encephalomyelitis (EAE) mouse models, high-resolution morphological sections of the mouse retina were obtained. Using this technology, the protective capacities of different substances were demonstrated[17]. The thickness values of the inner retinal layers (IRL) obtained are in good accordance with the numbers of retinal ganglion cells (RGC) obtained by histological staining of retinal wholemounts (**Figure 4**).

OKR monitoring provides a functional readout of the neurodegeneration seen by OCT. In these experiments, visual function assessed as spatial frequency by OKR, and neuroaxonal damage assessed as IRL thinning by OCT, were in close correlation[17]. Various protocols can be employed to examine the visual acuity by changing the spatial or temporal frequency, contrast sensitivity, orientation or speed of the moving grid. In the EAE model, an improved spatial frequency of 0.05 cycles/degree (c/d) of animals treated with substance 1 was detected compared to untreated MOG-EAE mice (**Figure 5**).

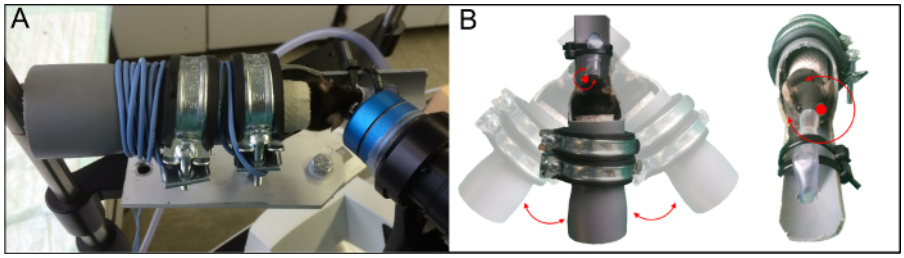

Figure 1: Custom holder for OCT measurement. (**A**) OCT imaging of a C57BL/6J mouse using the custom holder[33] and (**B**) rotational axis around the rodent eye. Rotation in the transverse plane (left) and in the axial plane (right) is demonstrated. This figure has been modified from Dietrich, M. et al.[33]. Please click here to view a larger version of this figure.

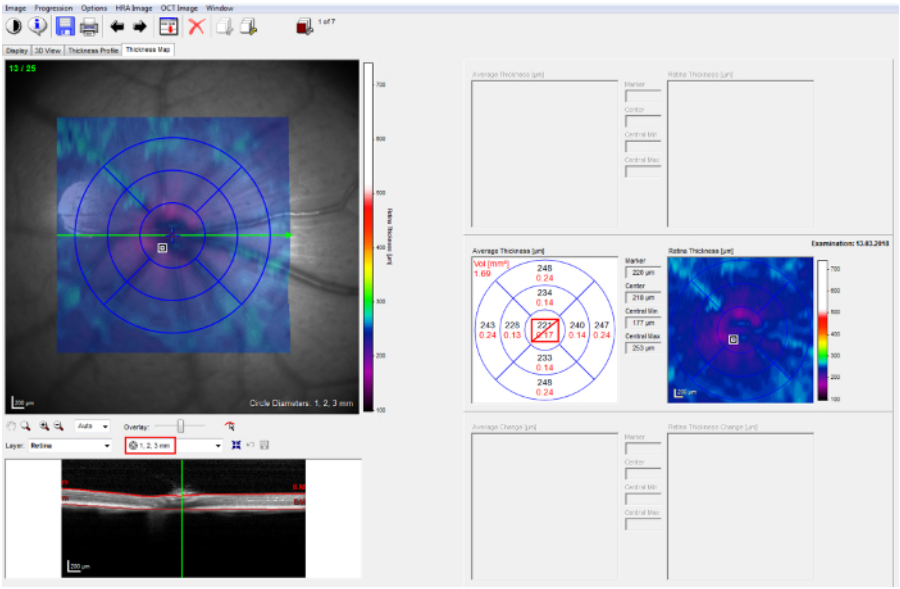

Figure 2: OCT post acquisition analysis. "1, 2, 3 mm" ETDRS grid on the 25 B-scan volume protocol (left). The thickness of retinal layers is provided for the different retinal sectors by the software (right). Please click here to view a larger version of this figure.

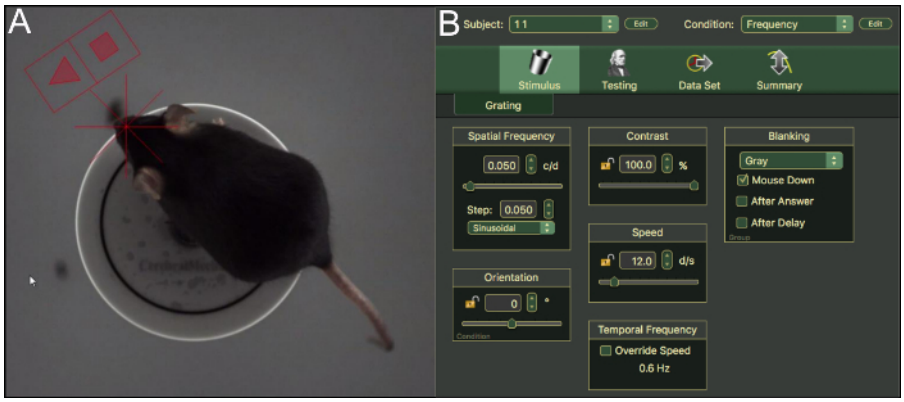

Figure 3: OKR measurement of mice and stimulus settings. (**A**) Top view through the camera analyzing a C57BL/6J mouse on the platform in the chamber. (**B**) User interface and settings of the OKR software. Please click here to view a larger version of this figure.

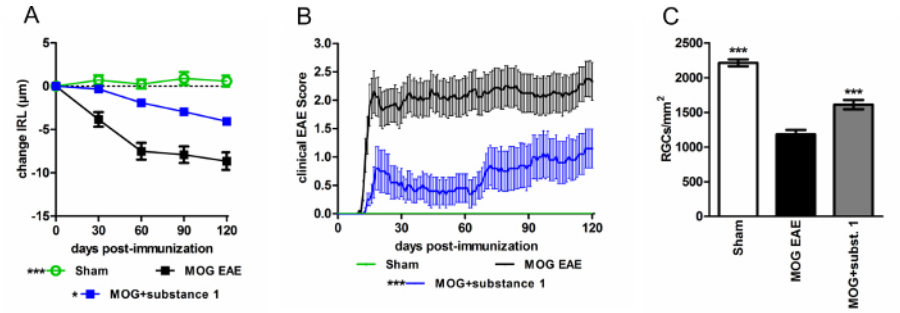

Figure 4: C57BL/6J mice with MOG EAE show an attenuated disease course when treated with substance 1 compared to untreated controls. (**A**) The degeneration of the inner retinal layers is reduced (**B**) and the clinical EAE score is attenuated during the EAE course when substance 1 was administered. Mice were scored daily, and OCT measurements were performed monthly over a period of 120 days. The graphs represent the mean and standard error of at least ten animals per group. (*$p < 0.05$, ***$p < 0.001$, area under the curve compared by ANOVA with Dunnett's post hoc test). (**C**) The IRL thickness change is in good accordance with RGC loss (***$p < 0.001$, by ANOVA with Dunnett's post hoc test compared to MOG untreated mice). Please click here to view a larger version of this figure.

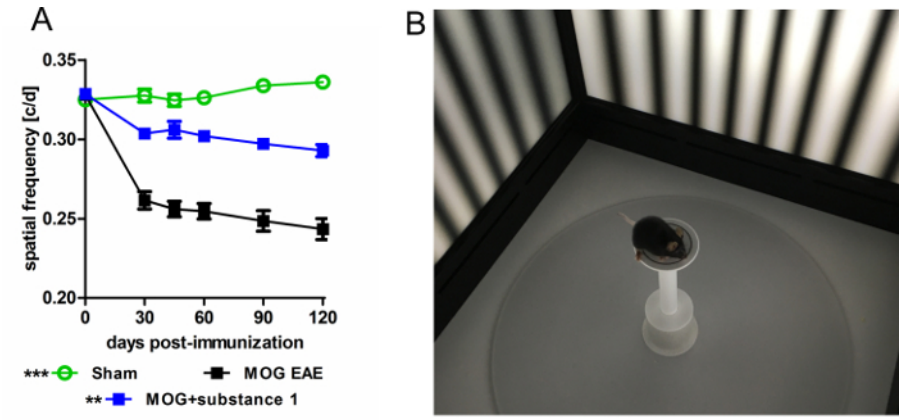

Figure 5: OKR measurement of C57BL/6J mice with MOG-EAE. (**A**) OKR reveals an improved visual acuity of animals treated with substance 1 compared to untreated MOG EAE mice measured by spatial frequency threshold testing over a period of 120 days. The graphs represent the mean and standard error of at least six animals per group (**p < 0.01, ***p < 0.001, area under the curve compared by ANOVA with Dunnett's post hoc test). (**B**) Image of a C57BL/6J mouse in the testing chamber. Please click here to view a larger version of this figure.

Discussion

This protocol provides an instruction for the thickness measurements and the examination of visual function in rodents. Visual readouts are increasingly used in translational research[18,26,38,39,40] and are easily transferable to clinical trials. The significant advantage of OCT in comparison to histological investigations in animal experiments is that longitudinal analyses are possible allowing the investigation of dynamic pathological processes, largely reducing the variability and the number of animals needed per study. Furthermore, in vivo imaging with OCT is not subject to fixation, cutting or staining artifacts, which may affect the layer thickness in histological investigations.

However, the orthogonal orientation of the laser beam in all planes in relation to the retina is a critical step to ensure the quality and reproducibility of the thickness values. It requires some training of the investigator and is mandatory before the acquisition of OCT scans. Additionally, as the commercial devices are built for human applications, the quality of rodent OCT images is still inferior compared to B-scans of human patients. In the authors' experience, it may be difficult to distinguish the different inner retinal layers (retinal nerve fiber layer, ganglion cell layer and inner plexiform layer) during manual correction. We therefore recommend analyzing these layers as a compound readout (IRL).

The experimental setup provides an option for volatile anesthesia, e.g., inhalant isoflurane, which is, in our experience, safer and easier to control than injectable anesthesia, e.g., ketamine-xylazine[41,42] and reduces the risk of premature awakening of rodents in case of longer acquisition times (e.g., when performing imaging of fluorescently labelled cells). In a preliminary study, volume scans were identified as the protocols with the highest validity and reliability. The inter-rater and test retest reliability was excellent when volume scans excluding the central part containing the optic disc were assessed with ICC (intra-class correlation coefficient) values above 0.85 for all assessments.

The measurement of the optokinetic response is based on the involuntary optokinetic reflex, which occurs in response to a continuously moving field. In rodents, in contrast to other species, the movement involves not only the eyes, but the whole head, which can easily be detected using the camera.

Distinguishing between "tracking" or normal behavioral movements of the animals requires some training of the investigator and it is important to be blinded for the experimental group. In addition, the animals need an adaption phase to accommodate to the experimental setting and during long-time measurement protocols, the animals have to be animated repeatedly to assure that "no tracking" is due to reaching the OKR threshold and not to decreasing attention. There is also a significant strain variability regarding the visual function of laboratory mice and rats[43,44]. The visual acuity of the rodent should therefore be evaluated before they are tested and some strains, such as SJL mice, may not even be suitable for OKR measurements, as they are homozygous for the allele Pde6brd1 (retinal degeneration 1).

In summary, the examination of retinal morphology and visual function in animal models allows for non-invasive, longitudinal investigations of structural and functional damage occurring in the context of EAE and may be helpful in other models involving the visual system, including but not limited to the models of retinopathies or optic nerve injury.

Disclosures

Unrelated to the work presented the authors declare the following financial disclosures:

Michael Dietrich received speaker honoraria from Novartis. Andrés Cruz-Herranz is a postdoctoral fellow of the National Multiple Sclerosis Society. Ari J. Green served on the scientific advisory board of MedImmune, Novartis, OCTIMS, Inception 5 Biosciences, and Bionure; is an associate editor of JAMA Neurology; was an editorial board member of Neurology; holds a patent for remyelination molecules and pathways; consulted for Inception 5 Sciences; received research support from Novartis Pharma OCTIMs, Inception Sciences SRA, NINDS, NIA, National MS Society, Sherak Foundation, and Hilton Foundation; holds stock or stock options in Inception 5; and served as an expert witness at Mylan v Teva Pharma. Hans-Peter Hartung has received fees for serving on steering committees from Biogen Idec, GeNeuro, Sanofi Genzyme, Merck, Novartis Pharmaceuticals, Octapharma, Opexa Therapeutics, Teva Pharmaceuticals, MedImmune, Bayer HealthCare, Forward Pharma, and Roche, fees for serving on advisory boards from Biogen Idec, Sanofi Genzyme, Merck, Novartis Pharmaceuticals, Octapharma, Opexa

Therapeutics, Teva Pharmaceuticals, and Roche, and lecture fees from Biogen Idec, Sanofi Genzyme, Merck, Novartis Pharmaceuticals, Octapharma, Opexa Therapeutics, Teva Pharmaceuticals, MedImmune, and Roche. Philipp Albrecht received compensation for serving on Scientific Advisory Boards for Ipsen, Novartis, Biogen; he received speaker honoraria and travel support from Novartis, Teva, Biogen, Merz Pharmaceuticals, Ipsen, Allergan, Bayer Healthcare, Esai, UCB and Glaxo Smith Kline; he received research support from Novartis, Biogen, Teva, Merz Pharmaceuticals, Ipsen, and Roche. The other authors report no disclosures.

Acknowledgements

This work was supported by grants of the Dr. Robert Pfleger-Foundation and the Ilselore Luckow-Foundation, as well as Biogen and Novartis to PA. Figure 1B was reproduced from "Whole-body positional manipulators for ocular imaging of anaesthetized mice and rats: A do-it-yourself guide. Dietrich, M., Cruz-Herranz, A., Yiu, H., Aktas, O., Brandt, A. U., Hartung, HP., Green, A., Albrecht, P. BMJ Open Ophthalmology. 1 (1), e000008, 2017" with permission from BMJ Publishing Group Ltd.

References

1. Folgar, F.A., Jaffe, G.J., Ying, G.-S., Maguire, M.G., Toth, C.A. Comparison of optical coherence tomography assessments in the comparison of age-related macular degeneration treatments trials. *Ophthalmology.* **121** (10), 1956-1965, (2014).
2. Mowatt, G. *et al.* Optical coherence tomography for the diagnosis, monitoring and guiding of treatment for neovascular age-related macular degeneration: a systematic review and economic evaluation. *Health Technology Assessment.* **18** (69), 1-254, (2014).
3. Schlanitz, F.G. *et al.* Identification of Drusen Characteristics in Age-Related Macular Degeneration by Polarization-Sensitive Optical Coherence Tomography. *American Journal of Ophthalmology.* **160** (2), 335-344.e1, (2015).
4. Makiyama, Y. *et al.* Prevalence and spatial distribution of cystoid spaces in retinitis pigmentosa: investigation with spectral domain optical coherence tomography. *Retina.* **34** (5), 981-988, (2014).
5. Al Rashaed, S., Khan, A.O., Nowilaty, S.R., Edward, D.P., Kozak, I. Spectral-domain optical coherence tomography reveals prelaminar membranes in optic nerve head pallor in eyes with retinitis pigmentosa. *Graefe's Archive for Clinical and Experimental Ophthalmology.* **22,** (2015).
6. Albrecht, P. *et al.* Retinal pathology in idiopathic moyamoya angiopathy detected by optical coherence tomography. *Neurology.* **85** (6), 521-527, (2015).
7. Albrecht, P., Fröhlich, R., Hartung, H.-P., Kieseier, B.C., Methner, A. Optical coherence tomography measures axonal loss in multiple sclerosis independently of optic neuritis. *Journal of Neurology.* **254** (11), 1595-1596, (2007).
8. Albrecht, P. *et al.* Retinal neurodegeneration in Wilson's disease revealed by spectral domain optical coherence tomography. *PLoS One.* **7** (11), e49825, (2012).
9. Albrecht, P. *et al.* Optical coherence tomography in parkinsonian syndromes. *PLoS One.* **7** (4), e34891, (2012).
10. Albrecht, P. *et al.* Degeneration of retinal layers in multiple sclerosis subtypes quantified by optical coherence tomography. *Multiple Sclerosis Journal.* **18** (10), 1422-1429, (2012).
11. Bhaduri, B. *et al.* Detection of retinal blood vessel changes in multiple sclerosis with optical coherence tomography. *Biomedical Optics Express.* **7** (6), 2321-2330, (2016).
12. Knier, B. *et al.* Optical coherence tomography indicates disease activity prior to clinical onset of central nervous system demyelination. *Multiple Sclerosis Journal.* **22** (7), 893-900, (2016).
13. Ringelstein, M. *et al.* Subtle retinal pathology in amyotrophic lateral sclerosis. *Annals of Clinical and Translational Neurology.* **1** (4), 290-297, (2014).
14. Ringelstein, M. *et al.* Retinal pathology in Susac syndrome detected by spectral-domain optical coherence tomography. *Neurology.* **85** (7), 610-618, (2015).
15. Satue, M. *et al.* Relationship between Visual Dysfunction and Retinal Changes in Patients with Multiple Sclerosis. *PLoS One.* **11** (6), e0157293, (2016).
16. Thomson, K.L., Yeo, J.M., Waddell, B., Cameron, J.R., Pal, S. A systematic review and meta-analysis of retinal nerve fiber layer change in dementia, using optical coherence tomography. *Alzheimer's & Dementia.* **1** (2), 136-143, (2015).
17. Dietrich, M. *et al.* Early alpha-lipoic acid therapy protects from degeneration of the inner retinal layers and vision loss in an experimental autoimmune encephalomyelitis-optic neuritis model. *Journal of Neuroinflammation.* **15** (1), 71, (2018).
18. Knier, B. *et al.* Neutralizing IL-17 protects the optic nerve from autoimmune pathology and prevents retinal nerve fiber layer atrophy during experimental autoimmune encephalomyelitis. *Journal of Autoimmunity.* **56**, 34-44, (2014).
19. Augustin, M. *et al.* In Vivo Characterization of Spontaneous Retinal Neovascularization in the Mouse Eye by Multifunctional Optical Coherence Tomography. *Investigative Ophthalmology & Visual Science.* **59** (5), 2054-2068, (2018).
20. Tode, J. *et al.* Thermal Stimulation of the Retina Reduces Bruch's Membrane Thickness in Age Related Macular Degeneration Mouse Models. *Translational Vision Science & Technology.* **7** (3), 2, (2018).
21. Gabriele, M.L. *et al.* Optic nerve crush mice followed longitudinally with spectral domain optical coherence tomography. *Investigative Ophthalmology & Visual Science.* **52** (5), 2250-2254, (2011).
22. Carpenter, C.L., Kim, A.Y., Kashani, A.H. Normative Retinal Thicknesses in Common Animal Models of Eye Disease Using Spectral Domain Optical Coherence Tomography. *Advances in Experimental Medicine and Biology.* **1074**, 157-166, (2018).
23. Alam, N.M. *et al.* A mitochondrial therapeutic reverses visual decline in mouse models of diabetes. *Disease Models & Mechanisms.* **8** (7), 701-710, (2015).
24. Bricker-Anthony, C., Rex, T.S. Neurodegeneration and Vision Loss after Mild Blunt Trauma in the C57Bl/6 and DBA/2J Mouse. *PLoS One.* **10** (7), e0131921, (2015).
25. Segura, F. *et al.* Assessment of Visual and Chromatic Functions in a Rodent Model of Retinal Degeneration. *Investigative Ophthalmology & Visual Science.* **56** (11), 6275-6283, (2015).
26. Fischer, M.D. *et al.* Noninvasive, in vivo assessment of mouse retinal structure using optical coherence tomography. *PLoS One.* **4** (10), e7507, (2009).

27. Ward, M.E. *et al.* Individuals with progranulin haploinsufficiency exhibit features of neuronal ceroid lipofuscinosis. *Science Translational Medicine.* **9** (385), (2017).
28. Chauhan, B.C. *et al.* Longitudinal in vivo imaging of retinal ganglion cells and retinal thickness changes following optic nerve injury in mice. *PLoS One.* **7** (6), e40352, (2012).
29. Lidster, K. *et al.* Neuroprotection in a novel mouse model of multiple sclerosis. *PLoS One.* **8** (11), e79188, (2013).
30. Munguba, G.C. *et al.* Nerve fiber layer thinning lags retinal ganglion cell density following crush axonopathy. *Investigative Ophthalmology & Visual Science.* **55** (10), 6505-6513, (2014).
31. Kokona, D., Jovanovic, J., Ebneter, A., Zinkernagel, M.S. In Vivo Imaging of Cx3cr1gfp/gfp Reporter Mice with Spectral-domain Optical Coherence Tomography and Scanning Laser Ophthalmoscopy. *Journal of Visualized Experiments.* (129), (2017).
32. Leung, C. K. S. *et al.* In vivo imaging of murine retinal ganglion cells. *Journal of Neuroscience Methods.* **168** (2), 475-478, (2008).
33. Dietrich, M. *et al.* Whole-body positional manipulators for ocular imaging of anaesthetised mice and rats: A do-it-yourself guide. *BMJ Open Ophthalmology.* **1** (1), e000008, (2017).
34. Cruz-Herranz, A. *et al.* The APOSTEL recommendations for reporting quantitative optical coherence tomography studies. *Neurology.* **86** (24), 2303-2309, (2016).
35. Tewarie, P. *et al.* The OSCAR-IB consensus criteria for retinal OCT quality assessment. *PLoS One.* **7** (4), e34823, (2012).
36. Fan, Q., Teo, Y.-Y., Saw, S.-M. Application of advanced statistics in ophthalmology. *Investigative Ophthalmology & Visual Science.* **52** (9), 6059-6065, (2011).
37. Prusky, G.T., Alam, N.M., Beekman, S., Douglas, R.M. Rapid quantification of adult and developing mouse spatial vision using a virtual optomotor system. *Investigative Ophthalmology & Visual Science.* **45** (12), 4611-4616, (2004).
38. Groh, J., Stadler, D., Buttmann, M., Martini, R. Non-invasive assessment of retinal alterations in mouse models of infantile and juvenile neuronal ceroid lipofuscinosis by spectral domain optical coherence tomography. *Acta Neuropathologica Communications.* **2**, 54, (2014).
39. Seeliger, M.W. *et al.* In vivo confocal imaging of the retina in animal models using scanning laser ophthalmoscopy. *Vision Research.* **45** (28), 3512-3519, (2005).
40. Shindler, K.S., Guan, Y., Ventura, E., Bennett, J., Rostami, A. Retinal ganglion cell loss induced by acute optic neuritis in a relapsing model of multiple sclerosis. *Multiple Sclerosis Journal.* **12** (5), 526-532 (2006).
41. Calderone, L., Grimes, P., Shalev, M. Acute reversible cataract induced by xylazine and by ketamine-xylazine anesthesia in rats and mice. *Experimental Eye Research.* **42** (4), 331-337 (1986).
42. Szczesny, G., Veihelmann, A., Massberg, S., Nolte, D., Messmer, K. Long-term anaesthesia using inhalatory isoflurane in different strains of mice-the haemodynamic effects. *Zeitschrift für mikroskopisch-anatomische Forschung.* **38** (1), 64-69, (2004).
43. Prusky, G.T., Harker, K., Douglas, R.M., Whishaw, I.Q. Variation in visual acuity within pigmented, and between pigmented and albino rat strains. *Behavioural Brain Research.* **136** (2), 339-348, (2002).
44. Wong, A.A., Brown, R.E. Visual detection, pattern discrimination and visual acuity in 14 strains of mice. *Genes, Brain, and Behavior.* **5** (5), 389-403, (2006).

Monitoring of retinal changes with optical coherence tomography predicts neuronal loss in experimental autoimmune encephalomyelitis in the mouse

Michael Dietrich [2*], Andrés Cruz-Herranz[1*], Alexander M. Hilla[3], Hao H. Yiu[1], Marc H. Levin[4,5], Christina Hecker[2], Andrea Issberner[2], Angelika Hallenberger[6], Christian Cordano[1], Klaus Lehmann-Horn[7], Lisanne J. Balk[8], Orhan Aktas[2], Jens Ingwersen[2], Charlotte von Gall[6], Hans-Peter Hartung[2], Scott S. Zamvil[1,9], Dietmar Fischer[3], Philipp Albrecht[2*], Ari J. Green[1,4*]

1. Division of Neuroimmunology and Glial Biology, Department of Neurology, University of California San Francisco, San Francisco, United States
2. Department of Neurology, Medical Faculty, Heinrich-Heine University, Düsseldorf, Germany
3. Department of Cell Physiology, Faculty of Biology and Biotechnology, Ruhr-University Bochum, Bochum, Germany
4. Department of Ophthalmology, University of California San Francisco, San Francisco, United States
5. Department of Ophthalmology, Palo Alto Medical Foundation, Palo Alto, CA, United States
6. Institute of Anatomy II, Medical Faculty, Heinrich-Heine University, Düsseldorf, Germany
7. Department of Neurology, Klinikum rechts der Isar, Technische Universität München, Munich, Germany
8. Department of Neurology, Amsterdam UMC, Vrije Universiteit Amsterdam, Amsterdam, The Netherlands
9. Program in Immunology, University of California, San Francisco, San Francisco, United States

*Equally contributing first/senior authors

The presented manuscript was accepted for publication in the “Journal of Neuroinflammation” in September 2019.

Contribution:
-Shared first authorship
-Design of the study and experiments (40%)
-Execution, analysis and statistics of the following methods: OCT measurements (50%); OKR measurements (100%); EAE experiments: MOG EAE in C57Bl/6J mice (50%), MBP EAE in C57Bl/6J mice (90%), MOG EAE in 2D2^{TCR} mice (90%); histology of optic nerve (90%) and retina (50%); Electron microscopy of optic nerve (50%)
-Writing and drafting of the manuscript (50%)

Title: Monitoring retinal changes with optical coherence tomography predicts neuronal loss in experimental autoimmune encephalomyelitis

Authors: Michael Dietrich [2*], Andrés Cruz-Herranz[1*], Alexander M. Hilla[3], Hao H. Yiu[1], Marc H. Levin[4,5], Christina Hecker[2], Andrea Issberner[2], Angelika Hallenberger[6], Christian Cordano[1], Klaus Lehmann-Horn[7], Lisanne J. Balk[8], Orhan Aktas[2], Jens Ingwersen[2], Charlotte von Gall[6], Hans-Peter Hartung[2], Scott S. Zamvil[1,9], Dietmar Fischer[3], Philipp Albrecht[2*], Ari J. Green[1,4*]

1. Division of Neuroimmunology and Glial Biology, Department of Neurology, University of California San Francisco, San Francisco, United States
2. Department of Neurology, Medical Faculty, Heinrich-Heine University, Düsseldorf, Germany
3. Department of Cell Physiology, Faculty of Biology and Biotechnology, Ruhr-University Bochum, Bochum, Germany
4. Department of Ophthalmology, University of California San Francisco, San Francisco, United States
5. Department of Ophthalmology, Palo Alto Medical Foundation, Palo Alto, CA, United States
6. Institute of Anatomy II, Medical Faculty, Heinrich-Heine University, Düsseldorf, Germany
7. Department of Neurology, Klinikum rechts der Isar, Technische Universität München, Munich, Germany
8. Department of Neurology, Amsterdam UMC, Vrije Universiteit Amsterdam, Amsterdam, The Netherlands
9. Program in Immunology, University of California, San Francisco, San Francisco, United States

*Equally contributing first/ senior authors.

Corresponding authors: phil.albrecht@gmail.com, agreen@ucsf.edu

ABSTRACT

BACKGROUND: Retinal optical coherence tomography (OCT) is a clinical and research tool in multiple sclerosis, where it has shown significant retinal nerve fiber (RNFL) and ganglion cell (RGC) layer thinning, while postmortem studies have reported RGC loss. Although retinal pathology in experimental autoimmune encephalomyelitis (EAE) has been described, comparative OCT studies among EAE models are scarce. Furthermore, the best practices for the implementation of OCT in the EAE lab, especially with afoveate animals like rodents, remain undefined. We aimed to describe the dynamics of retinal injury in different mouse EAE models and outline the optimal experimental conditions, scan protocols, and analysis methods, comparing these to histology to confirm the pathological underpinnings.

METHODS: Using spectral-domain OCT, we analyzed the test-retest and the inter-rater reliability of volume, peripapillary, and combined horizontal and vertical line scans. We then monitored the thickness of the retinal layers in different EAE models: in wild-type (WT) C57Bl/6J mice immunized with myelin oligodendrocyte glycoprotein peptide (MOG_{35-55}) or with bovine myelin basic protein (MBP); in TCR^{2D2} mice immunized with MOG_{35-55}, and in SJL/J mice immunized with myelin proteolipid lipoprotein ($PLP_{139-151}$). Strain-matched control mice were sham-immunized. RGC density was counted on retinal flatmounts at the end of each experiment.

RESULTS: Volume scans centered on the optic disc showed the best reliability. Retinal changes during EAE were localized in the inner retinal layers (IRL, the combination of the RNFL and the ganglion cell plus the inner plexiform layers). In WT, MOG_{35-55} EAE, progressive thinning of IRL started rapidly after EAE onset, with 1/3 of total loss occurring during the initial 2 months. IRL thinning was associated with the degree of RGC loss and the severity of EAE. Sham-immunized SJL/J mice showed progressive IRL atrophy, which was accentuated in PLP-immunized mice. MOG_{35-55}-immunized TCR^{2D2} mice showed severe EAE and retinal thinning. MBP immunization led to very mild disease without significant retinopathy.

CONCLUSIONS: Retinal neuroaxonal damage develops quickly during EAE. Changes in retinal thickness mirror neuronal loss and clinical severity. Monitoring of the IRL thickness after immunization against MOG_{35-55} in C57Bl/6J mice seems the most convenient model to study retinal neurodegeneration in EAE.

Keywords: experimental autoimmune encephalomyelitis- experimental optic neuritis- optical coherence tomography- optokinetic response- multiple sclerosis- neurodegeneration

Introduction

Optic neuritis (ON) is an acute, inflammatory demyelinating disease of the optic nerve resulting in impairment of vision. Fifty percent of patients with multiple sclerosis (MS) experience ON during the course of the disease. In up to 20 percent of them, ON is the presenting feature of MS[1]. Optical coherence tomography (OCT) allows for non-invasive, reproducible imaging of the live retina and its non-myelinated axons, and serves as a potential biomarker for estimating the neuroaxonal loss in the central nervous system (CNS).

While no animal model can fully recapitulate all pathophysiological aspects involved in MS, some models have proven useful for shedding light on the pathogenic mechanisms underlying neuroinflammatory injury, as well as to test candidate therapeutics. The most commonly studied animal model of MS is murine experimental autoimmune encephalomyelitis (EAE), where mice develop varying degrees of optic neuritis, white matter injury, and ascending myelitis[2].

After immunization of SJL/J mice with $PLP_{139-151}$, Shindler et al. detected loss of retinal ganglion cells (RGC, the neurons whose axons form the optic nerve) at day 14, starting with a 43 percent reduction which increased to 50 percent by day 18. RGC loss was correlated with the severity of inflammation, suggesting that RGC loss in EAE is a direct consequence of optic neuritis[3]. In C57B1/6 mice, active immunization with myelin oligodendrocyte glycoprotein peptide (MOG_{35-55}) or adoptive transfer of MOG-specific T cells causes severe optic neuritis [4]. Because MOG expression is higher in the optic nerves than in the spinal cord, even suboptimal doses of MOG can induce experimental optic neuritis in the absence of clinically evident paraparesis in EAE[5]. The TCR^{2D2} mouse line has a MOG-specific T-cell receptor leading to severe clinical disability of immunized animals. While TCR^{2D2} mice can develop spontaneous ON more frequently than they develop spontaneous EAE, the use of pertussis toxin (PT) promotes higher, timely incidence of ON and EAE[6]. In this context, Guan et al. found that RGC loss occurred progressively, reaching 39 percent at day 16 after injection with PT[6]. Horstmann and colleagues studied the retinas and optic nerves of C57B1/6 mice 23 days after the induction of MOG_{35-55}-EAE [7]. In this study, the severity of cellular infiltration and demyelination of the optic nerve as assessed by chemical staining techniques (such as hematoxylin-eosin and luxol fast blue staining respectively), correlated with the clinical EAE score. In this setting, EAE led to an 18 percent loss of RGC although no change in thickness of any retinal layer could be identified by measuring retinal sections under the microscope likely because of artifacts induced by fixation and tissue preparation.

Although these in vivo models of experimental ON have proven potentially useful to study mechanisms of neurodegeneration and neuronal survival with an autoimmune reaction mediated by stimulating an adaptive immune response, they are mainly focused upon histological measures (either by staining or retrograde labeling of RGC). Most of these studies had short observational periods of 21 to 40 days after immunization and lacked longitudinal assessments for time tracking of cell injury and loss. Neurodegeneration, however, is a dynamic process. In recent years, the development of non-invasive, retinal imaging techniques for animal models, such as OCT, has helped shed light on the longitudinal neurodegenerative changes during neuroinflammation. This approach has, additionally, emerged as a platform for the preclinical screening of candidate

neuroprotective compounds in MS and other neuroinflammatory diseases[8,910].

Studies comparing anterior visual pathway pathology and in-vivo imaging characteristics of different EAE models are lacking. A detailed characterization of retinal injury in animals is essential as it can facilitate translational research employing experimental designs that are directly adaptable to human clinical trials. To date, the most appropriate animal model to study ON in EAE has not been defined. The utilization of spectral-domain (SD)-OCT in animal models has been constrained by technical and optical issues. To date, although different segmentation algorithms have been tested in volume scans[11], it is not apparent which OCT scanning protocol is most suitable to assess thickness changes of the retinal layers. Acceptable reproducibility and reliability have been reported using a custom made algorithm for automated segmentation of retinal layers in retinal volume scans from mice[12]. However, in 2D scans, the automatic segmentation of the different retinal layers in mice is often prone to errors. Thus, segmentation of retinal layers is conducted manually or semi-automatically with manual correction, a laborious task that can potentially introduce systematic errors (e.g., due to examiner subjectivity and fatigue bias). It is, therefore, crucial to assess the reproducibility of consecutive assessments and the inter-rater reliability to identify scan protocols associated with high validity and reliability.

This work aimed to describe the dynamics of retinal injury after acute ON in different mouse models of EAE and to define the optimal mouse model, experimental conditions and analysis methods for the assessment of neuroprotective therapies in EAE using OCT as a primary outcome measure.

Methods

Experimental design

As a first step, we investigated which OCT scanning protocols are associated with the best test-retest reliability for retinal layer measurements. We then ran a series of experiments aimed at determining the optimal duration and the ideal mouse model for studying retinal changes in EAE. We analyzed the dynamics of retinal injury after direct immunization against MOG_{35-55} and MBP in C57BL/6J mice, MOG_{35-55} EAE in TCR^{2D2} transgenic mice, and $PLP_{139-151}$ in SJL/J mice. We analyzed changes in retinal thickness as assessed by serial retinal OCT, using sham-immunized, age-matched female mice from the same strain and/or WT littermates for TCR^{2D2} transgenic mice as controls for each model.

Mice

We bred C57Bl/6J and TCR^{2D2} transgenic mice from parents purchased from the Jackson Laboratories (Bar Harbor, ME, USA). SJL/J mice were provided by S. S. Zamvil, University of California, San Francisco. We performed our experiments on female and male (for TCR^{2D2}) 8 to 10-week-old mice.

Anesthesia

Before imaging, mice were anesthetized by mask inhalation of isoflurane vaporized at concentrations of 1.5% (2 liters/min) and their pupils were dilated with 1% tropicamide ophthalmic solution (Akorn, Lake Forest, IL). Compared to the use of intraperitoneal (i.p.) injection of ketamine and xylazine, this approach has proved to be simpler and safer,

allowing for rapid induction and easy control of the depth of anesthesia, with a low percentage of complications[13]. Furthermore, this method avoids the xylazine-induced acute, reversible cataract in rodents[14].

Optical Coherence Tomography

We performed retinal imaging using Spectralis™ OCT (Heidelberg Engineering, Heidelberg, Germany). During the exams, mice were placed on a custom-made mouse restrainer allowing free rotation and alignment of the eye to ensure the retinal laser was properly centered on the optic nerve head[15]. SD-OCT imaging was performed with and without the help of the TruTrack™ eye tracker that uses the fundus image to achieve imaging, maintaining registration of the image to enhance fidelity brought with averaging and to reduce breathing artifacts. We adapted for the optical properties of the mouse eye by using a custom contact lens during the examination, along with hydroxypropyl methylcellulose 0.3% (GenTeal™ ophthalmic gel, Novartis, Basel, Switzerland) to keep the eye moist and to ensure refraction continuity. Furthermore, we altered the Spectralis™ hardware by adding a 78-diopter lens in front of the camera and by adjusting the length of the reference arm (an option of the Spectralis software). All scans were acquired with an initial focus distance of 42D followed by manual correction. For volume scans, retinal layer thicknesses were calculated using the ETDRS grid with diameters of 1, 2, and 3 mm centered on the optic disc. We calculated the thickness of each retinal layer by averaging each sector of the grid, excluding the center which corresponded to the optic nerve head. Each volume scan consisted of 49 B-Scans recorded in high-resolution mode at 100 ART (rasterized from 100 averaged A-scans). The current version of the software does not allow for the exclusion of the center in horizontal and vertical line scans, which we combined into a cross-line by averaging individual horizontal and vertical layer thicknesses. We corrected segmentation artifacts at the disc by drawing straight lines between its opposing borders (figure 1). For each experiment, OCT imaging was performed at the time points indicated in the results section.

Investigation of the test-retest and inter-rater reliability for retinal layer assessments

We performed volume, peripapillary ring, as well as horizontal and vertical line scans to analyze the thickness of each retinal layer in 10 C57BL/6J mice obtained from Jackson Laboratories (Bar Harbor, ME, USA). We assessed the repeatability of OCT acquisition by removing and replacing the subject mouse onto the mount after each completed scan program, repeating the imaging with and without the Spectralis follow-up function – which utilizes the Spectralis eye tracking function to register images during follow up scans. We assessed the quality scores (a measure of signal intensity) for each protocol and considered them acceptable if above 20 and excellent if above 30. Using automated segmentation by the Heidelberg Eye ExplorerTM software (version 1.7.1.0 with the 5.10 beta version of the segmentation algorithm) and subsequent manual correction of segmentation errors, we obtained the thickness of the retinal layers on each scan. Two independent investigators determined the segmented thicknesses of each OCT scan. We assessed the total retinal thickness, individual retinal layers, and the inner retinal layers (IRL), defined as the combination of the retinal nerve fiber layer (RNFL) and the ganglion cell and the inner plexiform layer (GCIPL)[16].

Optokinetic Response

The optokinetic response was assessed as a measure for the visual acuity with a testing chamber and the OptoMotry™ software from CerebralMechanics™ (Lethbridge, Canada). A detailed description of the device[17] and methodology[8] is given elsewhere. In brief, we positioned the mice on a platform surrounded by TFT monitors displaying a virtual cylinder of black gratings (100% contrast) rotating in varying directions and at different frequencies. The mice' head movements tracking the grating were evaluated by an investigator blinded for the experimental groups. The spatial threshold frequency at which tracking was no longer possible was determined as a measure of visual function.

Induction and clinical scoring of EAE

Direct immunization against MOG_{35-55} in C57Bl/6J and TCR^{2D2} mice: animals were immunized subcutaneously with 100 µg of MOG_{35-55} peptide (Genemed Synthesis, San Antonio, TX, USA) in complete Freund's adjuvant (CFA) containing 400 µg Mycobacterium tuberculosis (Mt) H37Ra (Difco Laboratories, Detroit, MI, USA). Mice received 200 ng PT (List Biological, Campbell, CA, USA) by i.p. injection at the time of and 48 hours post-immunization. Control mice were sham-immunized with phosphate-buffered saline in CFA and received the same PT dosage. Direct immunization against $PLP_{139-151}$ in SJL/J mice: SJL/J mice were injected with 100 µg $PLP_{139-151}$ in 400 µg CFA subcutaneous and 2 x 50 ng PT i.p. on days 0 and 2. Control mice were sham-immunized with phosphate buffer saline in CFA and received the same PT dosage. Direct immunization against MBP in C57Bl/6J mice: animals were immunized with 400 µg of bovine MBP (Sigma, Darmstadt, Germany), emulsified in 200 µl of CFA, supplemented with 4 mg of Mt H37Ra, both purchased from Difco and additional i.p. injections of 200 ng of PT (Sigma-Aldrich, Darmstadt, Germany) on days 0 and 2 after immunization. We recorded daily clinical scores, as detailed in table 1.

Table 1. EAE clinical severity scores

0	No signs of disease.
0.5	Mild tail paresis: tip of the tail is weak and/or mouse doesn't spin tail.
1	Obvious tail paresis or plegia.
1.5	When flipped on its back, the mouse doesn't turn instantly in ≥50% of the cases (this score can only be assigned when signs of tail weakness as described in 0.5 and 1 are present at the same time).
2	Mild signs of hind limb paresis, like abnormal or slow gait, abnormal posture of the posterior part of the body.
2.5	Obvious signs of hind limb paresis, like abnormal, slow and weak movements of one or both hind limbs.
3	Signs of hind limb plegia: drags one hind limb behind (if the limb is moved a little but it doesn't help the mouse to move, this will count as a 3).
3.5	Signs of hind limb plegia: drags both hind limbs behind (if the limbs are moved a little but it doesn't help the mouse to move, this will count as a 3.5).
4	Mild signs of quadriparesis (weakness of all 4 limbs), as described in 2-3.5 and signs of weakness of one or both front limbs, like reduced speed when pulling itself forward, inability to push its chest up from ground or reduced ability (shorter duration) to hold itself up against gravity on the edge of the cage.
4.5	Quadriplegia: can not or barely pull itself forward or hold itself on the edge of the cage (in this stage the mouse has to be monitored closely and has to be sacrificed before 24 hours if the condition doesn't improve).
5	Mouse found dead.

Post-acquisition analysis

Using automated segmentation by the Heidelberg Eye Explorer™ software (version 1.7.1.0 with the 5.10 beta version of the segmentation algorithm) and subsequent manual correction of segmentation errors, we obtained the thickness of the retinal layers on each scan. For volume scans, retinal layer thicknesses were calculated using the early treatment of diabetic retinopathy (ETDRS) study grid (1, 2, 3 mm) centered on the optic disc (figure 1). We calculated the thickness of each retinal layer by averaging each sector of the grid, excluding the center which corresponded to the optic nerve head. In line scans, we corrected segmentation artifacts at the disc by drawing straight lines between the opposing borders of the optic disc. We determined the thickness of individual retinal layers and the IRL[16]. Thickness data were exported from the segmentation software onto an Excel spreadsheet (Microsoft, WA, USA). In the case of SJL/J mice, which are homozygous for the allele Pde6b^{rd1} (retinal degeneration 1), we used an 8x8 grid, obtaining retinal thickness values only in those sectors where imaging of the inner retinal layers was feasible (figure 1D).

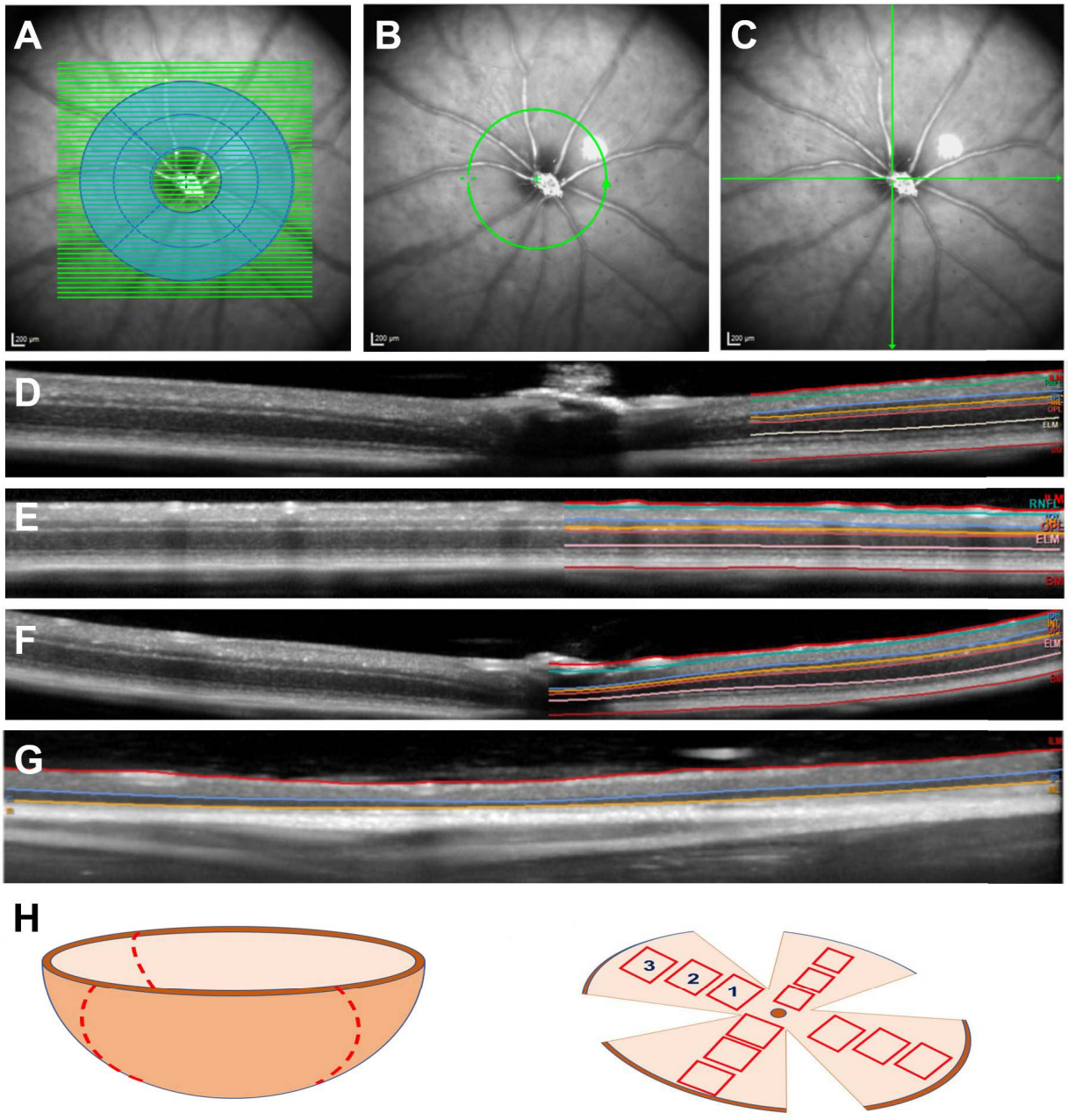

Figure 1 (A through C), Fundus Image of Mouse Retina with Segmentation of OCT, where each green line depicts a B-scan. (A), Volume scan taken from raster scan of the optic nerve head. Area in blue includes the region of calculated volume. (B), Peripapillary ring and (C), horizontal and vertical line scans. (D through F), examples of B-scans obtained from volume (D), peripapillary ring (E) and (F) line scans. On the right half of each B-scan, the results of the semi-automated segmentation of the layers are shown with retinal layers labeled. (G), horizontal B-scan in a SJL/J mouse, with atrophy of outer retinal layers, a characteristic finding in retinal degeneration 1. (H), Schematic representation of a retina dissected from an eyeball (left) and a whole-mount for histological analysis (right). The dotted line represents cuts made on the retina; the red squares represent areas analyzed in the central (1), mid-peripheral (2), and far-peripheral retina (3).

Histological analysis and Immunofluorescence Microscopy

Mice were sacrificed with an overdose of isoflurane. Cardiac perfusion was performed, optic nerves and retinae were dissected. Optic nerves were fixated in 4% paraformaldehyde (PFA) overnight and dehydrated in sucrose solutions with increasing concentrations. After embedding in O.C.T. compound (Sakura™ Finetek), longitudinal sections of 5 µm were cut for immunohistological analysis. The antibodies used for immunofluorescence microscopy are listed in table 2. To examine adaptive immune infiltration by CD3+ lymphocytes and innate immune activation – microglial/macrophage infiltration - as well as the myelin status of the optic nerves, slices were incubated with CD3 (1:400, Dako), Iba1 (1:500, Wako chemicals) and MBP (1:500, Millipore) antibodies, respectively. For a further rating of immune cell infiltration in optic nerves, hematoxylin and eosin (HE) staining was performed. RGC count was calculated by a semi-automated count of βIII-tubulin or Brn3a positive cells on retinal flatmounts. Briefly, retinae were stained with Brn3a (1:200, Santa Cruz Biotechnology, cat # sc-31984) or βIII-tubulin antibody (1:1000, Biolegend) and flat-mounted on glass slides. Each retina was then divided into four quadrants (three areas per quadrant: central, mid-periphery, and far-periphery) (figure 1E). For each eye, Brn3a+ or βIII-tubulin+ cell count was summed up from all 12 areas imaged as previously described[18].

Table 2. List of antibodies used for immunofluorescence microscopy

	Type	Manufacturer	Catalog #	Host species	Dilution used
Primary antibodies	Anti-CD3	Dako, Hamburg, Germany	A0452	Mouse	1:400
	Anti-Iba1	Wako, Richmond, VA, USA	019-19741	Rabbit	1:500
	Anti-MBP	Millipore, Burlington, MA, USA	MAB386	Rat	1:500
	Anti-Brn3a	Santa Cruz Biotechnology, Dallas, TX, USA	sc-31984	Goat	1:200
	Anti-βIII-tubulin	Biolegend, San Diego, CA, USA	801201	Mouse	1:1000
Seconday antibodies	Alexa Fluor-555 Anti-Goat	Life Technologies, Carlsbad, CA, USA	A-21432	Donkey	1:200
	Alexa Fluor-488 Anti-Rabbit	Life Technologies, Carlsbad, CA, USA	A-21206	Donkey	1:200
	Cy3 anti-Rabbit	Millipore, Burlington, MA, USA	AP187c	Goat	1:500
	Cy3 anti-Mouse	Millipore, Burlington, MA, USA	AP124c	Goat	1:500
	Cy3 anti-Rat	Millipore, Burlington, MA, USA	AP183C	Goat	1:500

Electron microscopy
For transmission electron microscopy (TEM), mice were sacrificed and cardiac perfusion was performed with 2% PFA and 2.5% glutaraldehyde (GA). Optic nerves were dissected and incubated in the fixative containing 2% PFA and 2.5% GA at 4°C for 3 hours, followed by incubation in 1% osmium tetroxide for 2 hours. Dehydration was achieved using acetone at increasing concentrations and block contrast was applied (1% phosphotungstic acid/ 0.5% uranylacetate in 70% acetone). A Spurr embedding kit (Serva, Heidelberg, Germany) was used according to the manufacturer's protocol. Ultrathin sections of 70 nm were cut using an Ultracut EM UC7 (Leica) and stained with lead-citrate[19] and 1.5% uranyl-acetate. Images were captured at various magnifications using a TEM H7100/100KV (Hitachi, Tokyo, Japan) using a Moroda SIS Camera system and were subsequently processed by Olympus ITEM 5.0 Software.

Statistical Analysis.
We performed the statistical analysis with SPSS version 22 (IBM). Data are presented as mean ± standard error of the mean (SEM). We calculated the area under the curve of EAE daily scores for each group. For all OCT scans, we calculated the two-way mixed effect absolute agreement interclass correlation coefficient (ICC) to assess the reliability of the measurements of every layer obtained by the two independent raters ("inter-rater reliability"), and to assess the repeatability of consecutive scans ("test-retest reliability"). We report the ICC and the 95% confidence intervals. ICC values above 0.9 were considered as excellent, between 0.8 and 0.9 as good, between 0.7 and 0.8 as acceptable, between 0.6 and 0.7 questionable, between 0.5 and 0.6 as poor and below 0.5 as unacceptable [20]. Differences in retinal thickness were analyzed using generalized estimating equations (GEE) with an exchangeable correlation matrix to adjust for intrasubject inter-eye correlations. We studied the association of OCT results with EAE severity and RGC loss by GEE association analyses, to identify which measurements could be used as surrogates for neuronal injury. Differences in RGC survival were analyzed with a one-way ANOVA and Holm-Sidak *post hoc* test. P values are designated as follows: *P ≤ 0.05, **P ≤ 0.01, ***P ≤ 0.001. For calculation of the sample sizes required for neuroprotection studies, we performed a power analysis using G*Power (Version 3.1.9.2) for an α of 0.05 and a power (1-ß) of 0.8.

Results
The OCT quality scores were good for the ring and excellent for cross and volume scans (supplementary figure 1).

Inter-rater reliability: Semi-automated segmentation of the IRL was feasible for all retinal layers in all three scanning protocols (figure 1). Volume scans provided excellent inter-rater reliability with ICC values of above 0.9 for all assessments (supplementary figure 2). Cross scans (average of horizontal and vertical line scans) and peripapillary ring scans provided a good to excellent inter-rater reliability for the assessment of the IRL thickness (ICC 0.961, 95% CI 0.913- 0.983 and ICC 0.816, 95% CI 0.468 - 0.932, respectively) while the RNFL showed good reliability for cross scans and unacceptable reliability for ring scans (ICC 0.828, 95% CI 0.533-0.930 and ICC 0.278, 95% CI -0.244-0.666, respectively).

Test-retest reliability: We obtained the highest reproducibility with volume scans, which showed excellent reliability for the assessment of the IRL and the GCIPL (supplementary figure 3). Cross and peripapillary scans provided excellent reproducibility only for the measurement of IRL thickness (0.918 [95% CI 0.492-0.983] and 0.950 [95% CI 0.508-0.993]) and, in the case of cross scans, also for the GCIPL (0.937 [95% CI 0.746-0.985]) while the RNFL showed a poor reliability for cross scans and a questionable reliability for ring scans (0.551, [95% CI -0.568- 0.89] and 0.624, [95% CI -0.655- 0.937]). The follow-up function did not add significantly to reproducibility.
In summary, in vivo retinal imaging by OCT was associated for a high inter-rater and test-retest reliability for the IRL and can, therefore, be used for the in vivo monitoring of neuroaxonal loss, e.g. in the context of optic neuritis.

A summary of the longitudinal experiments performed in EAE and their results is outlined in table 3 .

Table 3. Summary of EAE experiments and results

Figures	Strain	Encephalytogenic peptide	OCT follow-up period	OCT time-points (months after immunization)	OCT findings	Histological findings	Additional findings
2, 3, 4, 6	WT C57Bl/6J	MOG_{35-55}	120 days	0, 0.5, 1, 2, 3, 4	Initial IRL swelling mirroring EAE onset and peak, followed by progressive thinning	Optic neuritis (T-cell infiltration, microglial activation, and de-myelination) with 32% RGC loss. Decrease of myelinated nerve fibers and destruction of the myelin structure.	Decreased visual acuity (OKR)
2, 3	WT C57Bl/6J	MBP	120 days	0, 0.5, 1, 2, 3, 4	No change	No optic neuritis or RGC loss	
2, 3	TCR^{2D2}	MOG_{35-55}	120 days	0, 0.5, 1, 2, 3, 4	IRL atrophy already present at two weeks	Severe optic neuritis with 49 % RGC loss	
5	WT C57Bl/6J	MOG_{35-55}	9 months	0, 1, 2, 5, 7, 9	Progressive IRL and INL thinning, more pronounced during the first 2 months	54 % RGC loss	
6	SJL/J	$PLP_{139-151}$	7 months	0, 1, 2, 5, 7	Progressive IRL atrophy, also present to a lesser degree in Sham-immunized mice		

Retinal changes during 120 days after immunization with MOG $_{35-55}$ or MBP in WT C57Bl/6J and with MOG $_{35-55}$ in TCR^{2D2} mice

IRL swelling was evident two weeks after immunization of WT mice with MOG $_{35-55}$, which corresponded to clinical EAE, and was followed by progressive thinning and loss of RGC.

After MOG$_{35-55}$ immunization, TCR^{2D2} mice developed a severe clinical disability. Those suffering from quadriparesis had to be fed with liquid gel and soaked chow. Some animals (n=2), that received sham immunization (PT and CFA), developed spontaneous clinical signs. Although C57BL/6 mice are often considered resistant to EAE induced by MBP, some data suggest otherwise [21,22]. Thus, we studied the disease course and phenotype of retinal injury in this model as well. Clinical signs where minimal, and started around the same day as MOG$_{35-55}$- induced EAE (figure 2).

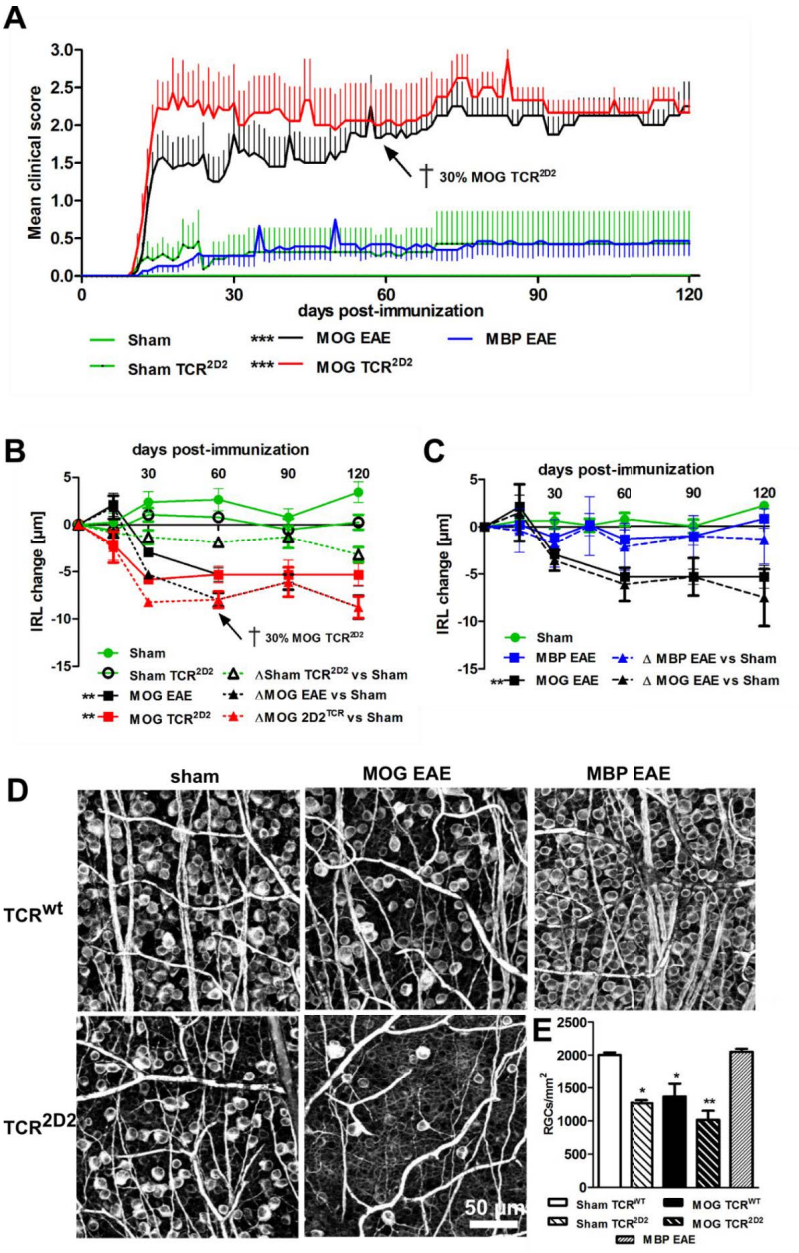

Figure 2 (A), Clinical EAE score of C57Bl/6J mice immunized with MOG-or MBP-peptide, as well as TCR^{2D2} transgenic mice immunized with MOG peptide. (B), Change of the inner retinal layers of TCR^{WT} and TCR^{2D2} mice. (C), IRL change of C57BL/6J mice immunized with MBP. (D), Retinal wholemounts stained by βIII-tubulin antibody from groups indicated in (A). The representative images display the most severe disease progression. (E), The bar graph shows the RGC density 120 days after immunization. Time courses and bar graphs represent the pooled mean ± SEM of two separate EAE experiments each with at least four animals per group, *p>0.05; **p<0.01; ***p<0.001, time courses (area under the curve) were compared to Sham, bar graph compared to Sham TCR^{WT} mice by ANOVA with Dunnett's post hoc test.

Contrary to our observations in WT C57Bl/6J mice immunized with MOG_{35-55}, IRL thinning was already evident after 2 weeks in TCR^{2D2} mice. However, after 60 days, no differences were observed between WT C57Bl/6J and TCR^{2D2} mice anymore, mainly because TCR^{2D2} animals (~30%) were sacrificed due to development of severe clinical EAE, reducing the number of animals with strong IRL degeneration. Mean IRL of the sham TCR^{2D2} group showed no thickness increase after a period of 120 days, while healthy WT controls gained up to 4 µm compared to the baseline measurement, suggesting that ON neurodegeneration occurs in TCR^{2D2} mice also in the absence of clinical EAE signs (figure 2B). As IRL thickness in control mice was subject to dynamic changes, we also analyzed the difference between EAE mice and the average, thickness of healthy control mice, at each time-point after immunization. This allowed for better visualization of the pace and extent of retinal atrophy after demyelinating injury in EAE mice. In line with the clinical disability of MBP immunized mice, neither degeneration of the IRL (figure 2C) nor the total retina (data not shown) was detected by OCT analysis and no significant reduction of retinal ganglion cells (RGC) (figure 2D+E) was observed at 120 days after MBP immunization compared to the sham control. Staining of the RGC from sham TCR^{2D2} mice confirmed the data of the OCT measurements, showing a reduced number of βIII-tubulin-positive cells in the retinae, also in those with no limb paresis. MOG-immunized TCR^{2D2} mice showed strong RGC reduction but also high variances between the single individuals (figure 2D+E).

HE-stained optic nerves from sham immunized TCR^{2D2} mice showed immune cell infiltration, compared to sham WT littermates, demonstrating the presence of ON, also in animals with no clinical signs. TCR^{2D2} mice immunized with MOG_{35-55} had severe inflammatory infiltration, exceeding the ON score of the WT control. Staining of the optic nerve revealed no significant cumulative infiltration of immune cells after MBP immunization, suggesting a mild disease pathology (figure 3).

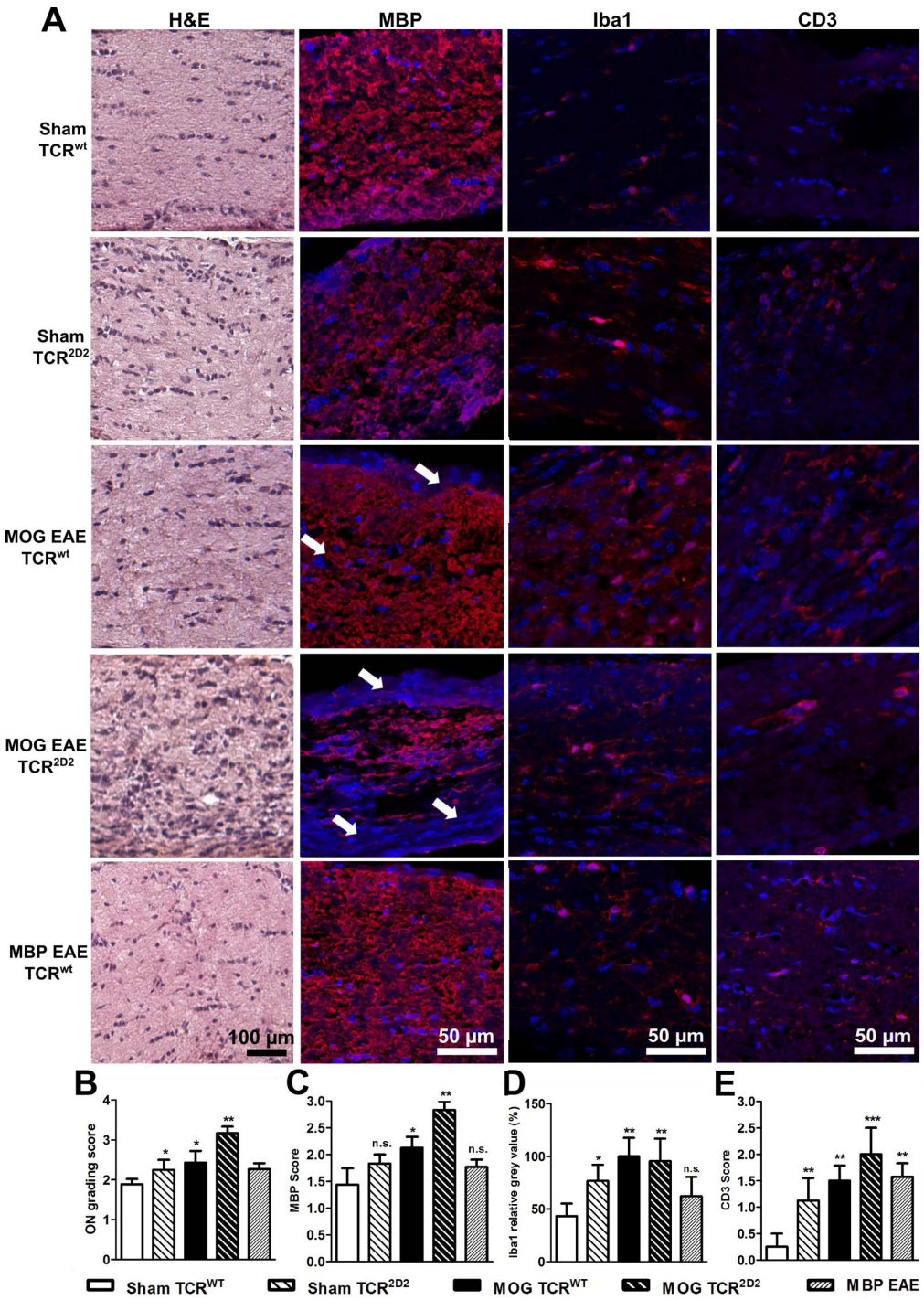

Figure 3 (A), Optic nerves of mice 120 days after MOG or MBP immunization stained by H&E and CD3, Iba1 or MBP antibodies. Optic nerves were compared by an established infiltration score according to H&E staining (B) (Shindler et al., 2006), MBP score for the myelin status (C), Iba1 fluorescence intensity measurement for microglia activation (D), and CD3+ cell infiltration (E). The bar graphs represent the pooled mean ± standard deviation of at least two separate EAE experiments each with at least 4 animals per group; one optic nerve per mouse was included, *p<0.05; **p<0.01; ***p<0.001; n.s. = not significant, by ANOVA with Dunnett's post hoc test compared to sham treated mice.

Increased T-cell infiltration, microglial activation, and demyelination of the optic nerve were observed 120 days after immunization of WT mice with MOG_{35-55} peptide. Microglia activation, as well as T-cell infiltration, was even present in TCR^{2D2} mice after sham immunization with CFA and PT. Even more severe infiltration of CD3 positive T-cells into the optic nerve and myelin degradation was observed in TCR^{2D2} EAE mice compared to WT animals, while microglial activation was similar (figure 3). Despite no significant changes in cellular infiltrates assessed by HE staining, we observed an increased infiltration of CD3-stained T-cells at day 120 in optic nerves of MBP immunized mice, while microglia activation and demyelination was unaltered.

To determine the effects of EAE on the ultrastructure of the myelin sheath, we performed electron microscopy of ultrathin cross sections of the optic nerve from sham and MOG_{35-55} immunized C57Bl/6J mice. Macroscopic analyses of the optic nerves revealed a normal myelin sheath in the sham immunized group while optic nerves of EAE mice displayed a prominent decrease of myelinated axons and destruction of the myelin structure (figure 4A). A quantitative analysis of the myelin structure revealed a significantly lower myelin-axon ratio in MOG- compared to sham immunized mice confirming the impression of myelin damage in MOG EAE from our macroscopic investigations (figure 4B).

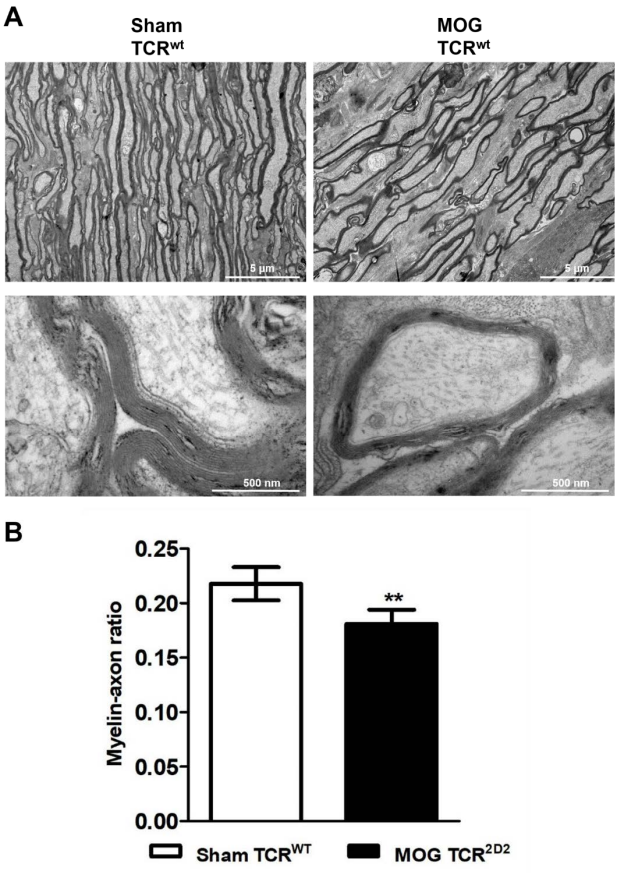

Figure 4 (A), Electron microscopy images of a longitudinal sections of the optic nerve fibers from sham and MOG35-55 treated C57Bl/6J wildtype mice. (B), The myelin-axon ratio was determined by the thickness of the myelin sheath and the axon. Bar graphs represent the pooled mean ± SD of an EAE experiment with four animals per group, **p<0.01 two-tailed student's t test compared to sham treated mice.

In summary, immunization of C5Bl/6J mice with MOG_{35-55} peptide but not MBP induced robust EAEON, detectable by ON histology and leading to a degeneration of the IRL and RGCs detectable by OCT and histology, respectively. This was even more pronounced

and often leading to death in TCR^{2D2} mice, which also displayed mild symptoms of ON when sham-immunized despite no motor symptoms.

Chronic retinal changes during 9 months after immunization and visual testing in MOG EAE in WT C57Bl/6J mice

In the eyes of control animals, we observed a progressive thickening of the retinae mirroring weight gain most likely corresponding to the natural growth of the eyes of the 6-8 week old mice (figure 5A). In EAE eyes, progressive thinning of the IRL started rapidly after the disease onset, with 1/3 of total loss occurring during the initial 2 months (-4.25 ± 0.87 µm compared to controls, P<0.001 at month 2; -13.39 ± 1.33 µm, P<0.001 at month 9). Inner nuclear layer (INL) thinning was detectable from the second month after immunization in EAE mice while INL thickness remained constant throughout the experiment in control mice.

As we identified the WT C57Bl/6J mice as a very suitable model for studying retinal injury in EAE, we chose to investigate the functional outcome of the structural results. Visual function was assessed by the optokinetic response of the mice, using the spatial frequency threshold as a readout for visual acuity. It was significantly reduced in EAE mice with values of 0.23 cycles per degree (c/d) compared to 0.33 c/d for sham-EAE control mice after 120 days of EAE (figure 5C).

After nine months, the RGC density halved (4665.83 ± 360 total Brn3a cells counted per eye *versus* 10206.78 ± 265, *P*<0.001) in immunized mice. This finding was consistent along all three retinal sectors (central, mid-peripheral and far peripheral) (figure 5D).

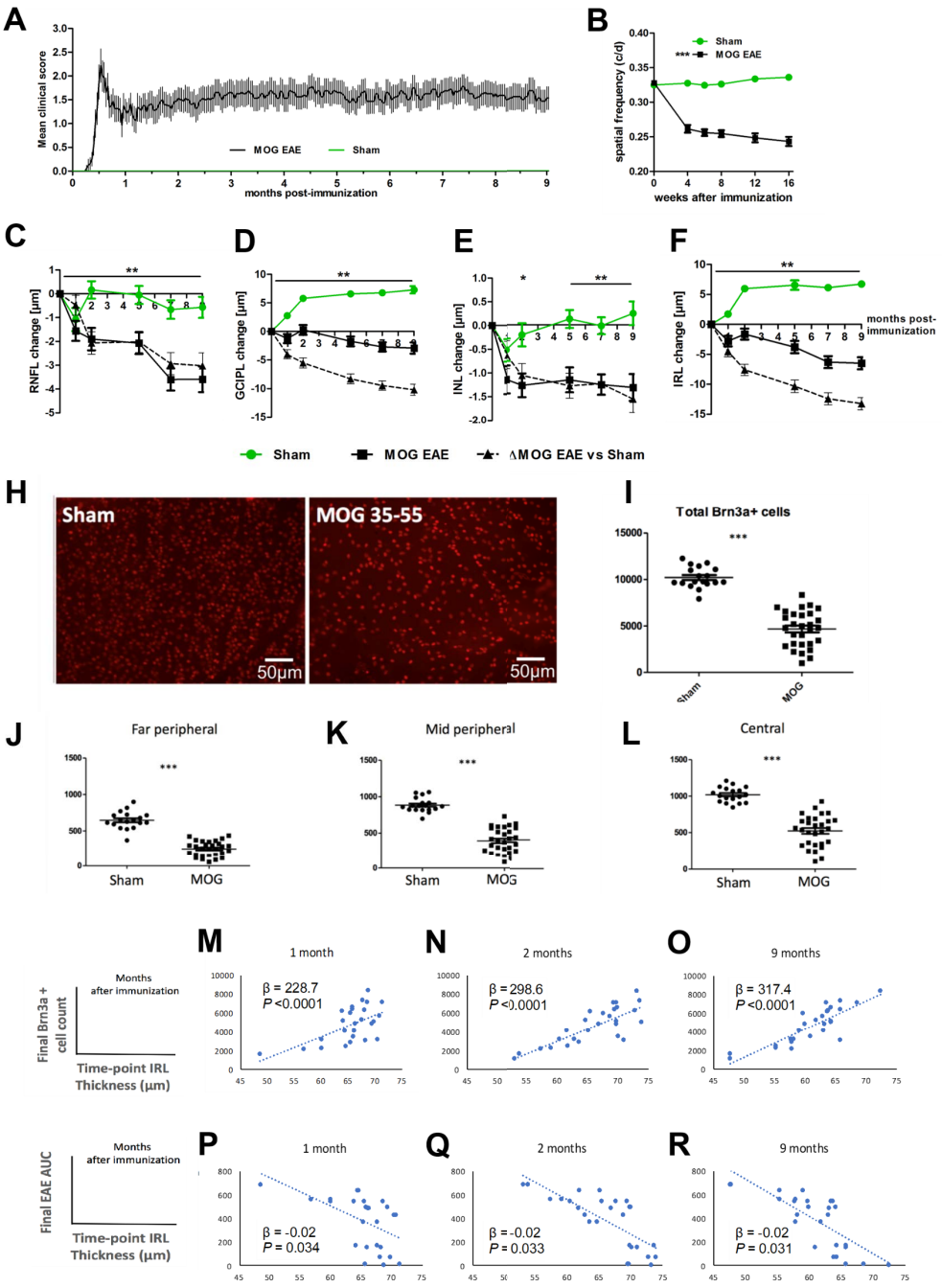

Figure 5 MOG 35-55 EAE in C57Bl/6J (n=17) vs. sham-immunized (n=12) mice. (A), EAE clinical scores. (B), Decreased visual acuity of EAE mice compared to untreated C57Bl/6J mice. OKR measurement was carried out for 120 days after MOG immunization as described above, area under the curve compared by ANOVA with Dunnett's post hoc test. (C through F), Thickness of retinal layers. (H through L), RGC count after 9 months. Data expressed as mean ± SEM, *p<0.05; ** p<0.01 ***p<0.001. P-values for OCT and RGC data obtained from generalized estimating equation models accounting for within-mouse, inter-eye correlations. (M through R), Linear regression analyses. IRL thickness during EAE is associated with ultimate neuronal loss (top row) and disease severity (bottom row). Similar results were obtained 5 and 7 months after immunization (data not shown). ß = Generalized estimating equation-association coefficient.

Investigating the IRL thickness at each time point (1, 2, 5, 7 and 9 months after immunization), we analyzed its association with the final RGC count (obtained at the end of the experiments, 9 months after immunization) and the total EAE score area under the curve (an indicator of the overall clinical severity and burden of disease) (figure 5E). IRL thinning during EAE was significantly associated with RGC loss (ß GEE -association coefficient 317.4, 95% IC 241.1, 393.7, *P*<0.0001 at month 9 after immunization) and disease severity (ß -0.02, 95% IC -0.03, -0.001, *P*=0.031 at month 9).

Chronic retinal changes during 7 months after immunization in $PLP_{139-151}$ EAE in SJL/J mice

We sought to characterize the dynamic changes in retinal thickness in SJL/J mice following immunization against $PLP_{139-151}$. In this mouse strain, not only immunized mice but also Sham-injected controls showed progressive IRL atrophy, due to the retinal degeneration linked to the homozygous mutation of the $Pde6b^{rd1}$ gene. However, in PLP-immunized mice, the IRL thinning was significantly aggravated after the second month following immunization (figure 6).

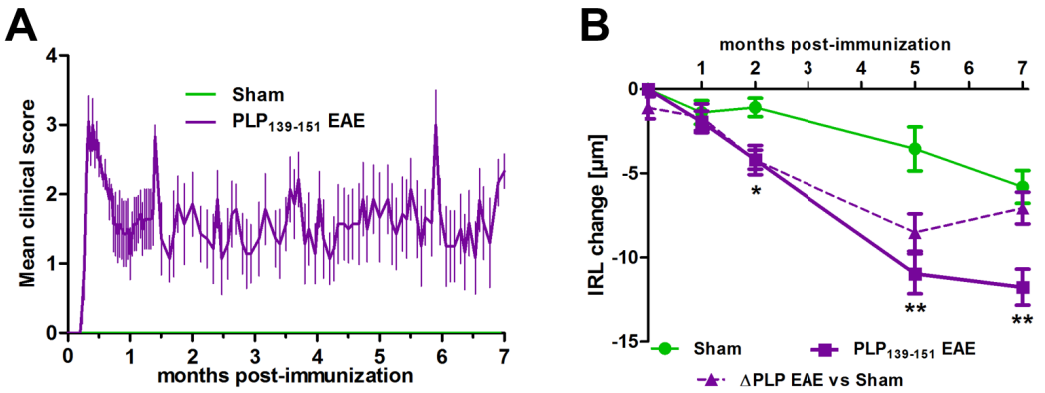

Figure 6 (A), Clinical EAE scores (top) and weight changes (bottom) in PLP139-151 EAE in SJL mice. The abscissa axis represents days after immunization. (B), IRL thickness in PLP 139-151-EAE (n= 10) vs. sham-immunized (n=5) SJL/J mice. Data expressed as mean ± SEM * p<0.05; **p<0.01.

We concluded that the retinal degeneration also occurring in sham-injected controls make the SJL mouse strain suboptimal for studies investigating the effects of optic neuritis.

Power analysis for neuroprotection studies

The results outlined above suggested that MOG_{35-55} EAE in C57Bl/6J model is particularly well suited for the investigation of therapeutic strategies aiming at preventing neuroaxonal loss. In this context, it is important to know the number of mice necessary to detect efficacy for given effect size. To this end we used data from a dataset from our recently published work on the protective effects of alpha-lipoic acid in EAE (Dietrich et al. 2018, J Neuroinflammation) comparing the results of the different structural and functional readouts in a power analysis. For OCT measurements at the endpoint 120 days after immunization we determined a minimum sample size of 14 animals per group to detect the 20% difference in IRL thickness change observed at an effect strength of 1.1, considering that the mean of the inner retinal layers changed by 1.7 µm in vehicle-treated

mice and was associated with a standard deviation of 1.52 µm. By performing several longitudinal measurements for each animal the sensitivity to detect treatment effects can be further increased. As a functional measure, a sample size of 3 animals per group was determined to detect alteration of the visual acuity of 15% at an effect strength of 3.7 (0.2286 c/d ± 0.011 c/d to 0.2686 c/d ± 0.011 c/d). For histological staining of RGCs in retinal wholemounts and the clinical EAE score at 120 days, the power analysis determined a sample size of 3 and 18 animals per group, respectively, to detect a change as low as 25% RGC survival and 50% EAE score at an effect strength of 4.45 (1181 RGCs/mm2 ± 200 RGCs to 1535 RGCs/mm2 ± 200 RGCs) and 0.93 (2.26 EAE score ± 1.27 vs 1.19 EAE score ± 0.93), respectively.
In summary, based on the results of our previous study we can conclude that OCT and OKR in the EAEON can detect protective treatment effects of 20 and 15% on retinal structure and visual function, respectively, with reasonable sample sizes.

Discussion

Retinal OCT is increasingly used as an outcome measure for clinical trials of candidate neuroprotective drugs in acute ON [23–26] and MS[27,28]. Preclinical investigations in experimental ON using in-vivo retinal outcomes can be readily transferred to a clinical trial scenario, yet the models best suited to address the different aspects of retinal neurodegeneration by in vivo OCT are still unknown. For this purpose, establishing the dynamics of retinal neuroaxonal loss in EAE is also crucial. Traditionally, EAE experiments mostly focus on clinical and/ or purely immunological aspects and extend for one month. Our results indicate that, in the MOG_{35-55} EAE model in C57BL/6J mice, IRL thickness changes during the course of the disease, reflecting the clinical severity and RGC survival. Here, we observed that slow retinal thinning after peak EAE continues until month 7 even though the clinical signs remain stable. EAE scores almost exclusively represent changes in motor function. This mirrors the current situation in the clinic and in clinical trials, where disability is measured through the EDSS scale, which relies heavily on the ambulatory capacity of patients. Additionally, while EAE scores and EDSS are ordinal scales and depend on the subjectivity of the scorer, OCT provides an objective, continuous quantitative anatomical readout.

We first analyzed the reproducibility and reliability of retinal OCT measurements in mice. Altogether, volume scans offered the best results, while the poorest were obtained with the peripapillary ring scans which, in fact, have been studied as an outcome parameter in animal models of MS [29]. A possible explanation is that the variability of the segmentation of single B-scans is averaged out when analyzing the mean of the 49 scans making up the volume scan. Our data indicate that, in mice, the separate assessment of the RNFL and GCIPL thickness can be challenging, since the segmentation of the limit between them is not very reproducible. We, therefore, also analyzed them jointly as the IRL, which yielded much more robust results. Another advantage of evaluating these layers together is that it reflects a combined outcome parameter for axonal (RNFL) and neuronal (GCIPL) loss.

We then investigated the extent and dynamics of retinal injury in different mouse EAE models. The genetic background of a mouse line, as well as the epitope used for immunization, affect the immune and inflammatory response during EAE. In Swiss-derived strains (e.g. SJL/J), PLP immunization leads to a relapsing remitting disease

course, while mice with a Bl/6 background develop a more chronic progression, thereby addressing different forms of the inflammatory CNS disease.[30]. Additionally, for neuroprotection studies, it may be particularly relevant to use models displaying severe retinal damage to ensure that even small effect sizes of neuroprotective interventions are detectable through OCT. We, therefore, chose to also include the model of $PLP_{139-151}$-induced EAE in SJL/J mice and MOG_{35-55}-induced EAE in TCR^{2D2} mice as models with particularly severe RGC degeneration[3] and ON, besides MOG_{35-55}-induced EAE in C57BL/6 WT mice[5]. Furthermore, we aimed to investigate the retinal degeneration in MBP-induced EAE in C57Bl/6J mice as a model characterized by a monophasic disease course and predominantly axonal damage but less demyelination[31]. In general, EAE induction in C57Bl/6J mice by MBP is not very feasible [21,22,32]; nevertheless, we were able to induce mild EAE signs with whole rat MBP, yet with no significant retinal thinning or relevant pathology of the optic nerve. Hence, we conclude that this model is not suitable for retinal studies. EAE in SJL/J mice following immunization against $PLP_{139-151}$ could be used to study retinal neurodegeneration in the context of repeated relapses. Even though OCT detected changes attributable to EAE in the retinas of SJL/J mice, the concomitant retinal dystrophy hinders further neurophysiological and histological investigations and significantly limits the usefulness of this mouse strain for our purposes. We, therefore, focused on mice with the C57BL/6J background, obtaining results by the findings of Knier et al.[9], and our own previous work [8,33]. We sought to also characterize the changes in retinal thickness during the acute phase of the disease. Serial OCT 6, 15, 30, 60, 90 and 120 days after immunization revealed three distinctive phases of retinal injury: no changes in retinal thickness were detectable 6 days after immunization (pre-EAE onset, data not shown); coinciding with clinical onset and peak of disease, there was considerable swelling of the IRL in WT mice, while retinal degeneration in TCR^{2D2} mice stared already at this early time point. The chronic phase of EAE was characterized by progressive IRL thinning below baseline levels both in WT and TCR^{2D2} mice. Histopathological examination revealed ON with T cell, and microglial infiltrates leading to RGC loss in the absence of clinical signs in TCR^{2D2} mice injected only with PT, in line with the observations of Guan et al. [17]. As IRL thickness is only slightly decreased at day 30 compared to baseline, loss of RGC might not be evident only one month after immunization. Taken together, these analyses indicated that, in the MOG_{35-55} EAE model through direct immunization of C57BL/6J mice, experiments using retinal OCT as a surrogate for neuronal damage should last more than one month and use IRL thickness as their primary outcome.

We measured retinal thickness until changes relative both to baseline levels and age-matched controls stabilized, which happened around month 9 after immunization. This continuation of IRL thinning far beyond the clinical stabilization of EAE suggests that OCT might be more sensitive to assess the chronic neurodegeneration after an acute inflammatory insult. Although significant IRL atrophy was already detectable after one month, these changes corresponded exclusively to the GCIPL, and only from the second month were we able also to detect thinning in the RNFL. By the end of the experiment, however, relative thinning of the RNFL was higher than that of the GCIPL. This aligns with studies of ON in humans describing GCL thinning as an early feature [34], detectable before that of the peripapillary RNFL [35], but with ultimate macular RNFL atrophy being more extensive than that of the macular GCIPL [36]. The different timing of RNFL versus GCIPL atrophy has been related to early edema of the RNFL during acute ON, or to RGC

shrinkage and loss before axonal atrophy occurs. According to this interpretation, RGC degeneration in ON would be driven by two related mechanisms: an initial wave of RGC injury, caused by early signals from damaged axons in the optic nerve, and a later wave of RGC loss, as a consequence of a dying-back process following axonal loss [36]. Our findings in the animal laboratory seem to support these observations. Like in patients with ON [37], we saw changes in the IRL thickness occurring most rapidly in the first months after the acute episode.

Nine months after immunization, surviving RGC were halved in MOG- versus sham-immunized mice. However, measuring IRL thickness longer than two months did not show to improve the association of IRL thickness and RGC survival substantially. These results indicated that MOG_{35-55} EAE studies using OCT as a surrogate for the ultimate survival of RGC do not necessarily provide additional meaningful information beyond two months after direct immunization unless investigating mechanisms of repair or specifically targeting processes that occur in the late phase. Similarly, because in the MOG-EAE model there is little clinical change beyond the fourth week after immunization, IRL thickness measured at 2 months was as good of a predictor of overall burden of disease (cumulative EAE score) as that measured 1 or 9 months after immunization (r^2 0.51, 0.47, and 0.52 at 1, 2 and 9 months, respectively).

It should be noted that OCT is a method to image tissue. It lacks real cellular resolution. Therefore, averaging while enhancing reproducibility does not necessarily improve fidelity. Each scan is the result of averaging 30 to 100 images, so the details of the interface between retinal layers might not be fully detected. We did not compare the results with the retinal layer thickness measurements to the layer thickness in histological sections or assessments by other OCT devices or segmentation algorithms. However, this was done in other studies[11,38] and was not the focus of our work. As a result of these limitations, measurements are obtained from an idealized representation of the retina and can be influenced by pathological changes that impact the optical properties of the tissue under study.
The power analysis using our previously published results with alpha-lipoic acid[8] revealed that protective effects of 20% on the retinal structure could be detected with 14 animals per group, which is in line with other studies using similar methodology[9,39,40]. Interestingly, OKR analysis of visual function and RGC counting in retinal wholemounts showed less variance resulting in numbers as low as 3 animals per group in the power analysis to detect 15% protection of visual function and 25% protection of RGCs. Of course, the power achieved by the different modalities depends on the mode of action of the therapeutic approaches studied.

Conclusions

IRL thickness, as assessed by retinal OCT, is a good surrogate for clinical severity and neuronal loss and survival in mouse models of EAE. During the onset and peak of disease, there is acute IRL thickening, followed by progressive thinning. In MOG-EAE in C57BL/6J mice, this occurs most rapidly between the height of disease and the 60th day after immunization, and only from that time-point on is it possible to detect associated thinning of the INL. In the otherwise healthy SJL/J adult mouse, which is a homozygous carrier of the allele $Pde6b^{rd1}$, there is progressive IRL thinning due to retinal dystrophy which is aggravated upon immunization with $PLP_{139-151}$. No significant retinal changes are found in MBP-EAE in C57BL/6J mice. MOG immunization in TCR^{2D2} mice results in severe EAE, therefore challenging animal care and survival during experiments.
We conclude that, among the models tested, MOG_{35-55} induced EAE in C57Bl/6J is the most convenient to study retinal neurodegeneration in the context of ON.

LIST OF ABBREVIATIONS

ARVO: Association for Research in Vision and Ophthalmology
AUC: Area Under the Curve
CFA: Complete Freund's Adjuvant
CNS: Central Nervous System
EAE: Experimental Autoimmune Encephalomyelitis
GCIPL: Ganglion cell-inner plexiform layer
GEE: Generalized Estimating Equations
HE: Hematoxylin and Eosin
IACUC: Institutional Animal Care and Use Committee
INL: Inner Nuclear Layer
IRL: Inner Retinal Layers
i.p: Intraperitoneal
MBP: Myelin Basic Protein
MOG: Myelin Oligodendrocyte Glycoprotein
MS: Multiple Sclerosis
OCT: Optical Coherence Tomography
ON: Optic Neuritis
PFA: Paraformaldehyde
PLP: Proteolipid Lipoprotein
PT: Pertussis Toxin
RGC: Retinal Ganglion Cell
RNFL: Retinal Nerve Fiber Layer
TCR^{2D2}: T Cell Receptor transgenic mouse specific for MOG_{35-55}
TEM: Transmission electron microscopy
TUNEL: Terminal Deoxynucleotidyl Transferase dUTP Nick End Labeling

DECLARATIONS

Ethics approval

This study was approved by the University of California, San Francisco Institutional Animal Care and Use Committee (IACUC), the German regional authorities (State Agency for Nature, Environment and Consumer Protection; AZ 84-02.4.2014.A059) and performed in adherence to the Association for Research in Vision and Ophthalmology (ARVO) Statement for the Use of Animals in Ophthalmic and Vision Research.

Consent for publication
Not applicable.

Availability of data and material
The datasets used and/or analyzed during the current study are available from the corresponding author on reasonable request.

Funding
A.C.-H. was a postdoctoral fellow of the National Multiple Sclerosis Society (FG 20102-A-1). K. L.-H. was a fellow of the Deutsche Forschungsgemeinschaft (DFG; Le 3079/1-1) and the National Multiple Sclerosis Society (FG 2067-A-1). C.C. was supported by a training/research fellowship FISM (Fondazione Italiana Sclerosi Multipla. cod 2013/B/4). The work was funded by grants from the Hilton Family Foundation, NINDS R01NS105741 (A.J.G.), the Forschungskommission of the Heinrich-Heine-University Duesseldorf, the charitable Doktor Robert Pfleger Foundation, the charitable Ilselore Luckow Foundation, Biogen and Novartis to P.A.

Competing interests
All authors declare no competing interests related to the work presented. Unrelated to the work presented, the authors declare the following financial disclosures: Michael Dietrich received speaker honoraria from Novartis. Hans-Peter Hartung has received fees for serving on steering committees from Biogen Idec, GeNeuro, Sanofi Genzyme, Merck, Novartis Pharmaceuticals, Octapharma, Opexa Therapeutics, Teva Pharmaceuticals, MedImmune, Bayer HealthCare, Forward Pharma, and Roche, fees for serving on advisory boards from Biogen Idec, Sanofi Genzyme, Merck, Novartis Pharmaceuticals, Octapharma, Opexa Therapeutics, Teva Pharmaceuticals, and Roche, and lecture fees from Biogen Idec, Sanofi Genzyme, Merck, Novartis Pharmaceuticals, Octapharma, Opexa Therapeutics, Teva Pharmaceuticals, MedImmune, and Roche. Klaus Lehmann-Horn received speaker honoraria and travel support from Novartis, Hoffmann-La Roche, and Merck Serono. He receives research support from Novartis. Philipp Albrecht received compensation for serving on Scientific Advisory Boards for Ipsen, Novartis, Biogen; he received speaker honoraria and travel support from Novartis, Teva, Biogen, Merz Pharmaceuticals, Ipsen, Allergan, Bayer Healthcare, Esai, UCB and Glaxo Smith Kline; he received research support from Novartis, Biogen, Teva, Merz Pharmaceuticals, Ipsen, and Roche. Ari J. Green served on the scientific advisory board of MedImmune, Novartis, OCTIMS, Inception 5 Biosciences, and Bionure; is an associate editor of JAMA Neurology; was an editorial board member of Neurology; holds a patent for Remyelination molecules and pathways; consulted for Inception 5 Sciences; received research support from Novartis Pharma OCTIMs, Inception Sciences SRA, NINDS, NIA, National MS Society, Sherak Foundation, and Hilton Foundation; holds stock or stock options in Inception 5; and served as an expert witness at Mylan v Teva Pharma. The other authors report no disclosures.

Authors' contributions
A. C-H. and M.D.: Conception of the work, data collection, data analysis and interpretation, drafting the article; H.H.Y, A.H. and C.H.: data collection, data analysis and interpretation; A.I., A.Ha., M.L., CC and K. L-H: data collection; L.J.B, O.A., J.I., C.vG., H-P.H., D.F. and S.S.Z.: critical revision of the article; P.A.: conception of the work, data collection, data analysis and interpretation; A.G.: Conception of the work, critical revision of the article. All authors read and approved the final manuscript.

Acknowledgements
Not applicable.

References

1. Balcer LJ. Clinical practice. Optic neuritis. *N Engl J Med*. 2006;354(12):1273-1280. doi:10.1056/NEJMcp053247
2. Kezuka T, Usui Y, Goto H. Analysis of the pathogenesis of experimental autoimmune optic neuritis. *J Biomed Biotechnol*. 2011;2011:294046. doi:10.1155/2011/294046
3. Shindler KS, Guan Y, Ventura E, Bennett J, Rostami A. Retinal ganglion cell loss induced by acute optic neuritis in a relapsing model of multiple sclerosis. *Mult Scler*. 2006;12(5):526-532. doi:10.1177/1352458506070629
4. Shao H, Huang Z, Sun SL, Kaplan HJ, Sun D. Myelin/oligodendrocyte glycoprotein-specific T-cells induce severe optic neuritis in the C57BL/6 mouse. *Invest Ophthalmol Vis Sci*. 2004;45(11):4060-4065. doi:10.1167/iovs.04-0554
5. Bettelli E, Pagany M, Weiner HL, Linington C, Sobel R a, Kuchroo VK. Myelin oligodendrocyte glycoprotein-specific T cell receptor transgenic mice develop spontaneous autoimmune optic neuritis. *J Exp Med*. 2003;197(9):1073-1081. doi:10.1084/jem.20021603
6. Guan Y, Shindler KS, Tabuena P, Rostami AM. Retinal ganglion cell damage induced by spontaneous autoimmune optic neuritis in MOG-specific TCR transgenic mice. *J Neuroimmunol*. 2006;178(1-2):40-48. doi:10.1016/j.jneuroim.2006.05.019
7. Horstmann L, Schmid H, Heinen AP, Kurschus FC, Dick HB, Joachim SC. Inflammatory demyelination induces glia alterations and ganglion cell loss in the retina of an experimental autoimmune encephalomyelitis model. *J Neuroinflammation*. 2013;10(1):120. doi:10.1186/1742-2094-10-120
8. Dietrich M, Helling N, Hilla A, et al. Early alpha-lipoic acid therapy protects from degeneration of the inner retinal layers and vision loss in an experimental autoimmune encephalomyelitis-optic neuritis model. *J Neuroinflammation*. 2018;15(1):71. doi:10.1186/s12974-018-1111-y
9. Knier B, Rothhammer V, Heink S, et al. Neutralizing IL-17 protects the optic nerve from autoimmune pathology and prevents retinal nerve fiber layer atrophy during experimental autoimmune encephalomyelitis. *J Autoimmun*. 2015;56:34-44. doi:10.1016/j.jaut.2014.09.003
10. Groh J, Hörner M, Martini R. Teriflunomide attenuates neuroinflammation-related neural damage in mice carrying human PLP1 mutations. *J Neuroinflammation*. 2018;15(1):194. doi:10.1186/s12974-018-1228-z
11. Dysli C, Enzmann V, Sznitman R, Zinkernagel MS. Quantitative Analysis of Mouse Retinal Layers Using Automated Segmentation of Spectral Domain Optical Coherence Tomography Images. *Transl Vis Sci Technol*. 2015;4(4):9. doi:10.1167/tvst.4.4.9
12. Antony BJ, Jeong W, Abràmoff MD, Vance J, Sohn EH, Garvin MK. Automated 3D Segmentation of Intraretinal Surfaces in SD-OCT Volumes in Normal and Diabetic Mice. *Transl Vis Sci Technol*. 2014;3(5):8. doi:10.1167/tvst.3.5.8
13. Szczesny G, Veihelmann A, Massberg S, Nolte D, Messmer K. Long-term anaesthesia using inhalatory isoflurane in different strains of mice-the haemodynamic effects. *Lab Anim*. 2004;38(1):64-69. doi:10.1258/00236770460734416
14. Calderone L, Grimes P, Shalev M. Acute reversible cataract induced by xylazine and by ketamine-xylazine anesthesia in rats and mice. *Exp Eye Res*. 1986;42(4):331-337. http://www.ncbi.nlm.nih.gov/pubmed/3754819. Accessed January 25, 2018.
15. Dietrich M, Cruz-Herranz A, Yiu H, et al. Whole-body positional manipulators for ocular imaging of anaesthetised mice and rats: a do-it-yourself guide. *BMJ open Ophthalmol*. 2017;1(1):e000008. doi:10.1136/bmjophth-2016-000008
16. Cruz-Herranz A, Balk LJ, Oberwahrenbrock T, et al. The APOSTEL recommendations for reporting quantitative optical coherence tomography studies. *Neurology*. 2016;86(24):2303-2309. doi:10.1212/WNL.0000000000002774

17. Prusky GT, Alam NM, Beekman S, Douglas RM. Rapid Quantification of Adult and Developing Mouse Spatial Vision Using a Virtual Optomotor System. *Investig Opthalmology Vis Sci*. 2004;45(12):4611. doi:10.1167/iovs.04-0541
18. Hilla AM, Diekmann H, Fischer D. Microglia Are Irrelevant for Neuronal Degeneration and Axon Regeneration after Acute Injury. *J Neurosci*. 2017;37(25):6113-6124. doi:10.1523/JNEUROSCI.0584-17.2017
19. REYNOLDS ES. The use of lead citrate at high pH as an electron-opaque stain in electron microscopy. *J Cell Biol*. 1963;17(1):208-212. doi:10.1083/jcb.17.1.208
20. George, D., & Mallery P. *SPSS for Windows Step by Step: A Simple Guide and Reference. 11.0 Update*. 4th ed. (Allyn & Bacon, ed.). Boston; 2003.
21. Faunce DE, Terajewicz A, Stein-Streilein J. Cutting edge: in vitro-generated tolerogenic APC induce CD8+ T regulatory cells that can suppress ongoing experimental autoimmune encephalomyelitis. *J Immunol*. 2004;172(4):1991-1995. http://www.ncbi.nlm.nih.gov/pubmed/14764660. Accessed June 10, 2018.
22. Linker RA, Gold R. MBP-induced experimental autoimmune encephalomyelitis in C57BL/6 mice. *J Immunol*. 2004;173(5):2896. http://www.ncbi.nlm.nih.gov/pubmed/15322142. Accessed June 10, 2018.
23. Diem R, Molnar F, Beisse F, et al. Treatment of optic neuritis with erythropoietin (TONE): a randomised, double-blind, placebo-controlled trial-study protocol. *BMJ Open*. 2016;6(3):e010956. doi:10.1136/bmjopen-2015-010956
24. Raftopoulos R, Hickman SJ, Toosy A, et al. Phenytoin for neuroprotection in patients with acute optic neuritis: a randomised, placebo-controlled, phase 2 trial. *Lancet Neurol*. 2016;15(3):259-269. doi:10.1016/S1474-4422(16)00004-1
25. Sühs K-W, Hein K, Sättler MB, et al. A randomized, double-blind, phase 2 study of erythropoietin in optic neuritis. *Ann Neurol*. 2012;72(2):199-210. doi:10.1002/ana.23573
26. Cadavid D, Balcer L, Galetta S, et al. Safety and efficacy of opicinumab in acute optic neuritis (RENEW): a randomised, placebo-controlled, phase 2 trial. *Lancet Neurol*. 2017;16(3):189-199. doi:10.1016/S1474-4422(16)30377-5
27. Aktas O, Albrecht P, Hartung H-P. Optic neuritis as a phase 2 paradigm for neuroprotection therapies of multiple sclerosis: update on current trials and perspectives. *Curr Opin Neurol*. 2016;29(3):199-204. doi:10.1097/WCO.0000000000000327
28. Dietrich M, Aktas O, Hartung H-P, Albrecht P. Assessing the anterior visual pathway in optic neuritis: recent experimental and clinical aspects. *Curr Opin Neurol*. 2019;32(3):346-357. doi:10.1097/WCO.0000000000000675
29. Lidster K, Jackson SJ, Ahmed Z, et al. Neuroprotection in a Novel Mouse Model of Multiple Sclerosis. Villoslada P, ed. *PLoS One*. 2013;8(11):e79188. doi:10.1371/journal.pone.0079188
30. Batoulis H, Recks MS, Addicks K, Kuerten S. Experimental autoimmune encephalomyelitis--achievements and prospective advances. *APMIS*. 2011;119(12):819-830. doi:10.1111/j.1600-0463.2011.02794.x
31. Gold R, Hartung HP, Toyka K V. Animal models for autoimmune demyelinating disorders of the nervous system. *Mol Med Today*. 2000;6(2):88-91. http://www.ncbi.nlm.nih.gov/pubmed/10652482. Accessed July 6, 2018.
32. Furlan R. MBP-specific experimental autoimmune encephalomyelitis in C57BL/6 mice. *J Immunol*. 2004;173(1):5; author reply 5-6. http://www.ncbi.nlm.nih.gov/pubmed/15210750. Accessed June 10, 2018.
33. Sagan SA, Winger RC, Cruz-Herranz A, et al. Tolerance checkpoint bypass permits emergence of pathogenic T cells to neuromyelitis optica autoantigen aquaporin-4. *Proc Natl Acad Sci*. 2016;113(51):14781-14786. doi:10.1073/pnas.1617859114
34. Kupersmith MJ, Garvin MK, Wang J-K, Durbin M, Kardon R. Retinal ganglion cell layer thinning within one month of presentation for optic neuritis. *Mult Scler*. 2016;22(5):641-648. doi:10.1177/1352458515598020

35. Petzold A, Balcer LJ, Calabresi PA, et al. Retinal layer segmentation in multiple sclerosis: a systematic review and meta-analysis. *Lancet Neurol*. 2017;16(10):797-812. doi:10.1016/S1474-4422(17)30278-8
36. Gabilondo I, Martínez-Lapiscina EH, Fraga-Pumar E, et al. Dynamics of retinal injury after acute optic neuritis. *Ann Neurol*. 2015;77(3):517-528. doi:10.1002/ana.24351
37. Balk LJ, Cruz-Herranz A, Albrecht P, et al. Timing of retinal neuronal and axonal loss in MS: a longitudinal OCT study. *J Neurol*. 2016;263(7):1323-1331. doi:10.1007/s00415-016-8127-y
38. Fischer MD, Huber G, Beck SC, et al. Noninvasive, in vivo assessment of mouse retinal structure using optical coherence tomography. *PLoS One*. 2009;4(10):e7507. doi:10.1371/journal.pone.0007507
39. Nishioka C, Liang H-F, Barsamian B, Sun S-W. Sequential phases of RGC axonal and somatic injury in EAE mice examined using DTI and OCT. *Mult Scler Relat Disord*. 2019;27:315-323. doi:10.1016/j.msard.2018.11.010
40. Manogaran P, Samardzija M, Schad AN, et al. Retinal pathology in experimental optic neuritis is characterized by retrograde degeneration and gliosis. *Acta Neuropathol Commun*. 2019;7(1):116. doi:10.1186/s40478-019-0768-5

Supplementary Files

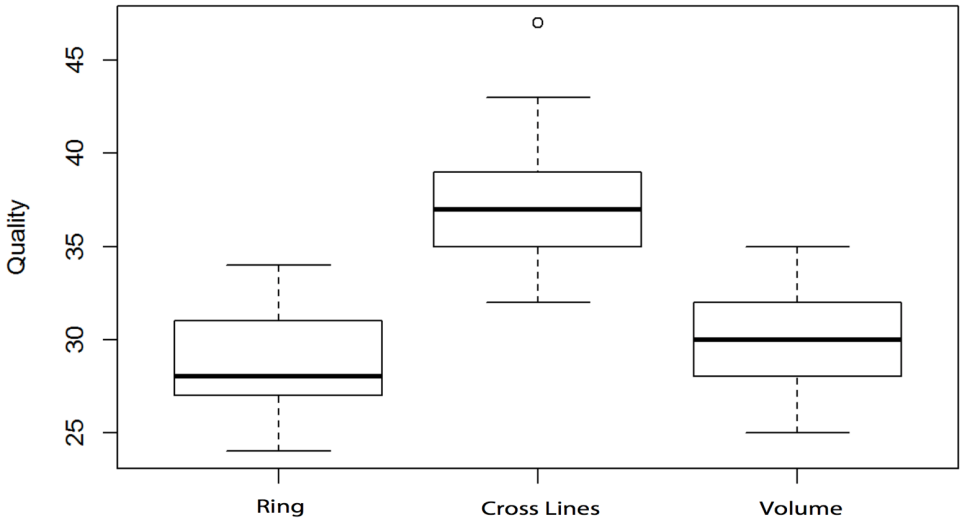

Supplementary figure 1 Quality scores (a measure of signal intensity). Quality above 20 is considered acceptable, quality above 30 is considered excellent.

A

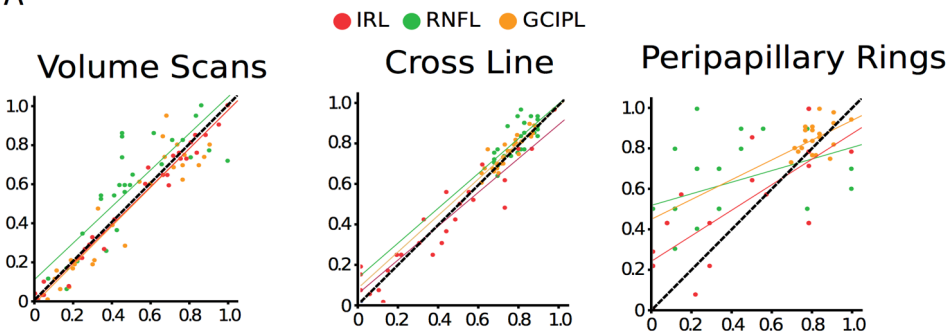

B

Scan	Layer	ICC	95%CI
Volume	IRL	0.995	0.989-0.998
	RNFL	0.902	0.771-0.957
	GCIPL	0.967	0.921-0.986
Cross Lines	IRL	0.961	0.913-0.983
	RNFL	0.828	0.533-0.930
	GCIPL	0.957	0.906-0.980
Ring	IRL	0.816	0.468-0.932
	RNFL	0.278	-0.244-0.666
	GCIPL	0.381	-0.673-0.764

Supplementary figure 2 A: OCT scans segmented by two independent raters with results plotted along a linear regression line. Each point represents a single eye of a mouse. The dotted line the reference for 100% agreement between both raters. Note the relatively improved performance characteristics for volume scans over line scans. B: Interclass correlation coefficients in the different protocols analyzed.

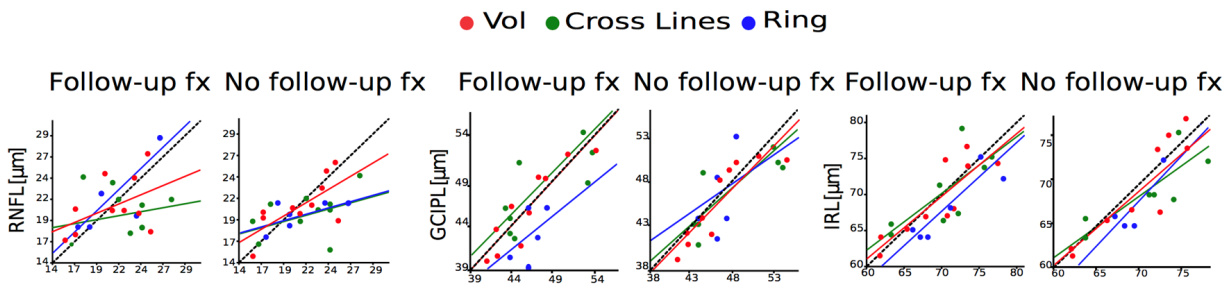

Protocol	Layer	Volume		Cross Lines		Ring	
		ICC	95%CI	ICC	95%CI	ICC	95%CI
Follow-up	IRL	0.927	(0.679-0.983)	0.886	(0.493-0.974)	0.891	(0.008-0.984)
	RNFL	0.657	(-0.693-0.923)	0.370	(-1.321- 0.848)	0.900	(0.454-0.984)
	GCIPL	0.954	(0.798-0.989)	0.877	(0.481-0.971)	0.780	(-0.284 -0.968)
No Follow-up	IRL	0.937	(0.741-0.985)	0.918	(0.492-0.983)	0.950	(0.508-0.993)
	RNFL	0.835	(0.255-0.962)	0.551	(-0.568-0.89)	0.624	(-0.655-0.937)
	GCIPL	0.938	(0.749-0.986)	0.937	(0.746-0.985)	0.787	(-0.648-0.968)

Supplementary figure 3 Serial OCT scans of wild-type mice segmented by a single rater. Note: animals were entirely removed and repositioned between scans. Table demonstrates the interclass correlation for different scan protocols. Note volume scans outperformed line scans and follow-up function adds little benefit to reproducibility. In addition, aggregating layers into either total retinal thickness or inner retinal layers generally outperforms individual layers.

Early alpha-lipoic acid therapy protects from degeneration of the inner retinal layers and vision loss in an experimental autoimmune encephalomyelitis-optic neuritis model

Michael Dietrich, Niklas Helling, Alexander Hilla, Annemarie Heskamp, Andrea Issberner, Thomas Hildebrandt, Zippora Kohne, Patrick Küry, Carsten Berndt, Orhan Aktas, Dietmar Fischer, Hans-Peter Hartung and Philipp Albrecht

Department of Neurology, Heinrich-Heine-University Düsseldorf, Germany

The presented manuscript was published in the “Journal of Neuroinflammation”, 2018

Contribution:
-First authorship
-Design of the study and experiments (50%)
-Execution, analysis and statistics of the following methods: Cell culture and toxicity assays (70%); OCT measurements (100%); OKR measurements (100%); EAE experiments: MOG EAE in C57Bl/6J mice and treatment with alpha-lipoic acid (100%); glutathione assay (70%); histology of optic nerve (90%) and retina (30%)
-Writing and drafting of the manuscript (80%)

Dietrich et al. Journal of Neuroinflammation (2018) 15:71
https://doi.org/10.1186/s12974-018-1111-y

Journal of Neuroinflammation

RESEARCH Open Access

Early alpha-lipoic acid therapy protects from degeneration of the inner retinal layers and vision loss in an experimental autoimmune encephalomyelitis-optic neuritis model

Michael Dietrich, Niklas Helling, Alexander Hilla, Annemarie Heskamp, Andrea Issberner, Thomas Hildebrandt, Zippora Kohne, Patrick Küry, Carsten Berndt, Orhan Aktas, Dietmar Fischer, Hans-Peter Hartung and Philipp Albrecht*

Abstract

Background: In multiple sclerosis (MS), neurodegeneration is the main reason for chronic disability. Alpha-lipoic acid (LA) is a naturally occurring antioxidant which has recently been demonstrated to reduce the rate of brain atrophy in progressive MS. However, it remains uncertain if it is also beneficial in the early, more inflammatory-driven phases. As clinical studies are costly and time consuming, optic neuritis (ON) is often used for investigating neuroprotective or regenerative therapeutics. We aimed to investigate the prospect for success of a clinical ON trial using an experimental autoimmune encephalomyelitis-optic neuritis (EAE-ON) model with visual system readouts adaptable to a clinical ON trial.

Methods: Using an in vitro cell culture model for endogenous oxidative stress, we compared the neuroprotective capacity of racemic LA with the R/S-enantiomers and its reduced form. In vivo, we analyzed retinal neurodegeneration using optical coherence tomography (OCT) and the visual function by optokinetic response (OKR) in $MOG_{35–55}$-induced EAE-ON in C57BL/6J mice. Ganglion cell counts, inflammation, and demyelination were assessed by immunohistological staining of retinae and optic nerves.

Results: All forms of LA provided equal neuroprotective capacities in vitro. In EAE-ON, prophylactic LA therapy attenuated the clinical EAE score and prevented the thinning of the inner retinal layer while therapeutic treatment was not protective on visual outcomes.

Conclusions: A prophylactic LA treatment is necessary to protect from visual loss and retinal thinning in EAE-ON, suggesting that a clinical ON trial starting therapy after the onset of symptoms may not be successful.

Keywords: Lipoic acid, EAE-ON, Optical coherence tomography, Optokinetic response, Multiple sclerosis, Neurodegeneration

* Correspondence: phil.albrecht@gmail.com
Department of Neurology, Medical Faculty, Heinrich-Heine University Düsseldorf, Moorenstr. 5, 40225 Düsseldorf, Germany

Background

Multiple sclerosis (MS) is an inflammatory autoimmune disorder that involves demyelination, oligodendrocyte death with subsequent axonal damage, and eventually loss of neurons in the central nervous system [1]. In the course of the disease, activated immune cells release mainly nitric oxide (NO) and other reactive oxygen species (ROS), leading to oxidative stress and contributing to the detrimental process of demyelination, axonal damage, and inflammation in both MS [2–5] and its animal model experimental autoimmune encephalomyelitis (EAE) [6, 7]. Especially in active phases of MS and in MS plaques, increased levels of free radicals along with particularly low levels of important antioxidants such as glutathione and vitamin E have been reported [8], suggesting a benefit of antioxidative and neuroprotective substances. However, until now, the vast majority of antioxidative therapeutic trials failed [9, 10], possibly due to the fact that readouts for neurodegeneration were not sensitive enough for short-term changes and not only detrimental aspects of reactive oxygen species (oxidative distress), but also essential signaling functions (oxidative eustress) were affected [9, 11].

Alpha-lipoic acid (LA), a naturally occurring sulfhydryl compound, is found in almost all plants and animals. It has strong antioxidant and anti-inflammatory properties [12]. Some authors have suggested that the (R)-enantiomer of LA is more potent [13] or that its reduced form dihydrolipoic acid (DHLA) is mainly responsible for the antioxidant effects [14]. A previous study has compared the efficacy of the different forms in EAE and demonstrated similar effects on inflammatory and clinical endpoints [15]. A randomized controlled clinical trial evaluating the effect of 1200 mg LA per day for 12 weeks on the antioxidant capacity and serum cytokine profiles revealed an increased total antioxidant capacity [16] and a reduction of pro-inflammatory cytokines INF-γ, ICAM-1, TGF-β, and IL-4 in relapsing-remitting MS [17] while the serum levels of TNF-α, IL-6, and MMP-9 and the clinical expanded disability status scale (EDSS) score were unchanged. In a recent phase II clinical study on secondary progressive MS (SPMS), the annualized percent change of brain volume (PCBV) was significantly reduced in patients receiving LA compared to placebo (− 0.21 ± 0.14 vs − 0.65 ± 0.10) [18].

Large conclusive phase III studies on LA efficacy to prevent clinical progression in MS are lacking. This is possibly owing to the fact that neurodegeneration progresses slowly and neuroprotective trials in MS require long observational periods and large sample sizes to evaluate efficacy on clinical outcomes making them very complicated and costly. Therefore, clinical trial designs with highly sensitive readouts for neurodegeneration and protection allowing shorter observational periods and smaller sample sizes are warranted.

In the past years, optical coherence tomography (OCT) has been established as a non-invasive and powerful tool for the evaluation of neurodegeneration in neurologic disorders [19–23]. This technology has been used in several clinical trials using ON as a model for screening protective and regenerative therapeutic approaches [24]. Furthermore, the high resolution of third-generation spectral-domain (SD)-OCT devices renders in vivo retinal imaging in small rodents possible and is therefore gaining an increasing importance in preclinical neurological research [25–29]. Neuroprotective effects of LA have been investigated in EAE, in the animal model of MS [15, 30–34], and in EAE-ON [35] using histological quantification of axons in the optic nerve. We aimed at comparing the neuroprotective properties of the single LA enantiomers and the reduced form using a model of endogenous oxidative stress in vitro and evaluating the neuroprotective effects of a prophylactic vs therapeutic LA treatment in EAE-ON using in vivo outcomes. The main purpose was to investigate if the previously observed preservation of optic nerve axons in EAE-ON translates to in vivo readouts of structure and function, namely OCT and optokinetic response (OKR), which can be applied in a phase II clinical trial on optic neuritis in patients.

Methods

Cell culture and glutamate toxicity assay

The HT22 cell line was cultured at 37 °C in a 5% CO2 atmosphere and Dulbecco's modified Eagle medium (DMEM) high glucose (ThermoFisher Scientific, GIBCO Life Technologies), containing 5% fetal calf serum (Hyclone), 100 U/mL penicillin, and 100 μg/mL streptomycin (GIBCO Life Technologies). For the cell viability assays, 5×10^3 HT22 cells were seeded in a 96-well plate and pre-incubated with either LA or DHLA (Sigma-Aldrich) for 9, 6, and 2 days or 1 day (d-9; d-6; d-2, − 24 h), treated at the same time (0 h), or hours (+ 3 h or + 6 h) after L-glutamate (Sigma-Aldrich) addition. Another 24 h later, cell viability was assessed using the CellTiter-Blue (Promega) assay as previously described [36].

Mice and induction of EAE

Female, 6-week-old C57BL/6J mice were purchased from Janvier Labs (Le Genest-Saint-Isle, France). Mice were immunized with 200 μg of myelin oligodendrocyte glycoprotein fragment 35–55 (MOG_{35-55}), purchased from BIOTREND emulsified in 200 μl of complete Freund's adjuvant (CFA), supplemented with 800 μg of heat-killed *Mt.*, H37Ra, both purchased from BD Difco (injected subcutaneous, distributed over four spots on the hind and front flank) and additional intraperitoneal

injections of 200 ng of pertussis toxin (PTX) from Sigma-Aldrich on days 0 and 2 after immunization. The sham control group (sham-EAE) also received PTX and CFA, but no MOG_{35-55} peptide. LA stock solution was prepared at 500 μM in dimethylsulfoxid (DMSO) and stored at − 80 °C until use. Treatment started either 1 week before (d-7), at the day of (d0), or 14 days after (d14) induction of EAE by adding LA stock solution (verum) or DMSO alone (vehicle) to the drinking water. Drinking water was replaced twice a week, uptake was measured daily, and the LA concentration was adjusted to a daily treatment dose of 100 mg/kg bodyweight (BW) per day. The clinical EAE score was graded daily according to the following criteria: (0) no disease, (0.5) mild tail paresis, (1) obvious tail paresis or plegia, (1.5) tail plegia and no righting reflex, (2) mild signs of hind limb paresis with clumsy gait, (2.5) obvious signs of hind limb paresis, (3) hind limb plegia; drags one hind limb behind, (3.5) hind limb plegia; drags both hind limbs behind (4) mild signs of quadriparesis (4.5) quadriplegia, and (5) death or moribund.

All animal procedures were performed in compliance with the experimental guidelines approved by the regional authorities (State Agency for Nature, Environment and Consumer Protection; AZ 84-02.4.2014.A059) and conform to the Association for Research in Vision and Ophthalmology (ARVO) Statement for the Use of Animals in Ophthalmic and Vision Research.

Optical coherence tomography

We report the OCT methodology in line with the APOSTEL recommendations [37], and an APOSTEL checklist is provided as supplementary material (see Additional file 1). The OCT measurements were performed with a Spectralis™ HRA+OCT device (Heidelberg Engineering, Germany) under ambient light conditions. The mice were positioned in a custom OCT holder described elsewhere [38] and anesthetized with isofluran vaporized at concentrations of 2.5% (2 L/min O_2). Their pupils were dilated with 2.5% phenylephrine-0.5% tropicamide ophthalmic solution (pharmacy of the University Hospital Düsseldorf). For imaging of the mouse retina, we used a custom contact lens and Visc-Ophtal eye gel (Dr. Winzer Pharma) during the examination to keep the eyes moist and to ensure a constant and homogenous refraction. A 25-diopter adaptor lens was placed on the objective lens of the OCT device to adapt the focus to the mouse eye and retina. The OCT imaging was carried out with the software integrated TruTrack™ eye tracking to diminish breathing artifacts and to achieve consistent ocular orientations.

We performed volume scans (25 × 25°) to analyze the thickness of the retinal layers. All scans were acquired with an initial focus distance of 38 diopters followed by manual correction. Each volume scan consisted of 25 B-Scans recorded in high-resolution mode at 50 automatic real time (ART, rasterized from 50 averaged A-Scans). We used automated segmentation by the Heidelberg Eye Explorer™ software version 1.9.10.0 followed by manual correction of a blinded investigator. The thickness measurements were derived from the circular 1, 2, and 3 mm early treatment of diabetic retinopathy study (ETDRS) grid centered on the optic disc, excluding the central part. We used the high-resolution mode; all scans had a quality of at least 20 dB. We calculated the thickness of the inner retinal layers (IRL), consisting of the retinal nerve fiber layer (RNFL), ganglion cell layer (GCL), and inner plexiform layer (IPL) by averaging each sector of the grid, excluding the center which corresponded to the optic nerve head.

Optokinetic response for visual function analysis

The optokinetic response analysis was carried out with a testing chamber and the OptoMotry™ software from CerebralMechanics™, Lethbride, Canada [39]. The mice were positioned on a platform in a box containing four screens displaying a moving grid creating a virtual cylinder with varying frequencies. The mice were monitored from above by a camera, and the head movements (tracking) were evaluated by an investigator blinded on the experimental groups. As a measure for visual acuity, we used the threshold of the highest spatial frequency at which the 100% contrast moving grid was still tracked by the mice. Clockwise tracking represented the left and counterclockwise the right eye. A more detailed description of the device and methodology is given elsewhere [40].

Tissue sampling and histological analysis

After 120 days of EAE, mice were sacrificed with an overdose of isofluran (Piramal Critical Care) and cardiac perfusion was performed with cold phosphate-buffered saline (PBS). Brains were extracted, washed in PBS, and frozen; optic nerves and retinae were isolated. Optic nerves were fixated in 4% paraformaldehyde (PFA) over night and dehydrated in sucrose solutions with increasing concentrations. After embedding in O.C.T. compound (Sakura™ Finetek), longitudinal sections of 5 μm were cut for immunohistological analysis. To examine $CD3^+$ lymphocyte and microglial infiltration and activation, as well as the myelin status of the optic nerves, slices were incubated with CD3- (1:400, Dako), Iba1- (1:500, Wako chemicals), and myelin basic protein (MBP)- (1:500, Millipore) antibodies, respectively. Cy3 anti-rat and Cy5 anti-rabbit (1:500, Millipore) were used as secondary antibodies. For rating the immune cell infiltration in optic nerves, hematoxylin and eosin (HE) staining was performed. Retinae were fixated in 4% PFA for 30 min and stained with βIII-tubulin antibody

(1:1000, Biolegend) and secondary antibody donkey anti-mouse IgG conjugated to Alexa Fluor 488 (1:1000, Invitrogen) for ganglion cell counting.

Microglial infiltration and activation were quantified by fluorescence intensity measurement of the Iba1 staining. The HE and CD3 staining results were rated by an investigator blinded to the experimental groups by a score [41] 0, no infiltration; 1, mild cellular infiltration; 2, moderate infiltration; 3, severe infiltration; and 4, massive infiltration.

The pathologic findings of the MBP staining were graded from 0 to 3 as previously described [42] by a blinded investigator: 0, no demyelination; 1, rare foci; 2, a few areas of demyelination; 3, large/confluent areas of demyelination.

Fluorescence-stained longitudinal optic nerve sections were acquired with a Leica HyD detector attached to a Leica DMi8 confocal microscope (× 63 objective lens magnification) and HE images with a camera (Olympus Color View III) attached to a Olympus BX51 microscope (× 20 objective lens magnification). At least four sections of the optic nerve, exclusively of the right eye of each mouse, were analyzed per staining. The entire longitudinal section of each optic nerve was included for rating and intensity measurement.

Detection of carbonylated proteins

Cortical brain samples were homogenized with a micro pestle on ice and re-suspended in NP-40 lysis buffer. The homogenate was incubated on ice for 30 min and vortexed every 10 min. Ice cold lysates were then sonicated three times at 10% power using a Bandelin Sonoplus UW2070 sonifier and cleared by centrifugation (4 °C, 12.000*g*, 15 min). Total protein carbonylation level was determined using the OxyBlot Protein Oxidation Detection Kit (Millipore) according to the manufacturer's protocol; the secondary antibody was replaced by the IRDye™ 680RD-conjugated goat-anti-rabbit (LI-COR Bioscience). The total fluorescence intensities were measured using a Li-COR Odyssey Clx Infrared Imaging System and normalized to β-actin (1:5000, Sigma).

Quantification of total glutathione

For estimation of reduced glutathione (GSH), 3×10^5 of HT22 cells were seeded in a 60-mm dish with 25 μM LA or vehicle DMSO treatment. After 24 h, glutamate was added at the indicated concentrations for 8 h and cells were harvested with lysis buffer. For measurement of GSH levels in tissue, frozen mouse cortices were homogenized with a micro pestle in PBS/EDTA buffer, sonicated, and transferred to lysis buffer. Tissue and cell samples were further processed and measured enzymatically as described previously [36] with a bicinchoninic acid assay for normalization against whole protein amount.

Statistics

Statistical analysis was performed using Microsoft Excel and Prism 5.0 (Graphpad). Data of the glutamate toxicity assays were fitted by sigmoid curves using the least squares method to estimate EC_{50}. A two-tailed analysis of variance (ANOVA) with Dunnett's post hoc test was used to compare the area under the curve for the glutamate toxicity assays, OCT courses and cumulative EAE scores. Group means were compared by one-way ANOVA with Dunnett's post hoc test using the means of both eyes of each animal for in vivo data and one eye per animal for the different histological investigations. Spearman correlations were performed to analyze the association between IRL thickness, OKR and clinical scores.

Results

LA and its reduced form protect from oxidative glutamate toxicity

To identify the effective concentrations and compare if both LA enantiomers and the reduced form DHLA are equally bioactive, we investigated their neuroprotective capacities in oxidative glutamate toxicity, an in vitro model of endogenous oxidative stress using the HT22 hippocampal mouse cell line. In this model, high concentrations of extracellular glutamate block the glutamate-cystine antiporter system (xc^-), resulting in GSH depletion and oxidative damage due to a lack of cellular cysteine.

LA or DHLA provided neuroprotective properties when pre-incubated 24 h before glutamate exposure. We observed no difference between the natural occurring (R)-(+)- and the (S)-(−)-enantiomers and similar EC_{50} values (Fig. 1a, b). At 10 mM glutamate, the EC_{50} value of DHLA was significantly improved compared to LA, suggesting that the reduced form has superior antioxidant capacities. The structural differences between the compounds are shown in Fig. 1c. Total intracellular GSH was measured 8 h after glutamate addition. An increase of the GSH levels in LA-treated cells was detected after a pretreatment of 24 h (Fig. 1d).

To examine the dynamics of these protective effects, several time course experiments were performed. An incubation with LA and its enantiomers 24 h before glutamate treatment led to a saturated protective effect while later treatment resulted in decreased cell survival (Fig. 2). Earlier LA treatment (days 9, 6, or 2), did not result in increased protection for the (R)-(+)- and (S)-(−)- enantiomers or the racemic mixture (see Additional file 2). The protective effect of DHLA was already saturated when it was added at the same time as the glutamate

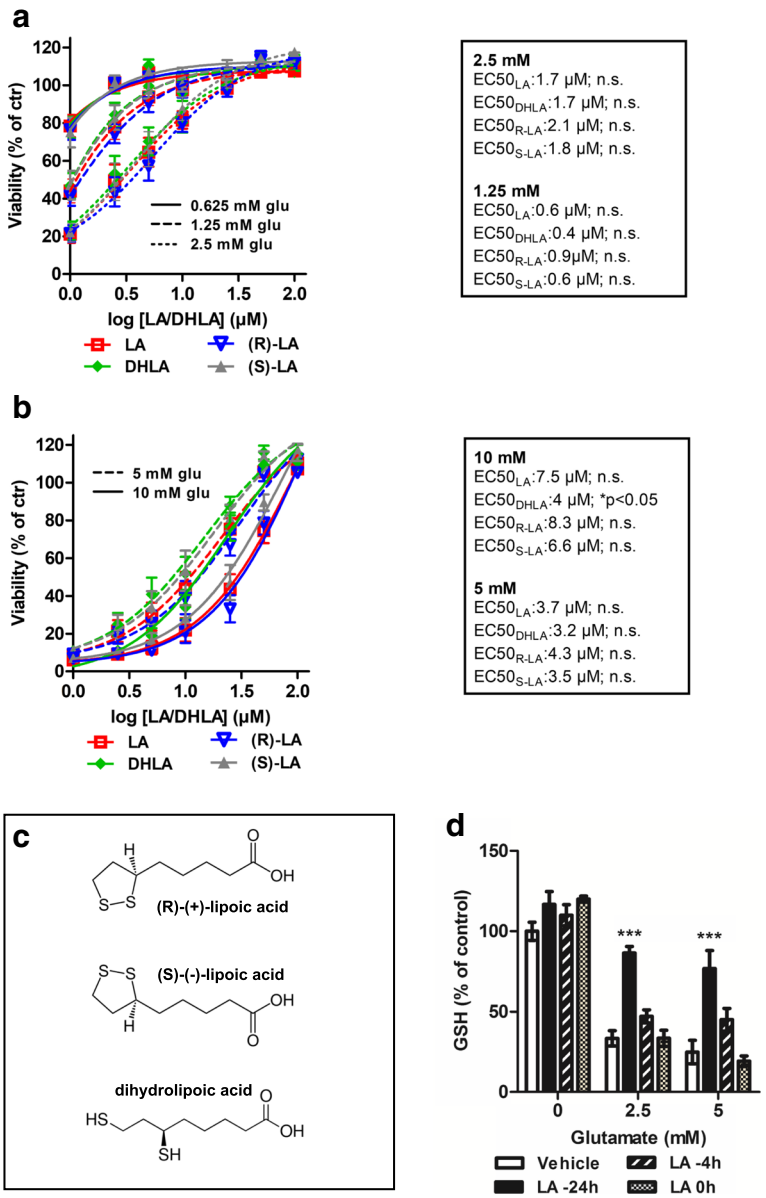

Fig. 1 Alpha-lipoic acid as well as its enantiomers and DHLA show protective effects in a model of oxidative glutamate toxicity. Five thousand HT22 cells were seeded into 96-well plates and treated with either vehicle or different concentrations of LA, DHLA, (S)-LA, or (R)-LA, followed by glutamate 24 h later. Graphs represent curve fits ± SEM for 0.625, 1.25, and 2.5 mM (**a**) and 5 or 10 mM (**b**) glutamate (glu) of five independent experiments, each performed in triplicates with corresponding EC_{50} values. Significant differences between LA and DHLA, (R)-LA, or (S)-LA treatments are indicated by asterisks (*$p < 0.05$, area under the curve compared by ANOVA with Dunnett's post hoc test). Structural formulas of the used compounds (**c**). For GSH, cells were treated with 25 μM LA for indicated time points and glutamate for additional 8 h before harvesting for protein extraction and enzymatic assay (**d**) (***$p < 0.001$, compared by two-way ANOVA with Dunnett's post hoc test to vehicle treatment)

addition, providing further evidence that antioxidant effects are mediated by the reduced form. However, all forms revealed the same protective capacity after a 24-h pretreatment. Our experiments demonstrated a few hour difference only between LA and DHLA. We therefore decided to carry out all following in vivo experiments with the racemic mixture of LA.

LA reduces the disability score and retinal degeneration in an EAE model

In order to test the potential of LA to protect from acute inflammatory relapses like optic neuritis, we investigated retinal neurodegeneration in $MOG_{33–55}$ peptide-induced EAE-ON in C57BL/6J mice. In this model, the rate of optic neuritis was very high with approximately 92% of

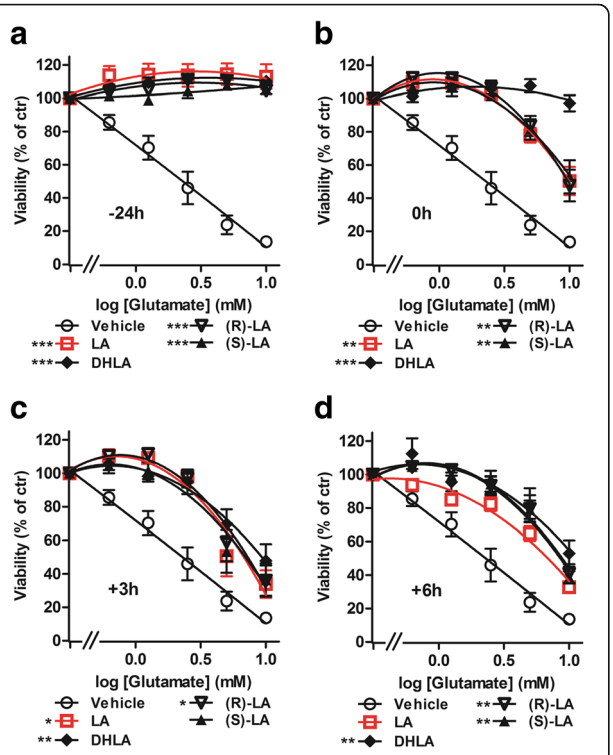

Fig. 2 Time course experiments reveal that DHLA acts faster than the precursor LA. Five thousand HT22 cells were seeded into 96-well plates and treated with either vehicle or 25 μM of LA, DHLA, (S)-LA, or (R)-LA starting 24 h before (**a**), at the same time (**b**), 3 h (**c**), or 6 h (**d**) after glutamate addition. Graphs represent curve fits ± SEM of four independent experiments, each performed in triplicates. Significant differences between vehicle and substance treatment are indicated by asterisks (*$p < 0.05$; **$p < 0.01$; ***$p < 0.001$, area under the curve compared by ANOVA with Dunnett's post hoc test)

nerves showing infiltrates in HE-stained longitudinal histological sections. Prophylactic treatment (d-7) with 100 mg/kg BW LA per day reduced the clinical score over a period of 120 days compared to vehicle (DMSO)-treated control mice ($p < 0.001$, one-way ANOVA analysis). A later initiation of LA therapy starting at days 0 and 14 after immunization led to a higher first peak of disease around day 14 and to subsequent higher clinical scores compared to mice treated with LA starting 7 days before MOG injection ($p < 0.01$, one-way ANOVA analysis) (Fig. 3a). Untreated sham control mice showed a nearly constant IRL thickness with minor growth over a period of 120 days, while MOG peptide-immunized animals presented a prominent loss of IRL thickness until day 60 and then a slow and steady decrease continuing until day 120 when they were sacrificed. Prophylactic LA treatment starting 7 days before and at the day of immunization resulted in an attenuated degeneration reflecting the course of the clinical EAE score. Therapeutic LA therapy starting at day 14 at the peak of the disease failed to preserve the inner retinal layers from degeneration (Fig. 3b). The clinical EAE score significantly correlated with the results of the OCT measurements (Fig. 3c) ($r = -0.51$, $p < 0.001$, Spearman). Prophylactic LA treatment increased GSH levels in the mouse cortex, while later treatment had no effect on the GSH concentration (Fig. 3d). However, the carbonylation of the proteins in the brain was not changed after LA treatment compared to untreated MOG control 120 days after EAE immunization (see Additional file 3).

Visual function and correlation of OKR and OCT readouts with the clinical EAE score

To analyze the visual function, we assessed the optokinetic response of the mice using the spatial frequency OKR threshold as a surrogate for visual acuity. The spatial frequency threshold was significantly reduced in EAE mice with values of 0.23 cycles per degree (c/d) compared to 0.33 c/d for sham-EAE control mice. A prophylactic LA treatment starting 7 days before or at the day of immunization (d0) reduced visual loss with spatial frequency values of 0.27 and 0.25 c/d, respectively, compared to 0.23 in vehicle-treated mice ($p < 0.001$, one-way ANOVA analysis). Therapeutic treatment starting at the first peak of disease (d14) had no beneficial effect on vision (Fig. 4a). These OKR values correlated significantly with the clinical EAE scores (Fig. 4b) ($r = -0.74$, $p < 0.001$, Spearman) and inversely with the thinning of the inner retinal layers (Fig. 4c) ($r = 0.49$, $p < 0.001$, Spearman).

Retinal ganglion cells are preserved after LA treatment

To elucidate, if the more severe IRL thinning and vision loss in therapeutically treated mice was a direct consequence of the degeneration of retinal ganglion cells (RGCs) or rather of the axons in the RNFL and/or the dendritic arbor in the IPL, we performed histological immunostainings of RGCs in retinal flat mounts using βIII-tubulin (Fig. 5a). The number of RGCs after 120 days was significantly lower ($p < 0.001$, one-way ANOVA analysis) in EAE mice (1181 cells/mm^2) compared to the sham-EAE control group (2214 cell/mm^2) confirming the results of the OCT scans. Interestingly, prophylactic ($p < 0.001$, one-way ANOVA analysis) as well as therapeutic LA treatment ($p < 0.01$, one-way ANOVA analysis) led to a higher viability of the RGCs compared to untreated EAE mice (Fig. 5b).

LA is anti-inflammatory but does not affect demyelination

As LA can reportedly reduce pro-inflammatory cytokines in relapsing-remitting MS [17], we performed histological analyses of immune cell infiltrates in optic nerve sections. We used antibodies directed against Iba1 and CD3, to stain for macrophages/microglia and CD3$^+$ lymphocytes, respectively (Fig. 6a). No significant

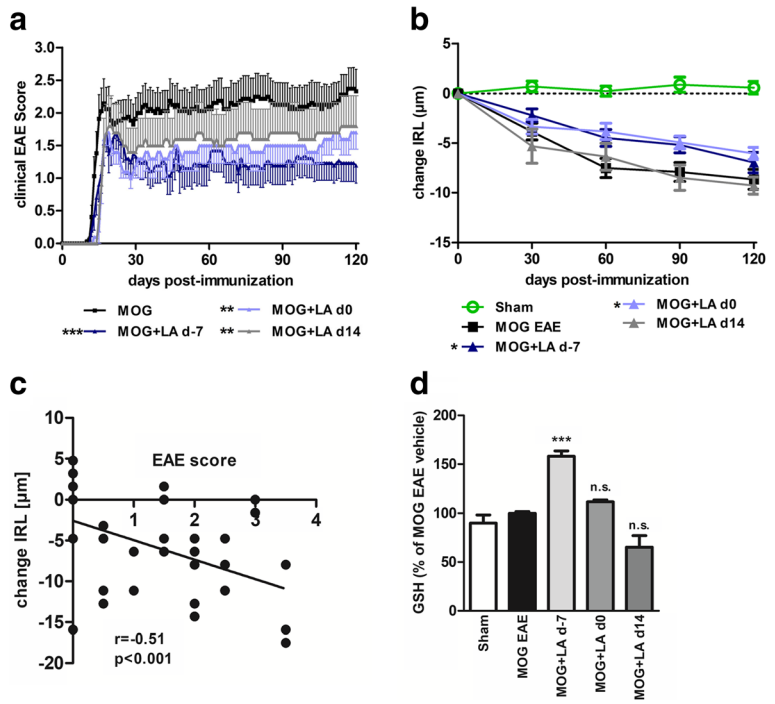

Fig. 3 The clinical course of MOG-induced EAE in C57BL/6J was attenuated, and the degeneration of the inner retinal layers was less pronounced in LA-treated mice. Prophylactic LA treatment acted beneficial on clinical EAE scores while later therapy had less pronounced effects (**a**). Thinning of the inner retinal layers was reduced during the EAE only when LA was administered prophylactically at the day of immunization or 7 days before while treatment at the onset of disease at day 14 had no effect (**b**). The correlation between the IRL thickness change and the EAE score at day 120 (**c**). GSH levels in the mouse cortices were significantly reduced after prophylactic LA treatment (**d**). Mice were scored daily, and OCT measurements were performed once a month over 120 days. GSH analysis was performed 120 days after EAE immunization. The time courses and bar graph present the pooled results of three independent EAE experiments with at least four mice per group (*$p < 0.05$; **$p < 0.01$; ***$p < 0.001$, area under the curve compared by ANOVA with Dunnett's post hoc test for time courses. Associations were calculated with Spearman correlation; each point represents an eye, some data points overlap. ***$p < 0.001$; n.s. = not significant, by ANOVA with Dunnett's post hoc test compared to MOG-untreated mice for bar graphs)

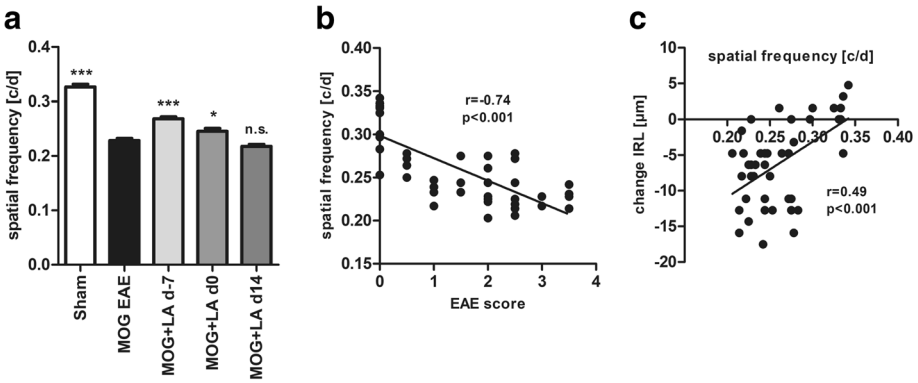

Fig. 4 Prophylactic LA treatment improved visual acuity of C57BL/6J mice compared to untreated mice with MOG EAE. OKR measurement was carried out 120 days after MOG immunization as described above (**a**). The bar graph represents the pooled mean ± standard deviation of at least three separate EAE experiments each with at least four animals per group (***$p < 0.001$, *$p < 0.05$, n.s. = not significant, by ANOVA with Dunnett's post hoc test compared to MOG-untreated mice). We found a correlation between clinical EAE score and the spatial frequency threshold from OKR measurements at day 120 (**b**) as well as the OKR values and the thickness change of the inner retinal layers at day 120 (**c**). Associations were calculated with Spearman correlation; each point represents an eye, some data points overlap. Results represent data from three pooled experiments each with at least three mice per group

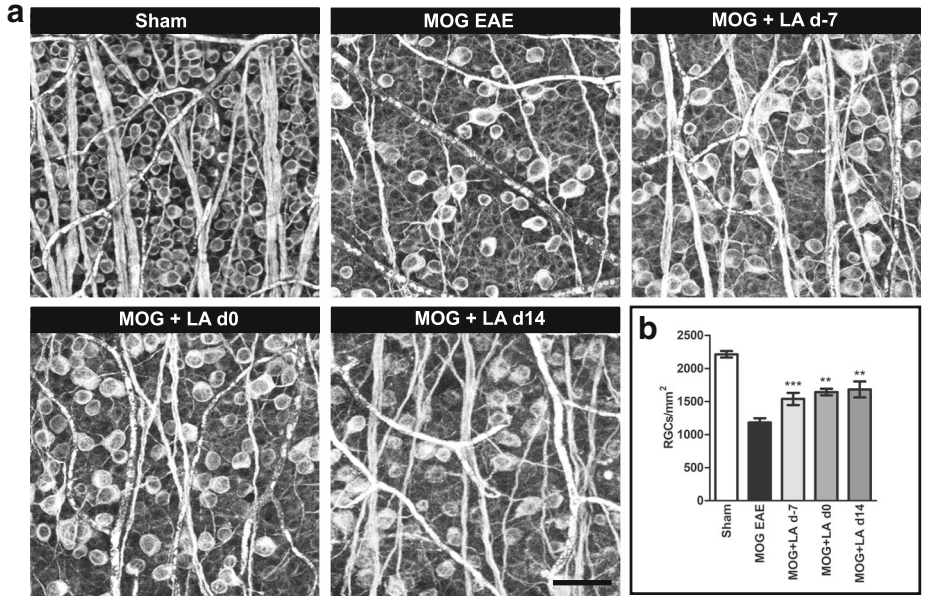

Fig. 5 In line with the results of the OCT measurements, LA treatment is beneficial for RGC survival in a MOG EAE in C57BL/6J. One hundred twenty days after immunization with MOG peptide, mice were sacrificed and an enucleation was performed followed by isolation and mounting of the retinae. RGCs were stained with βIII-tubulin antibody (**a**). The bar graph shows the RGC cell number 120 days after immunization; bar = 50 μm (**b**). The bar graph represents the pooled mean ± SEM of three separate EAE experiments each with at least four animals per group; one retina per mouse was included. (*$p < 0.05$; ***$p < 0.001$, by ANOVA with Dunnett's post hoc test compared to MOG-untreated mice)

reduction of microglial/macrophage infiltration and activity or infiltration of $CD3^+$ T lymphocytes was observed in the mouse optic nerves that had been prophylactically treated with LA as compared to untreated EAE mice. There was, however, a non-significant trend towards a decreased activation/infiltration (Fig. 6b). Therapeutic LA treatment had no effect on microglial/macrophage or lymphocyte infiltration in the optic nerve (see Additional file 4: Figure S3a–b).

To analyze the degree of (de)myelination, we performed immunohistological stainings against the MBP protein. Optic nerves immunized with MOG peptide exhibited large areas of demyelination while sham-EAE mice showed a uniform MBP expression pattern after 120 days (Fig. 6b). The optic nerve myelin status, rated by investigators blinded for the experimental groups, was improved neither after prophylactic (Fig. 6b) nor after therapeutic (see Additional file 4: Figure S3c) LA therapy.

HE staining was then performed to investigate the overall infiltration of immune cells into the optic nerves (Fig. 7a). An investigator blinded for the experimental groups rated the degree of severity using an established score [41]. Optic nerves of the sham-immunized control group showed normal histology, whereas MOG immunization resulted in a severe infiltration of inflammatory cells, confirming an established neuritis in 92% of analyzed optic nerves/animals. Pretreatment with LA 7 days before immunization resulted in a significant reduction of infiltrates compared to the optic nerves of the untreated MOG group, while a later LA therapy (d0 or d14) had no effect on the number of immune cells (Fig. 7b).

Discussion

In multiple sclerosis (MS), permanent disability mainly results from neuronal degeneration which occurs already early on in the course of disease. There is still an unmet need for substances to prevent this degeneration and to prevent permanent disability. As oxidative damage is thought to play an important role in the pathogenesis of neurodegeneration [1], substances with antioxidant properties may be suitable therapeutics. LA is a natural antioxidant available as an oral food supplement. It has an excellent safety profile and has proven to be an effective therapy for EAE [30, 32, 35, 43]. Furthermore, in a recent randomized, placebo-controlled phase II clinical study, brain volume loss over 2 years measured by magnetic resonance imaging was significantly reduced in SPMS under oral treatment with 1200 mg LA per day compared to placebo [18].

The (R)-racemic form of LA is naturally occurring [44] and has been suggested to be superior to the (S)-enantiomer in terms of bioavailability [45–48]. To investigate their neuroprotective capacities independently of a possible immunomodulatory mode of action, we first compared these different forms of LA in a model of

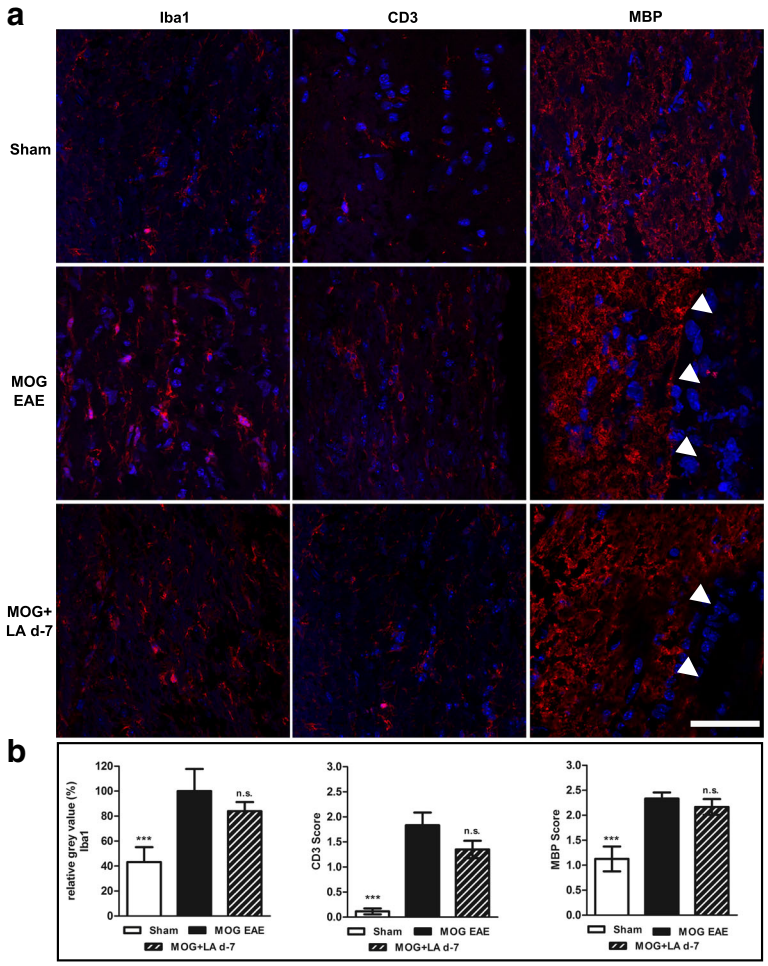

Fig. 6 Microglial activation and T cell infiltration were not altered in optic nerves of EAE mice after LA treatment. LA also failed to reduce demyelinating lesions. One hundred twenty days after MOG immunization, mice were sacrificed and optic nerves were extracted and processed, and longitudinal sections were prepared for Iba1, MBP, and CD3 staining (**a**). Optic nerves of sham-EAE, MOG EAE, and MOG EAE with LA-treated mice were compared for microglia activation by fluorescence intensity measurement, by an MBP myelination score for myelin status, and by a CD3 score for T cell Infiltration; quantitative analyses of the results of three independent EAE experiments with at least four mice are shown as bar graphs; bar = 50 μm (**b**); one optic nerve per mouse was included. (***$p < 0.001$, n.s. = not significant, by ANOVA with Dunnett's post hoc test compared to MOG-untreated mice)

endogenous oxidative glutamate stress in HT22 cells. We found that both enantiomers have identical antioxidative effects and that the racemic mixture can be used for further investigations. We then selected 25 μM LA (~ 5.2 μg/mL) for further in vitro investigations as this concentration is achieved in the serum of patients during oral therapy [31]. We determined the dynamics of the protection against oxidative damage by incubating HT22 cells starting from different time points, prior and after glutamate addition. Albeit the (R)-enantiomer of LA is reduced to DHLA 28 times faster by mitochondrial lipoamide dehydrogenase than (S)-LA [49] in our hands, (R)-LA had no superior effect in cell culture. Using DHLA, the neuroprotective capacity was already saturated when the drug was administered simultaneously with glutamate. This is consistent with the assumption that LA has to be reduced to develop its antioxidative potential. However, the difference between the racemic mixture of LA and DHLA was only 24 h, which is most likely irrelevant in a clinical context. Moreover, because racemic LA had a good safety profile in clinical studies, even at very high doses (1200 mg/day), we decided to carry out the in vivo studies with the commercially available racemic form of LA.

Our aim was to investigate if LA is also neuroprotective during the early, inflammatory disease stages of relapsing MS. Phase II and III studies with clinical endpoints related to neuroprotection are extremely time consuming and costly as neuronal degeneration in MS is a slow process and disability progresses over months

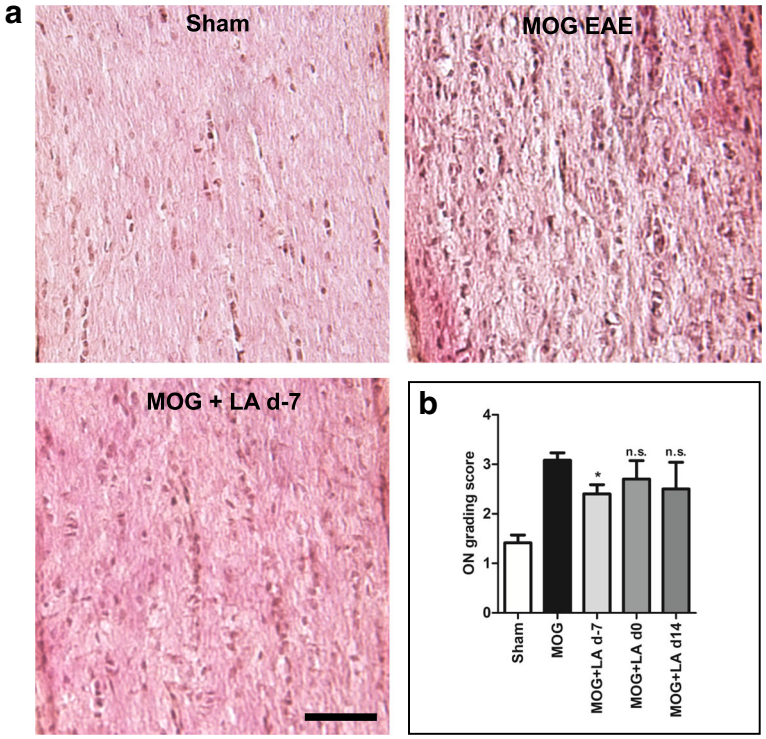

Fig. 7 Immune cell infiltration into the optic nerves was reduced after LA treatment. One hundred twenty days after MOG immunization, mice were sacrificed and optic nerves were extracted and processed and longitudinal cuts were prepared for HE staining, bar = 100 μm (**a**). Optic nerves from sham, MOG, and MOG with LA-treated mice were compared by an established infiltration score [41]; results are shown in the bar graph (**b**). The bar graph represents the pooled mean ± standard deviation of at least two separate EAE experiments each with at least four animals per group; one optic nerve per mouse was included (*$p < 0.05$, n.s. = not significant, by ANOVA with Dunnett's post hoc test compared to MOG-untreated mice)

and years. This deficiency of substitute models for clinical progression has limited the design of neuroprotection trials in MS. Preclinical study designs with readouts directly transferable to clinical trials are therefore of increasing interest. Our experiments aimed to evaluate whether a clinical optic neuritis trial could be reasonable since similar existing preclinical studies [35] lack of visual system readouts.

Moreover, the effect size of an OCT outcome is much higher in a study on optic neuritis where a greater loss of thickness occurs over a much shorter time period [24, 50, 51], therefore largely increasing the chances of a positive result. The MOG peptide-induced EAE-ON model used in the present study constitutes an ideal model to analyze the pathology occurring after an acute ON. It was therefore important to clarify whether the outcome of a previously published study [35] could be copied in our EAE-ON model with visual in vivo readouts as these are broadly used in ON studies. We tested if therapeutic or only prophylactic LA treatment during EAE might have a protective potential. The clinical EAE score was significantly improved after LA treatment, conclusive with many other studies [32, 35, 43], which, however, did not apply in vivo visual readouts. It was therefore crucial to analyze these animals by longitudinal methods such as OCT and OKR [32, 35, 43]. LA treatment starting at the same day or 7 days after MOG injection still had a beneficial effect on the clinical score but was less prominent as compared to early therapy. The inner retinal layers consisting of the retinal nerve fiber layer, the ganglion cell layer, and the inner plexiform layer containing their dendritic arbor is the ideal structure to study neuroprotection and retinal thinning in MS as all these layers show thinning in the context of MS and ON [19–21].

Over a period of 120 days, inner retinal layer degeneration and visual function loss of EAE mice treated with LA prophylactically (d-7) or at the day of immunization (d0) were reduced compared to untreated EAE mice. We found a link between the degeneration of the inner retinal layers and the loss of visual acuity in the EAE mice. A correlation between EAE score and vision loss was also observed in similar studies [52–54]. Single outliners might be due to the occurrence of optic neuritis in the absence of a clinical disability of the animals.

In order to assess the severity of RGC damage at later time points of therapy, we performed βIII-tubulin

staining of retinal flat mounts and counted their numbers. Remarkably, but in line with a previous study [35], the RGCs were protected to the same level by a therapeutic and prophylactic LA treatment. Even though the RGCs were little harmed after therapeutic treatment, visual function was not preserved and it had no effect on IRL thinning indicating an irreversible damage occurring at the very early phase of disease and a delayed protective effect of LA. Such discrepancy between the OCT outcome and RGC counts may be explained by a degeneration of the inner plexiform and retinal nerve fiber layers, which cannot be prevented by a treatment starting at the onset of symptoms while the cell bodies of the neurons remain intact. Robust protective effects have also been found by other researchers in a RGC line after hydrostatic pressure [55] and serum deprivation-induced injury, as well as in vivo after an optic nerve crush [56], suggesting a neuroprotective mode of action based on its antioxidant capacities. These abilities are generated by (1) direct scavenging of ROS and free radicals [43]; (2) the induction of detoxification enzymes, like NAD(P)H:quinone oxidoreductase and glutathione-S-transferase [57]; and (3) the increase of the GSH levels in the tissue [58]. In line with this, we observed increased GSH levels under prophylactic LA therapy in the brain of our mice.

However, besides its neuroprotective capacities, the decreased infiltrates observed in our HE-stained sections suggest additional anti-inflammatory effects. Anti-inflammatory properties of LA have so far been attributed to inhibitory effects of LA on T cell migration as it has been reported to inhibit matrix metalloproteinase-9 and the adhesion molecules ICAM-1 and VCAM-1 on the endothelium of the central nervous system [35]. Additionally, it was shown to increase cAMP levels in natural killer cells and thereby inhibiting their function [32]. The fact that in our study numbers on the infiltration of $CD3^+$ lymphocytes, on microglia presence, and on degree of demyelination failed to reach significance may be due to the sample size, which was powered for the in vivo readout and on RGC staining.

Conclusions

Therapeutic treatment with LA attenuates the clinical disability and preserves the survival of RGCs in the EAE-ON model. However, only a prophylactic therapy is capable of preserving visual function and of positively influencing OCT outcomes. We therefore conclude that LA might not be the ideal substance to be investigated in a clinical ON trial, which would use very similar in vivo readouts starting treatment after the onset of clinical symptoms. Nevertheless, our data provide strong evidence that a prophylactic treatment is superior to a therapeutic one and that it is effective already during the first relapse. This supports the concept of an early LA therapy, which should be started as early as possible and could be administered add-on to an immunomodulatory treatment.

Additional files

Additional file 1: Table S1. Advised Protocol for OCT Study Terminology and Elements (APOSTEL) checklist; each item discussed in the manuscript on the indicated page. (PDF 30 kb)

Additional file 2: Figure S1. LA treatment days before glutamate induced oxidative stress did not result in improved HT22 protection compared to a 24 h pre-incubation. 5000 cells were seeded into 96-well plates and pre-incubated 9 days (a), 6 days (b) or 2 days (c) before glutamate addition either with vehicle or 25 μM LA DHLA, (R)-LA or (S)-LA. Graphs represent curve fits ±SEM of four independent experiments, each performed in triplicates. Significant differences between vehicle- and substance-treatment are indicated by asterisks (***$p < 0.001$, area under the curve compared by ANOVA with Dunnett's post hoc test). (PDF 256 kb)

Additional file 3: Figure S2. The carbonylation of proteins did not change 120 days after EAE immunization. The bar graphs represent the pooled mean ± standard deviation of at least three separate EAE experiments each with at least three animals per group (n.s. = not significant, by ANOVA with Dunnett's post hoc test compared to MOG untreated mice). (PDF 165 kb)

Additional file 4: Figure S3. Optic nerves of sham-EAE, MOG-EAE and MOG-EAE with therapeutic LA treated mice were compared for microglia activation by fluorescence intensity measurement (a), by a CD3 score for T-cell Infiltration (b) and by a MBP myelination score for myelin status (c); quantitative analyses of the results of three independent EAE experiments with at least four mice are shown as bar graphs; one ON per mouse was included. (***$p < 0.001$, n.s. = not significant, by ANOVA with Dunnett's post hoc test compared to MOG untreated mice). (PDF 227 kb)

Abbreviations

ANOVA: Analysis of variance; ART: Automatic real time; BW: Bodyweight; c/d: Cycles per degree; CFA: Complete Freund's adjuvant; DHLA: Dihydrolipoic acid; DMEM: Dulbecco's modified Eagle medium; DMSO: Dimethylsulfoxid; EAE: Experimental autoimmune encephalomyelitis; EDSS: Expanded disability status scale; ETDRS: Early treatment of diabetic retinopathy study; GCL: Ganglion cell layer; glu: Glutamate; GSH: Glutathione; HE: Hematoxylin and eosin; IPL: Inner plexiform layer; IRL: Inner retinal layer; LA: Alpha-lipoic acid; MBP: Myelin basic protein; $MOG_{35–55}$: Myelin oligodendrocyte glycoprotein fragment 35–55; MS: Multiple sclerosis; NO: Nitric oxide; OCT: Optical coherence tomography; OKR: Optokinetic response; ON: Optic neuritis; PBS: Phosphate-buffered saline; PCBV: Percent change of brain volume; PFA: Paraformaldehyde; PTX: Pertussis toxin; RGCs: Retinal ganglion cells; RNFL: Retinal nerve fiber layer; ROS: Reactive oxygen species; SD-OCT: Spectral-domain OCT; SPMS: Secondary progressive multiple sclerosis

Acknowledgements

Not applicable.

Funding

This work was supported by grants to PA from the "Forschungskommission" of the Medical Faculty of the Heinrich-Heine University Düsseldorf.

Availability of data and materials

The dataset obtained and analyzed in the current study is available from the corresponding author on a reasonable request.

Authors' contributions

MD, NH, AH, AMH, AI, TH, and ZK performed the experiments and analyzed the data; MD and PA wrote the manuscript; PK, CB, OA, DF, and HPH were involved in revising the manuscript critically for important intellectual content and made substantial contributions to the interpretation of data. PA

conceived the study and supervised the experiments. All authors read and approved the final manuscript.

Ethics approval
All protocols involving animals were compliance with the experimental guidelines approved by the regional authorities (State Agency for Nature, Environment and Consumer Protection) and conform to the Association for Research in Vision and Ophthalmology (ARVO) Statement for the Use of Animals in Ophthalmic and Vision Research.

Consent for publication
Not applicable.

Competing interests
The authors declare that they have no competing interests. The following financial disclosures are unrelated to the work: Michael Dietrich received speaker honoraria from Novartis. Carsten Berndt received research support from Biogen. Patrick Küry performed consultancy work for Geneuro. Orhan Aktas received grants from the German Research Foundation (DFG) and the German Ministry of Education and Research (BMBF); grants and personal fees from Bayer HealthCare, Biogen, Genzyme, Novartis, and Teva; and personal fees from Almirall, MedImmune, Merck Serono, and Roche. Hans-Peter Hartung has received fees for serving on steering committees from Biogen Idec, GeNeuro, Sanofi Genzyme, Merck, Novartis Pharmaceuticals, Octapharma, Opexa Therapeutics, Teva Pharmaceuticals, MedImmune, Bayer HealthCare, Forward Pharma, and Roche; fees for serving on advisory boards from Biogen Idec, Sanofi Genzyme, Merck, Novartis Pharmaceuticals, Octapharma, Opexa Therapeutics, Teva Pharmaceuticals, and Roche; and lecture fees from Biogen Idec, Sanofi Genzyme, Merck, Novartis Pharmaceuticals, Octapharma, Opexa Therapeutics, Teva Pharmaceuticals, MedImmune, and Roche. Philipp Albrecht received compensation for serving on Scientific Advisory Boards for Ipsen, Novartis, and Biogen; he received speaker honoraria and travel support from Novartis, Teva, Biogen, Merz Pharmaceuticals, Ipsen, Allergan, Bayer Healthcare, Esai, UCB, and Glaxo Smith Kline; he received research support from Novartis, Biogen, Teva, Merz Pharmaceuticals, Ipsen, and Roche. The other authors report no disclosures.

Publisher's Note

Received: 23 January 2018 Accepted: 28 February 2018
Published online: 07 March 2018

References
1. Compston A, Coles A. Multiple sclerosis. Lancet. 2008;372:1502–17.
2. Witherick J, Wilkins A, Scolding N, Kemp K. Mechanisms of oxidative damage in multiple sclerosis and a cell therapy approach to treatment. Autoimmune Dis. 2010;2011:164608.
3. van der Goes A, Brouwer J, Hoekstra K, Roos D, van den Berg TK, Dijkstra CD. Reactive oxygen species are required for the phagocytosis of myelin by macrophages. J Neuroimmunol. 1998;92:67–75.
4. Wang P, Xie K, Wang C, Bi J. Oxidative stress induced by lipid peroxidation is related with inflammation of demyelination and neurodegeneration in multiple sclerosis. Eur Neurol. 2014;72:249–54.
5. van Horssen J, Witte ME, Schreibelt G, de Vries HE. Radical changes in multiple sclerosis pathogenesis. Biochim Biophys Acta. 2011;1812:141–50.
6. Nikic I, Merkler D, Sorbara C, Brinkoetter M, Kreutzfeldt M, Bareyre FM, et al. A reversible form of axon damage in experimental autoimmune encephalomyelitis and multiple sclerosis. Nat Med. 2011;17:495–9.
7. Ruuls SR, Bauer J, Sontrop K, Huitinga I, A't Hart B, Dijkstra CD. Reactive oxygen species are involved in the pathogenesis of experimental allergic encephalomyelitis in Lewis rats. J Neuroimmunol. 1995;56:207–17.
8. Gilgun-Sherki Y, Melamed E, Offen D. The role of oxidative stress in the pathogenesis of multiple sclerosis: the need for effective antioxidant therapy. J Neurol. 2004;251:261–8.
9. Lepka K, Berndt C, Hartung H-P, Aktas O. Redox events as modulators of pathology and therapy of neuroinflammatory diseases. Front Cell Dev Biol. 2016;4:63.
10. Carvalho AN, Firuzi O, Gama MJ, van Horssen J, Saso L. Oxidative stress and antioxidants in neurological diseases: is there still hope? Curr Drug Targets. 2017;18:705–18.
11. Sies H, Berndt C, Jones DP. Oxidative stress. Annu Rev Biochem. 2017; 86:715–48.
12. Odabasoglu F, Halici Z, Aygun H, Halici M, Atalay F, Cakir A, et al. α-Lipoic acid has anti-inflammatory and anti-oxidative properties: an experimental study in rats with carrageenan-induced acute and cotton pellet-induced chronic inflammations. Br J Nutr. 2011;105:31–43.
13. Uchida R, Okamoto H, Ikuta N, Terao K, Hirota T. Enantioselective pharmacokinetics of α-lipoic acid in rats. Int J Mol Sci. 2015;16:22781–94.
14. Holmquist L, Stuchbury G, Berbaum K, Muscat S, Young S, Hager K, et al. Lipoic acid as a novel treatment for Alzheimer's disease and related dementias. Pharmacol Ther. 2007;113:154–64.
15. Marracci GH, Jones RE, McKeon GP, Bourdette DN. Alpha lipoic acid inhibits T cell migration into the spinal cord and suppresses and treats experimental autoimmune encephalomyelitis. J Neuroimmunol. 2002;131:104–14.
16. Khalili M, Eghtesadi S, Mirshafiey A, Eskandari G, Sanoobar M, Sahraian MA, et al. Effect of lipoic acid consumption on oxidative stress among multiple sclerosis patients: a randomized controlled clinical trial. Nutr Neurosci. 2014;17:16–20.
17. Khalili M, Azimi A, Izadi V, Eghtesadi S, Mirshafiey A, Sahraian MA, et al. Does lipoic acid consumption affect the cytokine profile in multiple sclerosis patients: a double-blind, placebo-controlled, randomized clinical trial. Neuroimmunomodulation. 2014;21:291–6.
18. Spain R, Powers K, Murchison C, Heriza E, Winges K, Yadav V, et al. Lipoic acid in secondary progressive MS: a randomized controlled pilot trial. Neurol Neuroimmunol Neuroinflamm. 2017;4:e374.
19. Albrecht P, Müller A-K, Ringelstein M, Finis D, Geerling G, Cohn E, et al. Retinal neurodegeneration in Wilson's disease revealed by spectral domain optical coherence tomography. PLoS One. 2012;7:e49825.
20. Albrecht P, Ringelstein M, Muller AK, Keser N, Dietlein T, Lappas A, et al. Degeneration of retinal layers in multiple sclerosis subtypes quantified by optical coherence tomography. Mult Scler. 2012;18:1422–9.
21. Albrecht P, Muller A-K, Sudmeyer M, Ferrea S, Ringelstein M, Cohn E, et al. Optical coherence tomography in parkinsonian syndromes. PLoS One. 2012;7:e34891.
22. Thomson KL, Yeo JM, Waddell B, Cameron JR, Pal S. A systematic review and meta-analysis of retinal nerve fiber layer change in dementia, using optical coherence tomography. Alzheimers Dement (Amst). 2015;1:136–43.
23. Knier B, Berthele A, Buck D, Schmidt P, Zimmer C, Mühlau M, et al. Optical coherence tomography indicates disease activity prior to clinical onset of central nervous system demyelination. Mult Scler. 2016;22:893–900.
24. Aktas O, Albrecht P, Hartung HP. Optic neuritis as a phase 2 paradigm for neuroprotection therapies of multiple sclerosis: update on current trials and perspectives. Curr Opin Neurol. 2016;29:199–204.
25. Groh J, Stadler D, Buttmann M, Martini R. Non-invasive assessment of retinal alterations in mouse models of infantile and juvenile neuronal ceroid lipofuscinosis by spectral domain optical coherence tomography. Acta Neuropathol Commun. 2014;2:54.
26. Knier B, Rothhammer V, Heink S, Puk O, Graw J, Hemmer B, Korn T. Neutralizing IL-17 protects the optic nerve from autoimmune pathology and prevents retinal nerve fiber layer atrophy during experimental autoimmune encephalomyelitis. J Autoimmun. 2014;56:34–44.
27. Berger A, Cavallero S, Dominguez E, Barbe P, Simonutti M, Sahel J-A, et al. Spectral-domain optical coherence tomography of the rodent eye: highlighting layers of the outer retina using signal averaging and comparison with histology. PLoS One. 2014;9:e96494.
28. Hein K, Gadjanski I, Kretzschmar B, Lange K, Diem R, Sättler MB, Bähr M. An optical coherence tomography study on degeneration of retinal nerve fiber layer in rats with autoimmune optic neuritis. Invest Ophthalmol Vis Sci. 2012;53:157–63.
29. Fischer MD, Huber G, Beck SC, Tanimoto N, Muehlfriedel R, Fahl E, et al. Noninvasive, in vivo assessment of mouse retinal structure using optical coherence tomography. PLoS One. 2009;4:e7507.
30. Wang K-C, Tsai C-P, Lee C-L, Chen S-Y, Lin G-J, Yen M-H, et al. α-Lipoic acid enhances endogenous peroxisome-proliferator-activated receptor-gamma to ameliorate experimental autoimmune encephalomyelitis in mice. Clin Sci (Lond). 2013;125:329–40.
31. Yadav V, Marracci GH, Munar MY, Cherala G, Stuber LE, Alvarez L, et al. Pharmacokinetic study of lipoic acid in multiple sclerosis: comparing mice and human pharmacokinetic parameters. Mult Scler. 2010;16:387–97.
32. Salinthone S, Schillace RV, Marracci GH, Bourdette DN, Carr DW. Lipoic acid stimulates cAMP production via the EP2 and EP4 prostanoid receptors and

inhibits IFN gamma synthesis and cellular cytotoxicity in NK cells. J Neuroimmunol. 2008;199:46–55.
33. Jones RE, Moes N, Zwickey H, Cunningham CL, Gregory WL, Oken B. Treatment of experimental autoimmune encephalomyelitis with alpha lipoic acid and associative conditioning. Brain Behav Immun. 2008;22:538–43.
34. Morini M, Roccatagliata L, Dell'Eva R, Pedemonte E, Furlan R, Minghelli S, et al. Alpha-lipoic acid is effective in prevention and treatment of experimental autoimmune encephalomyelitis. J Neuroimmunol. 2004;148:146–53.
35. Chaudhary P, Marracci G, Yu X, Galipeau D, Morris B, Bourdette D. Lipoic acid decreases inflammation and confers neuroprotection in experimental autoimmune optic neuritis. J Neuroimmunol. 2011;233:90–6.
36. Albrecht P, Bouchachia I, Goebels N, Henke N, Hofstetter HH, Issberner A, et al. Effects of dimethyl fumarate on neuroprotection and immunomodulation. J Neuroinflammation. 2012;9:163.
37. Cruz-Herranz A, Balk LJ, Oberwahrenbrock T, Saidha S, Martinez-Lapiscina EH, Lagreze WA, et al. The APOSTEL recommendations for reporting quantitative optical coherence tomography studies. Neurology. 2016;86:2303–9.
38. Dietrich M, Cruz-Herranz A, Yiu H, Aktas O, Brandt AU, Hartung HP, et al. Whole-body positional manipulators for ocular imaging of anaesthetised mice and rats: a do-it-yourself guide. BMJ Open Ophthalmol. 2017;1:e000008.
39. Prusky GT, Alam NM, Beekman S, Douglas RM. Rapid quantification of adult and developing mouse spatial vision using a virtual optomotor system. Invest Ophthalmol Vis Sci. 2004;45:4611–6.
40. Prusky GT, West PW, Douglas RM. Behavioral assessment of visual acuity in mice and rats. Vis Res. 2000;40:2201–9.
41. Shindler KS, Guan Y, Ventura E, Bennett J, Rostami A. Retinal ganglion cell loss induced by acute optic neuritis in a relapsing model of multiple sclerosis. Mult Scler. 2006;12:526–32.
42. Calida DM, Constantinescu C, Purev E, Zhang GX, Ventura ES, Lavi E, Rostami A. Cutting edge: C3, a key component of complement activation, is not required for the development of myelin oligodendrocyte glycoprotein peptide-induced experimental autoimmune encephalomyelitis in mice. J Immunol. 2001;166:723–6.
43. Schreibelt G, Musters RJP, Reijerkerk A, de Groot LR, van der Pol SMA, Hendrikx EML, et al. Lipoic acid affects cellular migration into the central nervous system and stabilizes blood-brain barrier integrity. J Immunol. 2006;177:2630–7.
44. Brookes MH, Golding BT, Howes DA, Hudson AT. Proof that the absolute configuration of natural α-lipoic acid is R by the synthesis of its enantiomer [(S)-(−)-α-lipoic acid] from (S)-malic acid. J Chem Soc Chem Commun. 1983;19:1051–3.
45. Niebch G, Büchele B, Blome J, Grieb S, Brandt G, Kampa P, et al. Enantioselective high-performance liquid chromatography assay of (+)R- and (−)S-alpha-lipoic acid in human plasma. Chirality. 1997;9:32–6.
46. Hermann R, Mungo J, Cnota PJ, Ziegler D. Enantiomer-selective pharmacokinetics, oral bioavailability, and sex effects of various alpha-lipoic acid dosage forms. Clin Pharmacol. 2014;6:195–204.
47. Hermann R, Niebch G, Borbe HO, Fieger-Büschges H, Ruus P, Nowak H, et al. Enantioselective pharmacokinetics and bioavailability of different racemic α-lipoic acid formulations in healthy volunteers. Eur J Pharm Sci. 1996;4:167–74.
48. Gleiter CH, Schug BS, Hermann R, Elze M, Blume HH, Gundert-Remy U. Influence of food intake on the bioavailability of thioctic acid enantiomers. Eur J Clin Pharmacol. 1996;50:513–4.
49. Biewenga GP, Dorstijn MA, Verhagen JV, Haenen GR, Bast A. Reduction of lipoic acid by lipoamide dehydrogenase. Biochem Pharmacol. 1996;51:233–8.
50. Raftopoulos R, Hickman SJ, Toosy A, Sharrack B, Mallik S, Paling D, et al. Phenytoin for neuroprotection in patients with acute optic neuritis: a randomised, placebo-controlled, phase 2 trial. Lancet Neurol. 2016;15:259–69.
51. Syc SB, Saidha S, Newsome SD, Ratchford JN, Levy M, Ford E, et al. Optical coherence tomography segmentation reveals ganglion cell layer pathology after optic neuritis. Brain. 2012;135:521–33.
52. Matsunaga Y, Kezuka T, An X, Fujita K, Matsuyama N, Matsuda R, et al. Visual functional and histopathological correlation in experimental autoimmune optic neuritis. Invest Ophthalmol Vis Sci. 2012;53:6964–71.
53. Larabee CM, Desai S, Agasing A, Georgescu C, Wren JD, Axtell RC, Plafker SM. Loss of Nrf2 exacerbates the visual deficits and optic neuritis elicited by experimental autoimmune encephalomyelitis. Mol Vis. 2016;22:1503–13.
54. Smith AW, Rohrer B, Wheless L, Samantaray S, Ray SK, Inoue J, et al. Calpain inhibition reduces structural and functional impairment of retinal ganglion cells in experimental optic neuritis. J Neurochem. 2016;139:270–84.
55. Liu B, Ma X, Guo D, Guo Y, Chen N, Bi H. Neuroprotective effect of alpha-lipoic acid on hydrostatic pressure-induced damage of retinal ganglion cells in vitro. Neurosci Lett. 2012;526:24–8.
56. Koriyama Y, Nakayama Y, Matsugo S, Kato S. Protective effect of lipoic acid against oxidative stress is mediated by Keap1/Nrf2-dependent heme oxygenase-1 induction in the RGC-5 cellline. Brain Res. 2013;1499:145–57.
57. Flier J, van Muiswinkel FL, Jongenelen CAM, Drukarch B. The neuroprotective antioxidant alpha-lipoic acid induces detoxication enzymes in cultured astroglial cells. Free Radic Res. 2002;36:695–9.
58. Packer L, Witt EH, Tritschler HJ. Alpha-lipoic acid as a biological antioxidant. Free Radic Biol Med. 1995;19:227–50.

Summary and Discussion

Multiple Sclerosis (MS) is an inflammatory autoimmune disorder, where chronic disability is mainly due to neuronal degeneration. Visual dysfunction is a symptom appearing in 50% of all MS patients, where optic neuritis is the heralding event. (Thompson et al. 2018; Wingerchuk and Carter 2014; Kale 2016). Strategies to effectively prevent chronic neurodegenerative processes or to promote repair are still lacking (Vargas and Tyor 2017). Different preclinical approaches are used to gain a better insight into the pathological processes and to find therapeutic targets. Among these, a variety of experimental autoimmune encephalomyelitis (EAE) models exist (Miller et al. 2010; Lassmann and Bradl 2017).

Whole-body positional manipulators for ocular imaging of anesthetized mice and rats: A do-it-yourself guide

After the invention of spectral domain OCT, this technology has also become applicable in rodent models (Knier et al. 2014; Dietrich et al. 2018; Zhang et al. 2017; Talla et al. 2013; Huang et al. 2012; Hein et al. 2012; Fischer et al. 2009). For an optimal reproducibility and quality in these assessments, the proper orientation of the light beam in an orthogonal angel to the retina is essential. Most commercially available OCT devices are constructed for human use and have to be adapted for preclinical research. “Some OCT devices only allow movements in the vertical axis, so the adjustment of the angle as well as the horizontal and vertical axis has to be performed by moving the animal.” (Dietrich et al. 2017:4). With the holder described in our publication, the beam-to-target angle can be adjusted by a manual rotation of the tube housing the animal. We proved the holder to be highly functional in over 2000 OCT measurements and measured a time benefit (2.8 times faster) over unrestrained positioning of the rodents, which keeps the time the animal is under anesthesia limited. The option for volatile anesthesia using this holder is another advantage, which is in our experience safer and easier to control than injectable anesthesia (Calderone et al. 1986; Szczesny et al. 2004). Nevertheless, a limitation of our “do-it yourself” holder is that the rotations have to be executed manually instead of controlled dials, which may reduce the precision of very fine adjustments. We do however think that the manual serves as a useful guide for researchers aiming to establish retinal imaging in rodents at their laboratories. Improving the prototype by using higher quality materials according to specific needs and interests is also possible.

Using optical coherence tomography and optokinetic response as structural and functional visual system readouts in mice and rats

“One of the first *in vivo* assessments in preclinical models of ON was the measurement of visual function by determining the optokinetic response (OKR) threshold (Quinn et al. 2011;

Prusky et al. 2004) […]. To test the OKR, rodents are placed on a platform in the center of a chamber while a rotating virtual cylinder of black gratings is projected at varying spatial frequencies […]. This measure is associated with the severity of optic neuritis and RGC loss in optic neuritis (Dietrich et al. 2018; Larabee et al. 2016; McDougald et al. 2018; An et al. 2013)." (Dietrich et al. 2019a:350). Hence, combining both cSLO/OCT and OKR allows a quantitative *in vivo* investigation of structure and function. The protocol published in "The Journal of Visualized Experiments" aimed to provide a manual for acquisition and analysis of high quality retinal scans in mice and rats, and is intended as an instructional manual for researchers using optokinetic response analysis in rodents. The substantial advantage of these techniques in comparison to histological investigations in animal experiments is, that longitudinal analyses are possible, allowing the investigation of dynamic pathological processes, largely reducing the variability and the number of animals needed per study (Huang et al. 1991; Prusky et al. 2004). When using OKR, the investigator should be blinded for the experimental group and it requires some training to distinguish between normal behavior and the actual "tracking" movements. Additionally, the visual acuity of the rodent should be evaluated before they are measured as there is a significant strain variability (Prusky et al. 2002; Wong and Brown 2006). Some mouse lines might not even be suitable for OKR measurements, e.g. SJL mice, as they are homozygous for the allele Pde6b^{rd1} (retinal degeneration 1) (Pittler and Baehr 1991). Alternative functional *in vivo* measurements of the visual system applicable in rodent models also exist, namely the visual evoked potentials (VEP) (Zhang et al. 2017; You et al. 2011) and electroretinography (ERG) (Talla et al. 2013; Talla et al. 2014). The latter techniques do not depend on the animals' willingness to cooperate and/or visual acuity over a certain distance, they are, however, more challenging to establish.

Monitoring retinal changes with optical coherence tomography predicts neuronal loss in experimental autoimmune encephalomyelitis

Despite the increasing research in preclinical EAE-ON models using the visual pathway, comparative OCT studies are still rare. Moreover, the best practices for the implementation of OCT in EAE mice are undefined. We initially identified the OCT scanning protocol for mice with the best reproducibility and reliability. We obtained the best results with volume scans, while peripapillary ring scans led to the poorest outcome, but has also been considered as an outcome parameter in animal models of MS (Lidster et al. 2013). This is possibly because the variability of the manual correction is averaged out by several B-scans compared to only one. Since the manual separation of the limits between the RNFL, GCL and IPL can be challenging, we analyzed them jointly as the IRL.

For models with severe retinal damage and optic neuritis, we chose the $PLP_{139-151}$-induced EAE in SJL/J mice and MOG_{35-55}-induced EAE in TCR^{2D2} mice (Shindler et al. 2006). Furthermore, we aimed to investigate the retinal degeneration in MBP-and MOG_{35-55}-induced EAE in C57Bl/6J mice (Gold et al. 2000; Bettelli et al. 2003). We were able to induce mild EAE signs in C57Bl/6J mice by immunization with whole rat MBP, with no significant retinal thinning, and according to the literature, induction also not seems to be very feasible in general (Faunce et al. 2004; Furlan 2004; Linker and Gold 2004). Hence, we conclude that this model is not suitable for retinal studies. EAE in SJL/J mice after immunization with $PLP_{139-151}$ resulted in detectable changes; however, retinal dystrophy occurring in this mouse line even in sham control animals ($Pde6b^{rd1}$ mutation) (Pittler and Baehr 1991), limits the usefulness for our purposes. The MOG immunization in TCR^{2D2} mice resulted in a severe progression with a loss rate of 30%, 60 days after EAE induction (death or sacrifice due to heavy burden of the animals). The challenging animal care and survival during the experiments led to the decision that this model might also not ideally suited. In the MOG_{35-55} induced EAE in C57Bl/6J mice, there was an acute IRL thickening until the onset and peak of disease, followed by progressive thinning, occurring most rapidly between the peak of disease and the 60^{th} day after immunization. This is similar to patients with ON, where changes occur most rapidly in the first months after the acute episode (Balk et al. 2016). In addition, according to our results, EAE studies using OCT as a surrogate for the survival of RGC do not provide additional meaningful information beyond two months, unless investigating mechanisms of repair or specifically targeting processes that occur in the late phase. Concluding all these data, we selected the MOG_{35-55}/C57Bl/6J model as the most appropriate for neuroprotection studies using visual system readouts, also in accordance with the findings of other research groups (Knier et al. 2014).

Typically, in preclinical EAE-ON studies, histological analysis of the optic nerve and the retina are applied, additionally to the *in vivo* visual readouts (Table 2).

Table 2. Typical readouts for animal ON models (modified from Dietrich et al. 2019a). In animal models for MS/ON, diverse *in vivo* readouts are combined with the histological analysis of the optic nerve and the retina. Ganglion cell layer (GCL), inner plexiform layer (IPL), inner nuclear layer (INL).

Sample/device	Type	Target	Staining/Readout
Optic nerve	Histology	Cellular infiltrates	Haematoxylin and eosin staining
Optic nerve	Histology	T-cells	CD3 antibody
Optic nerve	Histology	Microglia	Iba1 antibody
Optic nerve	Histology	Myelin	MBP antibody, Luxol fast blue
Retina	Histology	RGCs	Tubulin-βIII antibody, Brn3a antibody, FluoroGold injection
Retina	Histology	Microglia	Iba1
OCT	Visual readout	Retinal structure	Retinal layer thickness, mainly RNFL, GCL, IPL, INL
OKR	Visual readout	Visual function	Visual acuity
VEP	Visual readout	Visual function	Visual system conductivity
ERG	Visual readout	Visual function	Retinal function

Early alpha-lipoic acid therapy protects from degeneration of the inner retinal layers and vision loss in an experimental autoimmune encephalomyelitis-optic neuritis model

During the progression of MS, nitric oxide and other reactive oxygen species are released, leading to oxidative stress in the CNS. This is contributing to the detrimental process of demyelination, axonal damage and inflammation in both MS (Witherick et al. 2010; van der Goes et al. 1998; Wang et al. 2014; van Horssen et al. 2011) and EAE (Nikic et al. 2011; Ruuls et al. 1995). These increased levels of free radicals suggesting a benefit of antioxidative and neuroprotective substances. As a natural antioxidant, LA has exhibited beneficial effects in EAE (Schreibelt et al. 2006; Salinthone et al. 2008; Chaudhary et al. 2011; Wang et al. 2013). and in a phase II study of secondary progressive MS (Spain et al. 2017). Therefore, the purpose of our study was to investigate, whether LA also acts neuroprotective during the earlier phases of relapsing remitting MS. Our preclinical experiments aimed to evaluate if a clinical optic neuritis trial, especially using visual system readouts, could be reasonable. As a first step, we performed an *in vitro* experiment of endogenous oxidative glutamate stress, identifying reduced LA (dihydrolipoic acid) as the form exerting the ant-oxidative properties. No superior effects were however discovered by the (R)-racemic form of LA, contrary to the literature (Niebch et al. 1997; Hermann et al. 2014; Hermann et al. 1996; Gleiter et al. 1996). In the MOG_{35-55}/C57Bl/6J EAE model, the clinical score of the mice was significantly attenuated, conclusive with many other studies (Chaudhary et al. 2011; Salinthone et al. 2008; Schreibelt et al. 2006), which, however, lack of *in vivo* visual readouts such as OCT or OKR. The IRL

degeneration as well as the loss of the visual acuity was prevented after a prophylactic LA treatment of the EAE mice. Unfortunately, we could not detect these effects after a therapeutic treatment 14 days after MOG immunization. Remarkably, but in line with a previous study (Chaudhary et al. 2011), the RGCs were protected to the same level as after prophylactic LA treatment. The discrepancy between the OCT measurement and RGC counts could be explained by a degeneration of the inner plexiform and retinal nerve fibre layers, which cannot be prevented by a treatment starting at the onset of symptoms. Additional anti-inflammatory effects of LA were revealed by hematoxylin and eosin staining of the optic nerve, revealing a reduced infiltration of immune cells. These properties have been attributed to inhibitory effects of LA on T-cell migration (Chaudhary et al. 2011) and the increase of cAMP levels in natural killer cells, thereby inhibiting their function (Salinthone et al. 2008). We identified significantly higher GSH levels in tissue of LA treated mice suggesting that antioxidant effects may also significantly contribute to its protective effects, which is in line with our observations in cell culture. After considering all the data, we concluded, that LA might not be the ideal substance to be investigated in a clinical setting using visual readouts. As treatment would start only after the onset of clinical symptoms, possible beneficial outcomes would not be detectable by OCT or visual ability measurements.

In conclusion, OCT and OKR are non-invasive, longitudinal research tools with huge scientific potential. The EAE model serves as a paradigm for MS and optic neuritis, as it recapitulates the disease pathologies like acute autoimmune infiltration, demyelination and neuroaxonal damage. It is therefore also suited for preclinical neuroprotection and neuronal/axonal repair studies. The outcome can be easily assessed through the retina by the structural and functional readouts, which makes the anterior visual pathway a perfect model for the preclinical evaluation of novel therapeutic strategies.

Publications as co-author/review articles

Liebmann M, Hucke S, Koch K, Eschborn M, Ghelman J, Chasan AI, Glander S, Schadlich M, Kuhlencord M, Daber NM, Eveslage M, Beyer M, **Dietrich M**, Albrecht P, Stoll M, Busch KB, Wiendl H, Roth J, Kuhlmann T, Klotz L (2018) Nur77 serves as a molecular brake of the metabolic switch during T cell activation to restrict autoimmunity. Proceedings of the National Academy of Sciences of the United States of America, 21;115(34):E8017-E8026.
Contribution: Execution and statistical analysis of the OKR measurements of Nur77 EAE mice. Manuscript writing and data interpretation (contribution to final manuscript: 5%).

Ingwersen J, Santi L de, Wingerath B, Graf J, Koop B, Schneider R, Hecker C, Schroter F, Bayer M, Engelke AD, **Dietrich M**, Albrecht P, Hartung H-P, Annunziata P, Aktas O, Prozorovski T (2018) Nimodipine confers clinical improvement in two models of experimental autoimmune encephalomyelitis. Journal of neurochemistry, epub ahead of print.
Contribution: Scoring and Nimodipine treatment of $PLP_{139–151}$ EAE mice, statistical analysis of EAE experiments (contribution to final manuscript: 15%).

Hoffmann C, **Dietrich M**, Herrmann A-K, Schacht T, Albrecht P, Methner A (2017) Dimethyl Fumarate Induces Glutathione Recycling by Upregulation of Glutathione Reductase. Oxidative medicine and cellular longevity 2017:6093903.
Contribution: HT22 cell culture, qPCR and glutathione measurements. Statistical analysis and interpretation of qPCR and glutathione data (contribution to final manuscript: 30%).

Merckx E, Albertini G, Paterka M, Jensen C, Albrecht P, **Dietrich M**, van Liefferinge J, Bentea E, Verbruggen L, Demuyser T, Deneyer L, Lewerenz J, van Loo G, Keyser J de, Sato H, Maher P, Methner A, Massie A (2017) Absence of system xc(-) on immune cells invading the central nervous system alleviates experimental autoimmune encephalitis. J Neuroinflammation, 13;14(1):9.
Contribution: Histological staining of optic nerve slices, fluorescence microscopy of histological samples (contribution to final manuscript: 10%).

Review:
Dietrich M, Aktas O, Hartung H-P, Albrecht P (2019) Assessing the anterior visual pathway in optic neuritis: Recent experimental and clinical aspects. Current opinion in neurology, 32(3):346-357 (contribution to final manuscript: 70%).

References

Aktas O, Albrecht P, Hartung HP (2016) Optic neuritis as a phase 2 paradigm for neuroprotection therapies of multiple sclerosis: update on current trials and perspectives. Current opinion in neurology 29:199–204

Albrecht P, Fröhlich R, Hartung H-P, Kieseier BC, Methner A (2007) Optical coherence tomography measures axonal loss in multiple sclerosis independently of optic neuritis. J. Neurol. 254:1595–1596

Albrecht P, Ringelstein M, Muller AK, Keser N, Dietlein T, Lappas A, Foerster A, Hartung HP, Aktas O, Methner A (2012) Degeneration of retinal layers in multiple sclerosis subtypes quantified by optical coherence tomography. Multiple Sclerosis Journal 18:1422–1429

An X, Kezuka T, Usui Y, Matsunaga Y, Matsuda R, Yamakawa N, Goto H (2013) Suppression of experimental autoimmune optic neuritis by the novel agent fingolimod. Journal of neuro-ophthalmology : the official journal of the North American Neuro-Ophthalmology Society 33:143–148

Balk LJ, Cruz-Herranz A, Albrecht P, Arnow S, Gelfand JM, Tewarie P, Killestein J, Uitdehaag, Bernard M J, Petzold A, Green AJ (2016) Timing of retinal neuronal and axonal loss in MS: a longitudinal OCT study. Journal of neurology 263:1323–1331

Bates GP, Dorsey R, Gusella JF, Hayden MR, Kay C, Leavitt BR, Nance M, Ross CA, Scahill RI, Wetzel R, Wild EJ, Tabrizi SJ (2015) Huntington disease. Nature reviews. Disease primers 1:15005

Bettelli E, Pagany M, Weiner HL, Linington C, Sobel RA, Kuchroo VK (2003) Myelin oligodendrocyte glycoprotein-specific T cell receptor transgenic mice develop spontaneous autoimmune optic neuritis. J Exp Med 197:1073–1081

Calderone L, Grimes P, Shalev M (1986) Acute reversible cataract induced by xylazine and by ketamine-xylazine anesthesia in rats and mice. Experimental eye research 42:331–337

Chaudhary P, Marracci G, Yu X, Galipeau D, Morris B, Bourdette D (2011) Lipoic acid decreases inflammation and confers neuroprotection in experimental autoimmune optic neuritis. Journal of neuroimmunology 233:90–96

Chauhan BC, Stevens KT, Levesque JM, Nuschke AC, Sharpe GP, O'Leary N, Archibald ML, Wang X (2012) Longitudinal in vivo imaging of retinal ganglion cells and retinal thickness changes following optic nerve injury in mice. PloS one 7:e40352

Cheng Y, Skinner DD, Lane TE (2018) Innate Immune Responses and Viral-Induced Neurologic Disease. Journal of clinical medicine 8

Compston A, Coles A (2008) Multiple sclerosis. Lancet 372:1502–1517

DePaula-Silva AB, Hanak TJ, Libbey JE, Fujinami RS (2017) Theiler's murine encephalomyelitis virus infection of SJL/J and C57BL/6J mice. Models for multiple sclerosis and epilepsy. Journal of neuroimmunology 308:30–42

Dietrich M, Aktas O, Hartung H-P, Albrecht P (2019a) Assessing the anterior visual pathway in optic neuritis. Recent experimental and clinical aspects. Current opinion in neurology

Dietrich M, Cruz-Herranz A, Yiu H, Aktas O, Brandt AU, Hartung H-P, Green A, Albrecht P (2017) Whole-body positional manipulators for ocular imaging of anaesthetised mice and rats. A do-it-yourself guide. BMJ Open Ophthalmol. 1:e000008

Dietrich M, Hecker C, Hilla A, Cruz-Herranz A, Hartung H-P, Fischer D, Green A, Albrecht P (2019b) Using Optical Coherence Tomography and Optokinetic

Response As Structural and Functional Visual System Readouts in Mice and Rats. J Vis Exp. 143
Dietrich M, Helling N, Hilla A, Heskamp A, Issberner A, Hildebrandt T, Kohne Z, Kury P, Berndt C, Aktas O, Fischer D, Hartung H-P, Albrecht P (2018) Early alpha-lipoic acid therapy protects from degeneration of the inner retinal layers and vision loss in an experimental autoimmune encephalomyelitis-optic neuritis model. J Neuroinflammation 15:71
Faunce DE, Terajewicz A, Stein-Streilein J (2004) Cutting edge. In vitro-generated tolerogenic APC induce CD8+ T regulatory cells that can suppress ongoing experimental autoimmune encephalomyelitis. J Immunol 172:1991–1995
Fischer MD, Huber G, Beck SC, Tanimoto N, Muehlfriedel R, Fahl E, Grimm C, Wenzel A, Remé CE, van de Pavert, Serge A, Wijnholds J, Pacal M, Bremner R, Seeliger MW (2009) Noninvasive, in vivo assessment of mouse retinal structure using optical coherence tomography. PloS one 4:e7507
Frohman EM, Fujimoto JG, Frohman TC, Calabresi PA, Cutter G, Balcer LJ (2008) Optical coherence tomography. A window into the mechanisms of multiple sclerosis. Nature clinical practice. Neurology 4:664–675
Furlan R (2004) MBP-specific experimental autoimmune encephalomyelitis in C57BL/6 mice. J Immunol 173:5; author reply 5-6
Galetta KM, Calabresi PA, Frohman EM, Balcer LJ (2011) Optical coherence tomography (OCT): imaging the visual pathway as a model for neurodegeneration. Neurotherapeutics 8:117–132
Gleiter CH, Schug BS, Hermann R, Elze M, Blume HH, Gundert-Remy U (1996) Influence of food intake on the bioavailability of thioctic acid enantiomers. European Journal of Clinical Pharmacology 50:513–514
Gobel K, Wedell J-H, Herrmann AM, Wachsmuth L, Pankratz S, Bittner S, Budde T, Kleinschnitz C, Faber C, Wiendl H, Meuth SG (2013) 4-Aminopyridine ameliorates mobility but not disease course in an animal model of multiple sclerosis. Exp Neurol. 248:62–71
Gold R, Hartung HP, Toyka KV (2000) Animal models for autoimmune demyelinating disorders of the nervous system. Molecular medicine today 6:88–91
Hein K, Gadjanski I, Kretzschmar B, Lange K, Diem R, Sättler MB, Bähr M (2012) An optical coherence tomography study on degeneration of retinal nerve fiber layer in rats with autoimmune optic neuritis. Invest Ophthalmol Vis Sci 53:157–163
Hermann R, Mungo J, Cnota PJ, Ziegler D (2014) Enantiomer-selective pharmacokinetics, oral bioavailability, and sex effects of various alpha-lipoic acid dosage forms. Clinical pharmacology : advances and applications 6:195–204
Hermann R, Niebch G, Borbe HO, Fieger-Büschges H, Ruus P, Nowak H, Riethmüller-Winzen H, Peukert M, Blume H (1996) Enantioselective pharmacokinetics and bioavailability of different racemic α-lipoic acid formulations in healthy volunteers. European Journal of Pharmaceutical Sciences 4:167–174
Hoffmann C, Dietrich M, Herrmann A-K, Schacht T, Albrecht P, Methner A (2017) Dimethyl Fumarate Induces Glutathione Recycling by Upregulation of Glutathione Reductase. Oxidative medicine and cellular longevity 2017:6093903
Huang D, Swanson EA, Lin CP, Schuman JS, Stinson WG, Chang W, Hee MR, Flotte T, Gregory K, Puliafito CA (1991) Optical coherence tomography. Science 254:1178–1181
Huang WC, Wright AF, Roman AJ, Cideciyan AV, Manson FD, Gewaily DY, Schwartz SB, Sadigh S, Limberis MP, Bell P, Wilson JM, Swaroop A, Jacobson SG (2012)

RPGR-associated retinal degeneration in human X-linked RP and a murine model. Invest Ophthalmol Vis Sci 53:5594–5608
Ingwersen J, Santi L de, Wingerath B, Graf J, Koop B, Schneider R, Hecker C, Schroter F, Bayer M, Engelke AD, Dietrich M, Albrecht P, Hartung H-P, Annunziata P, Aktas O, Prozorovski T (2018) Nimodipine confers clinical improvement in two models of experimental autoimmune encephalomyelitis. Journal of neurochemistry
Kale N (2016) Optic neuritis as an early sign of multiple sclerosis. Eye and brain 8:195–202
Knier B, Rothhammer V, Heink S, Puk O, Graw J, Hemmer B, Korn T (2014) Neutralizing IL-17 protects the optic nerve from autoimmune pathology and prevents retinal nerve fiber layer atrophy during experimental autoimmune encephalomyelitis. J Autoimmun 56:34–44
Kokona D, Jovanovic J, Ebneter A, Zinkernagel MS (2017) In Vivo Imaging of Cx3cr1gfp/gfp Reporter Mice with Spectral-domain Optical Coherence Tomography and Scanning Laser Ophthalmoscopy. Journal of Visualized Experiments
Lane CA, Hardy J, Schott JM (2018) Alzheimer's disease. European journal of neurology 25:59–70
Larabee CM, Desai S, Agasing A, Georgescu C, Wren JD, Axtell RC, Plafker SM (2016) Loss of Nrf2 exacerbates the visual deficits and optic neuritis elicited by experimental autoimmune encephalomyelitis. Molecular vision 22:1503–1513
Lassmann H, Bradl M (2017) Multiple sclerosis. Experimental models and reality. Acta Neuropathol 133:223–244
Lee H-J, Kim B, Waters P, Woodhall M, Irani S, Ahn S, Kim S-J, Kim S-M (2018) Chronic relapsing inflammatory optic neuropathy (CRION). A manifestation of myelin oligodendrocyte glycoprotein antibodies. J Neuroinflammation 15:302
Leung, Christopher K. S., Lindsey JD, Crowston JG, Ju W-K, Liu Q, Bartsch D-U, Weinreb RN (2008) In vivo imaging of murine retinal ganglion cells. Journal of neuroscience methods 168:475–478
Lidster K, Jackson SJ, Ahmed Z, Munro P, Coffey P, Giovannoni G, Baker MD, Baker D (2013) Neuroprotection in a novel mouse model of multiple sclerosis. PloS one 8:e79188
Liebmann M, Hucke S, Koch K, Eschborn M, Ghelman J, Chasan AI, Glander S, Schadlich M, Kuhlencord M, Daber NM, Eveslage M, Beyer M, Dietrich M, Albrecht P, Stoll M, Busch KB, Wiendl H, Roth J, Kuhlmann T, Klotz L (2018) Nur77 serves as a molecular brake of the metabolic switch during T cell activation to restrict autoimmunity. Proceedings of the National Academy of Sciences of the United States of America
Linker RA, Gold R (2004) MBP-induced experimental autoimmune encephalomyelitis in C57BL/6 mice. J. Immunol. 173:2896
Lisak RP, Nedelkoska L, Benjamins JA, Schalk D, Bealmear B, Touil H, Li R, Muirhead G, Bar-Or A (2017) B cells from patients with multiple sclerosis induce cell death via apoptosis in neurons in vitro. Journal of neuroimmunology 309:88–99
Manogaran P, Walker-Egger C, Samardzija M, Waschkies C, Grimm C, Rudin M, Schippling S (2018) Exploring experimental autoimmune optic neuritis using multimodal imaging. NeuroImage 175:327–339
Matsushima GK, Morell P (2001) The neurotoxicant, cuprizone, as a model to study demyelination and remyelination in the central nervous system. Brain Pathol 11:107–116
McDougald DS, Dine KE, Zezulin AU, Bennett J, Shindler KS (2018) SIRT1 and NRF2 Gene Transfer Mediate Distinct Neuroprotective Effects Upon Retinal Ganglion Cell

Survival and Function in Experimental Optic Neuritis. Invest Ophthalmol Vis Sci 59:1212–1220
Merckx E, Albertini G, Paterka M, Jensen C, Albrecht P, Dietrich M, van Liefferinge J, Bentea E, Verbruggen L, Demuyser T, Deneyer L, Lewerenz J, van Loo G, Keyser J de, Sato H, Maher P, Methner A, Massie A (2017) Absence of system xc(-) on immune cells invading the central nervous system alleviates experimental autoimmune encephalitis. J Neuroinflammation 14:9
Miller DH, Barkhof F, Frank JA, Parker GJM, Thompson AJ (2002) Measurement of atrophy in multiple sclerosis. Pathological basis, methodological aspects and clinical relevance. Brain : a journal of neurology 125:1676–1695
Miller SD, Karpus WJ, Davidson TS (2010) Experimental autoimmune encephalomyelitis in the mouse. Curr Protoc Immunol Chapter 15:Unit 15.1
Munguba GC, Galeb S, Liu Y, Landy DC, Lam D, Camp A, Samad S, Tapia ML, Lee RK (2014) Nerve fiber layer thinning lags retinal ganglion cell density following crush axonopathy. Investigative ophthalmology & visual science 55:6505–6513
Niebch G, Büchele B, Blome J, Grieb S, Brandt G, Kampa P, Raffel HH, Locher M, Borbe HO, Nubert I, Fleischhauer I (1997) Enantioselective high-performance liquid chromatography assay of (+)R- and (-)S-alpha-lipoic acid in human plasma. Chirality 9:32–36
Nikic I, Merkler D, Sorbara C, Brinkoetter M, Kreutzfeldt M, Bareyre FM, Bruck W, Bishop D, Misgeld T, Kerschensteiner M (2011) A reversible form of axon damage in experimental autoimmune encephalomyelitis and multiple sclerosis. Nature medicine 17:495–499
Olsson T, Barcellos LF, Alfredsson L (2017) Interactions between genetic, lifestyle and environmental risk factors for multiple sclerosis. Nat Rev Neurol 13:25–36
Optic Neuritis Study Group (1991) The clinical profile of optic neuritis. Experience of the Optic Neuritis Treatment Trial. Arch Ophthalmol 109:1673–1678
Petzold A, de Boer, Johannes F, Schippling S, Vermersch P, Kardon R, Green A, Calabresi PA, Polman C (2010) Optical coherence tomography in multiple sclerosis: a systematic review and meta-analysis. Lancet Neurol 9:921–932
Piguet F, Alves S, Cartier N (2017) Clinical Gene Therapy for Neurodegenerative Diseases. Past, Present, and Future. Human gene therapy 28:988–1003
Pittler SJ, Baehr W (1991) Identification of a nonsense mutation in the rod photoreceptor cGMP phosphodiesterase beta-subunit gene of the rd mouse. Proceedings of the National Academy of Sciences of the United States of America 88:8322–8326
Prusky GT, Alam NM, Beekman S, Douglas RM (2004) Rapid quantification of adult and developing mouse spatial vision using a virtual optomotor system. Invest Ophthalmol Vis Sci. 45:4611–4616
Prusky GT, Harker K, Douglas RM, Whishaw IQ (2002) Variation in visual acuity within pigmented, and between pigmented and albino rat strains. Behavioural Brain Research 136:339–348
Quinn TA, Dutt M, Shindler KS (2011) Optic neuritis and retinal ganglion cell loss in a chronic murine model of multiple sclerosis. Front Neurol 2:50
Ruuls SR, Bauer J, Sontrop K, Huitinga I, t' Hart BA, Dijkstra CD (1995) Reactive oxygen species are involved in the pathogenesis of experimental allergic encephalomyelitis in Lewis rats. Journal of neuroimmunology 56:207–217
Saidha S, Al-Louzi O, Ratchford JN, Bhargava P, Oh J, Newsome SD, Prince JL, Pham D, Roy S, van Zijl P, Balcer LJ, Frohman EM, Reich DS, Crainiceanu C, Calabresi

PA (2015) Optical coherence tomography reflects brain atrophy in multiple sclerosis: A four-year study. Ann Neurol 78:801–813
Salinthone S, Schillace RV, Marracci GH, Bourdette DN, Carr DW (2008) Lipoic acid stimulates cAMP production via the EP2 and EP4 prostanoid receptors and inhibits IFN gamma synthesis and cellular cytotoxicity in NK cells. Journal of neuroimmunology 199:46–55
Schreibelt G, Musters RJP, Reijerkerk A, Groot LR de, van der Pol SMA, Hendrikx EML, Dopp ED, Dijkstra CD, Drukarch B, Vries HE de (2006) Lipoic acid affects cellular migration into the central nervous system and stabilizes blood-brain barrier integrity. Journal of immunology (Baltimore, Md. : 1950) 177:2630–2637
Shindler KS, Guan Y, Ventura E, Bennett J, Rostami A (2006) Retinal ganglion cell loss induced by acute optic neuritis in a relapsing model of multiple sclerosis. Mult Scler. 12:526–532
Siger M, Dziegielewski K, Jasek L, Bieniek M, Nicpan A, Nawrocki J, Selmaj K (2008) Optical coherence tomography in multiple sclerosis. Thickness of the retinal nerve fiber layer as a potential measure of axonal loss and brain atrophy. J Neurol 255:1555–1560
Spain R, Powers K, Murchison C, Heriza E, Winges K, Yadav V, Cameron M, Kim E, Horak F, Simon J, Bourdette D (2017) Lipoic acid in secondary progressive MS: A randomized controlled pilot trial. Neurology(R) neuroimmunology & neuroinflammation 4:e374
Szczesny G, Veihelmann A, Massberg S, Nolte D, Messmer K (2004) Long-term anaesthesia using inhalatory isoflurane in different strains of mice-the haemodynamic effects. Zeitschrift für mikroskopisch-anatomische Forschung 38:64–69
Talla V, Porciatti V, Chiodo V, Boye SL, Hauswirth WW, Guy J (2014) Gene therapy with mitochondrial heat shock protein 70 suppresses visual loss and optic atrophy in experimental autoimmune encephalomyelitis. Invest Ophthalmol Vis Sci 55:5214–5226
Talla V, Yang C, Shaw G, Porciatti V, Koilkonda RD, Guy J (2013) Noninvasive assessments of optic nerve neurodegeneration in transgenic mice with isolated optic neuritis. Invest Ophthalmol Vis Sci 54:4440–4450
Thenganatt MA, Jankovic J (2014) Parkinson disease subtypes, United States
Thompson AJ, Baranzini SE, Geurts J, Hemmer B, Ciccarelli O (2018) Multiple sclerosis. Lancet 391:1622–1636
Toosy AT, Mason DF, Miller DH (2014) Optic neuritis. Lancet Neurol 13:83–99
van der Goes A, Brouwer J, Hoekstra K, Roos D, van den Berg TK, Dijkstra CD (1998) Reactive oxygen species are required for the phagocytosis of myelin by macrophages. Journal of neuroimmunology 92:67–75
van Horssen J, Witte ME, Schreibelt G, Vries HE de (2011) Radical changes in multiple sclerosis pathogenesis. Biochimica et biophysica acta 1812:141–150
Vargas DL, Tyor WR (2017) Update on disease-modifying therapies for multiple sclerosis. Journal of investigative medicine : the official publication of the American Federation for Clinical Research 65:883–891
Villoslada P, Sepulcre J, Toledo J, Bejarano B (2008) Retinal nerve fiber layer is associated with brain atrophy in multiple sclerosis. Neurology 71:1747; author reply 1747-8
Wang K-C, Tsai C-P, Lee C-L, Chen S-Y, Lin G-J, Yen M-H, Sytwu H-K, Chen S-J (2013) α-Lipoic acid enhances endogenous peroxisome-proliferator-activated

receptor-gamma to ameliorate experimental autoimmune encephalomyelitis in mice. Clinical science (London, England : 1979) 125:329–340
Wang P, Xie K, Wang C, Bi J (2014) Oxidative stress induced by lipid peroxidation is related with inflammation of demyelination and neurodegeneration in multiple sclerosis. European neurology 72:249–254
Ward ME, Chen R, Huang H-Y, Ludwig C, Telpoukhovskaia M, Taubes A, Boudin H, Minami SS, Reichert M, Albrecht P, Gelfand JM, Cruz-Herranz A, Cordano C, Alavi MV, Leslie S, Seeley WW, Miller BL, Bigio E, Mesulam M-M, Bogyo MS, Mackenzie IR, Staropoli JF, Cotman SL, Huang EJ, Gan L, Green AJ (2017) Individuals with progranulin haploinsufficiency exhibit features of neuronal ceroid lipofuscinosis. Science translational medicine 9
Wingerchuk DM, Carter JL (2014) Multiple sclerosis: current and emerging disease-modifying therapies and treatment strategies. Mayo Clinic proceedings 89:225–240
Witherick J, Wilkins A, Scolding N, Kemp K (2010) Mechanisms of oxidative damage in multiple sclerosis and a cell therapy approach to treatment. Autoimmune diseases 2011:164608
Wong AA, Brown RE (2006) Visual detection, pattern discrimination and visual acuity in 14 strains of mice. Genes, brain, and behavior 5:389–403
Wu Y, Zhong L, Geng J (2019) Visual impairment in neuromyelitis optica spectrum disorders (NMOSD). Journal of chemical neuroanatomy 97:66–70
You Y, Klistorner A, Thie J, Graham SL (2011) Latency delay of visual evoked potential is a real measurement of demyelination in a rat model of optic neuritis. Invest Ophthalmol Vis Sci 52:6911–6918
Zhang H-K, Ye Y, Zhao Z-N, Li K-J, Du Y, Hu Q-M, He J-F (2017) Neuroprotective effects of gypenosides in experimental autoimmune optic neuritis. International journal of ophthalmology 10:541–549

Appendix

List of abbreviations

AD: Alzheimer's Disease
CNS: central nervous system
cSLO: confocal scanning laser ophthalmoscopy
EAE: experimental autoimmune encephalomyelitis
ERG: electroretinography
GCL: ganglion cell layer
INL: inner nuclear layer
IPL: inner plexiform layer
IRL: inner retinal layer
LA: alpha-lipoic acid
MBP: myelin basic protein
MOG_{35-55}: myelin oligodendrocyte glycoprotein, fragment 35-55
MS: Multiple Sclerosis
OCT: optical coherence tomography
OKR: optokinetic response
ON: optic neuritis
PD: Parkinson's Disease
PLP: proteolipid protein
RGC: retinal ganglion cells
RNFL: retinal nerve fiber layer
TCR: T-cell receptor
TCR^{2D2}: T-cell receptor transgenic mouse, specific for MOG_{35-55}
VEP: visual evoked potential

Acknowledgment/Danksagung

Ich möchte mich zunächst ganz herzlich bei Philipp Albrecht bedanken, unter dessen stets kompetenter Anleitung ich diese Arbeit anfertigen durfte. Vielen Dank für die zahlreichen guten Ideen, viele spannende Projekte, Beharrlichkeit und Optimismus, konstruktive Kritik und Lob. Ich freue mich, dass ich die Möglichkeit hatte viel Neues zu lernen und Gelerntes weitergeben zu können, und, dass ich durch zahlreiche Kooperationen und die Teilnahme an spannenden Kongressen und Meetings viele interessante Menschen kennenlernen konnte.

Des Weiteren möchte ich mich bei Prof. Rose bedanken für Ihre Bereitschaft als Mentor aus der naturwissenschaftlichen Fakultät zur Verfügung zu stehen. Vielen Dank für das Lesen und die Begutachtung dieser Arbeit!

Auch bei Prof. Hartung bedanke ich mich für die Möglichkeit, in den Laboren der Neurologie zu Arbeiten, die konstruktive und hilfreiche Zusammenarbeit bei allen gemeinsamen Projekten und Publikationen.

Mein Dank gilt ebenso allen Koautoren für die produktive Zusammenarbeit, besonders aber Andrés Cruz-Herranz für seine Expertise in der Maus-OCT und EAE-Forschung, und die tolle Zusammenarbeit bei unserer gemeinsamen Publikation. Danken möchte ich auch Carsten Berndt, Thomas Hildebrand, Klaudia Lepka und Orhan Aktas für die Zusammenarbeit an zahlreichen Projekten, sowie Alexander Hilla und Dietmar Fischer für deren Expertise zur Retinaforschung.

Bedanken möchte ich mich auch bei allen Mitgliedern der Arbeitsgruppe und den Kollegen aus dem Labor im Life Science Center. Es macht Spaß, mit euch zusammen zu arbeiten! Ich danke ganz besonders Andrea für die das Segmentieren von OCT Scans, das Schneiden, Färben und Aufnehmen der histologischen Proben, Kaffeekochen, Gespräche und so weiter. Ohne Dich wäre meine Doktorarbeit so nicht möglich gewesen! Herzlichen Dank auch an Christina Hecker für die vielen Tage in der TVA, die gemeinsamen Experimente und die super Zusammenarbeit.
Danke auch an alle anderen Mitglieder der AG, Valeria Koska, Niklas Helling und Moritz Frenger für die Hilfe bei den Experimenten und Auswertungen.

Auch ein großes Dankeschön an meine Eltern, die mich auf meinem Weg immer unterstützt haben! Der größte Dank aber geht zum Abschluss an meine Ehefrau Sabine, die in den letzten elf Jahren immer an meiner Seite war und die mich einfach glücklich macht!

Declaration/Erklärung

Ich versichere an Eides Statt, dass die Dissertation von mir selbständig und ohne unzulässige fremde Hilfe unter Beachtung der „Grundsätze zur Sicherung guter wissenschaftlicher Praxis an der Heinrich-Heine-Universität Düsseldorf“ erstellt worden ist. Diese Dissertation wurde bei keiner anderen Institution in dieser oder ähnlicher Form bisher eingereicht und es wurden keine erfolglosen Promotionsversuche unternommen.

Michael Dietrich